UNIVERSITY OF OKLAHOMA

GRADUATE COLLEGE

THE IMPACT OF EL NINO SOUTHERN OSCILLATION ON THE CLIMATOLOGY OF U.S. WINTER AND EARLY SPRING TORNADO OUTBREAKS

A DISSERTATION

SUBMITTED TO THE GRADUATE FACULTY

in partial fulfillment of the requirements for the

Degree of

DOCTOR OF PHILOSOPHY

By

ASHTON ROBINSON COOK
Norman, Oklahoma
2014

THE IMPACT OF EL NINO SOUTHERN OSCILLATION ON THE CLIMATOLOGY OF U.S. WINTER AND EARLY SPRING TORNADO OUTBREAKS

A DISSERTATION APPROVED FOR THE
SCHOOL OF METEOROLOGY

BY

_____
Dr. Lance Leslie, Chair

_____
Dr. Lesley Rankin-Hill

_____
Dr. David Parsons

_____
Dr. Susan Postawko

_____
Dr. Joseph Schaefer

ACKNOWLEDGEMENTS

I never expected my road to a Ph.D. to be as lengthy, turbulent, traumatic, and full of unexpected twists and turns…all compounded by very emotional circumstances surrounding the sudden and unexpected death of my former committee chair Dr. Peter J. Lamb. Miraculously, I survived it all. And from it, I have emerged as a stronger, more confident meteorologist and human being. I have also learned that academic and career achievement is important and highly valued by many. But I have also learned the value of my fellow man and the importance of helping others in their time of need and in pursuit of their academic and career goals. I have the OU School of Meteorology and the National Weather Service to thank for this.

I could not have made it on this journey without the support of some amazing people. Dr. Lance Leslie has been supportive of my academic aspirations ever since I first took one of his courses in 2007. I have always admired his love for weather and through time I have come to appreciate the value and importance he places on the success of his students. Dr. Leslie was always aware of my ability to perform research and attain a Ph.D. and had faith in me. He was aware of the various challenges I faced and the words “don’t give up” resonate with me as clearly now as they did when he first said them to me at one of the most difficult points along the journey. I cannot overstate how grateful I am that he assumed chairmanship of my dissertation committee in the wake of the tragic passing

of Dr. Lamb. My hope is that my career can be a reflection of the powerful investment he has made in my academic career and my life.

My family has been a “rock” for me throughout this process. My mother, Dorothy, was an amazing example of unfailing love throughout this process and constantly expressed her support and pride in me no matter the circumstances. There were times when it seemed as if she knew just what to say at the perfect time to help me move forward with peace and optimism that somehow everything would be okay. My aunt, Vera, and my dad, Ray, were also constant sources of support. Their prayers, their visits, and phone calls were all reminders that even though I was fighting an uphill battle, I was never fighting that battle alone.

Several other individuals had key roles in helping me along the road to the degree. Luwanda Byrd was a constant source of encouragement, strength, and compassion throughout the Ph.D. journey. Dr. Lesley Rankin-Hill always had an open-door policy for her students and I took full advantage of that, relying on her for advice at critical junctures during the dissertation process. Dr. Amelia Adams was a source of experience and constant positivity regarding the challenges I faced in the dissertation program. These three ladies were not only helpful with regard to navigating the Ph.D. process, but also in helping me to grieve the unexpected loss of Dr. Lamb. They are truly outstanding individuals and I am forever grateful for their willingness to help me in my time of need.

Several other individuals played key roles in shaping the direction of the research. Dr. Joseph Schaefer showed interest and support in the research I conducted from day one, which culminated into a journal publication. Dr. Lamb took an interest in my work from day one also and played a key role in shaping the initial writing of the term paper I did for his Climate Dynamics class. Dr. Michael Richman provided statistics expertise that greatly enhanced the overall body of work. Dr. David Parsons provided several important points for ensuring that the work remained important, relevant, and applicable. Dr. Susan Postawko's probing questions about the impact of my research for society helped me communicate the potential applicability of the work to the seasonal tornado forecast problem. My co-workers, Dr. Israel Jirak and Dr. Patrick Marsh, were also helpful with initial revisions of the dissertation, and Dr. Phillip Bothwell also provided helpful guidance.

I also want to acknowledge five individuals who had very positive influences in my academic career: Dr. Jeff Kimpel, David Imy, Dr. Ashanti Johnson, Dr. Ambrose Jearld, and the late Dr. Ken Crawford. These honorable men and women were exemplary servant leaders that I had great fortune of interacting with during my time as a graduate student at OU. I have learned a tremendous amount from just observing their conduct in professional matters and I intend to carry their example with me throughout my career.

I certainly could not have made it to this point without several friendships that helped me maintain some semblance of the difficult, delicate art of work-life balance. To Renee Curry, Ryan Noel, Ashley Noel, Robin Williams, Diana Douglass, Liz Leitman, Jeff Leitman, Tim Marquis, Somer Erickson, Nick Biermann, Celina Bell, Greg Dial, Dr. Dewayne Branch, Dr. Ty White, Kurtis Dawson, Dana Jackson, Robert Dennis, Brian Shawn Kelly (and the rest of my OKC Diamondbacks and Bounty Hunters football teammates), my Harvest Church family, and countless others, your friendship has helped me through some of the most difficult days of my life and it means more to me than you will ever know.

Three men have made an immense impact in my life and I also want to honor them: Pastor Calvin Williams (and the Lighthouse Family Praise and Worship Center), Barry George, and Walter Sledge. I cannot thank these three individuals enough for the prayers, advice, and support they have given me in the past 15 years. I honestly do not know what my life would look like without them.

Last, and certainly not least, I thank GOD and my Savior Jesus Christ for helping me through this process. Through this relationship, I always know that I have HOPE and a FUTURE no matter the circumstance! (Jeremiah 29:11)

TABLE OF CONTENTS

LIST OF TABLES

LIST OF FIGURES

ABSTRACT

In recent years, the notion of a potential seasonal tornado outbreak prediction scheme has garnered the attention of several researchers. The studies that have arisen on this topic have focused mainly on the influence of large-scale climate drivers (e.g., El Niño Southern Oscillation, North Atlantic Oscillation, Pacific Decadal Oscillation) on tornado outbreaks. Studies on these relationships, however, have yielded conflicting results regarding the roles of the climate drivers on tornado intensity and frequency.

The present study addresses the need to establish linkages between winter and early spring U.S. tornado outbreaks to ENSO. Linkages between tornado outbreaks and ENSO are established in two ways: 1) statistically by relating raw counts of tornadoes in outbreaks (six or more in a 24 hour period in the U.S. east of the Rocky Mountains) and their destruction potential to sea surface temperature anomalies in the Niño 3.4 region and 2) qualitatively by relating shifts in synoptic-scale atmospheric phenomena contributing to tornado outbreak development to ENSO. The latter method for establishing these linkages is key as they help to avoid the weaknesses present in several previous studies of neglecting physical explanations of underlying shifts in tornado activity as a function of ENSO.

1. INTRODUCTION

1.1 Historical Overview of United States Tornado Occurrences

Tornadoes have posed a major threat to civilization in the United States, with their documentation after European settlement beginning as far back as the mid-1600s. The first recorded tornado in U.S. history, journaled by Massachusetts Governor John Winthrop in July 1643, touched down in the northeastern part of his state, killing one Native American, lifting one meeting house, and downing numerous trees (Ludlum 1970, p. 3). Tornadoes during the 17th and early 18th centuries were most often recorded in the northeastern U.S., and more documentation of tornado-like phenomena occurred from other parts of the present-day U.S., as settlers and pioneers migrated from the farthest eastern and northeastern parts of the country into the deep South, Great Plains, and the "old-northwest" (present-day areas from Pennsylvania to Iowa).

Poorly understood in those times, tornadoes had several different names: violent hurricanes, cyclones, tempests, and whirlwinds (Flora 1953, p. 169; Ludlum 1970, pp. 3, 4, 92, 182; Grazulis 1993, pp. 11-12, 195-196). Now, the *Glossary of Meteorology* of the American Meteorological Society (Glickman 2000) defines a tornado as "a violently rotating column of air, in contact with the surface, pendant from a cumuliform cloud, and often (but not always) visible as a funnel cloud." Despite various naming conventions, these violent storms had several common and undeniable traits: long and

distinct paths, sudden onsets, and utter destruction in their wake with incomprehensible force. Often times these tornadoes were signified by dark, turbulent clouds, a loud 'roar', frequent lightning, heavy rain, and large hail. Much destruction to trees, homes, businesses, and towns were left behind in their wake, and these violent storms often changed localities and livelihoods forever.

One of the most significant, pre-Civil War era tornadoes was the Natchez, Mississippi, tornado of May 7, 1840. This tornado was unique in that its effects were far-reaching and its economic impact was as great as any single tornado in recorded history to that point (Flora 1953, p. 111; Ludlow 1970, pp. 86-89). This large, violent tornado had extended across both sides of the Mississippi River (0.6 miles in width) at one point, and did significant damage on both sides of the river simultaneously for parts of its life span. Official death tolls were listed at greater than 300, although that number did not include slaves who were killed by the tornado, nor could it accurately account for the numbers of individuals who perished in the Mississippi River as the tornado struck the Natchez landing. Losses as a result of this tornado were conservatively estimated at $5 million (1840 U.S. dollars). Because the Mississippi River was a major shipping route for goods throughout the U.S. in a nation with strong dependence on shipping via waterways and tributaries for commerce, this economic disaster and loss of life affected not only the local area, but also many areas along much of the Mississippi, Wabash, Salt, and Ohio River transport systems (Ludlum

1970, pp. 86-89). Thus, it likely was the first tornado disaster in U.S. history to have a widespread impact.

The single deadliest tornado ever recorded in the U.S. occurred on March 18, 1925 (Flora 1953, pp. 121-123; C. Doswell, personal communication). Commonly referred to as the “Tri-State Tornado” that crossed eastern Missouri, southern Illinois, and southwestern Indiana, this violent storm was probably the most severe single tornado event in U.S. history in terms of its impacts. It killed 695 people, injured over 2000 people, destroyed over 15,000 buildings and farmsteads, and left deep scars across the American landscape that took decades to heal. This tornado was on the ground for approximately 219 miles and moved toward the east-northeast at roughly 50-75 miles per hour. Individuals in its path referred to the tornado as a “rolling black cloud” that was on the ground. Because of the common perception of tornadoes as a narrow funnel instead of a wide, large circulation, many mistook this tornado as a fog-bank, failing to realize the imminent danger they were in (Flora 1953, pp. 121-123).

Major tornado disasters, including large loss of life, numerous injuries, and property damage, aren’t limited to early American history. In more recent times (i.e., the “modern” era of tornado documentation), the focus has broadened from single tornadoes that have impacted localities to include multiple tornadoes occurring in short succession across larger areas, or ‘tornado outbreaks’. Three of the most notable recent outbreaks include the “Super Outbreak” of April 3-4, 1974, which affected parts of

Illinois, Michigan, Indiana, Ohio, Kentucky, West Virginia, Virginia, North Carolina, Georgia, Tennessee, Alabama, and Mississippi; the central Oklahoma outbreak of May 3, 1999; and the Deep South outbreak of April 27, 2011, affecting Alabama, Arkansas, Mississippi, Georgia, Tennessee, Virginia, North Carolina, and New York. In each of these outbreaks, an unprecedented number of violent tornadoes struck multiple areas in relatively short succession. Among them, over 650 people were killed, several thousand people were injured, and more than $16 billion in property losses were attributed to tornadoes in the outbreaks.

This dissertation focuses on winter and early spring tornado outbreaks across the United States east of the Rocky Mountains. Tornado 'outbreak days' are defined as days having six (6) or more tornadoes anywhere in that region. The foundation for the effort involves the development of a climatology of tornado outbreaks from 1950-2010 for the months of January through April. This foundation then is used to investigate the relationship between winter and early spring tornado outbreaks and El Niño Southern Oscillation (ENSO; Bjerknes 1969; Wyrtki 1975; Rasmusson and Carpenter 1982; Ropelewski and Halpert 1987; Peixoto and Oort 1992, pp. 415-426; Federov and Philander 2000) to identify the larger-scale teleconnections that influence the character of tornado outbreaks. In particular, linkages are made ENSO and its influence on thermodynamic and dynamic atmospheric structures deemed important to the development of tornado outbreaks.

1.2 Tornado Outbreaks

The term ‘tornado outbreak’ has undergone a complex evolution in time as scientists have learned more about the behavior of these storms. In early American history, terms such as tornado ‘swarms’ and/or ‘families’ were commonly used to describe tornado activity over multiple areas and in relatively short time frames (a few hours to several days). Ludlum (1970, p. 12) employs this terminology to describe some of the earliest recorded tornado events affecting the northeastern U.S. in the 1600s and he also used it to describe other American tornado occurrences through the 1800s (Ludlum 1970, pp. 98). Although various objective measures for defining tornado outbreaks have been used over the past century, the aforementioned tornado outbreak definition (6 or more tornadoes in a 24 hour period) was introduced by Pautz (1969), adopted in later studies (e.g., Cook and Schaefer 2008), and will be employed here.

One continuing problem with gauging U.S. tornado incidence and outbreaks during earlier times is that larger tornadoes striking major population centers with significant impacts were reported to a much greater extent than weaker or less-impactful ones (Flora 1953, p.86; Galway 1977). With the advent of tornado and storm spotter networks in the 1950s (Galway 1977) and Doppler radar technologies to help detect thunderstorm rotation in the 1970s and 1980s (Burgess et al. 1975, Crum and Alberty 1993, Simmons and Sutter 2005), individual tornado counts have increased and reported tornado outbreaks (as defined above) are becoming more frequent.

Thus, even though U.S. tornado outbreaks appear to have occurred more frequently, this increase likely also is influenced by non-meteorological factors (Doswell and Burgess 1988, Marzban and Schaefer 2001, Brooks et al. 2003, Verbout et al. 2006). For example, Brooks et al. (2003) showed that annual reported U.S. tornado occurrence has increased at an average rate of approximately 14 tornadoes per year from the mid-1950s to 2003, which resulted in the yearly report counts nearly doubling during that time. Marzban and Schaefer (2001), however, identified a decrease trend in the annual number of strong or violent tornadoes (i.e., tornadoes rated F2-F5 on the Fujita scale; Fujita 1971), indicating further the at least partly non-meteorological nature of the recent increase of total tornado reports.

Several attempts have been made to remove the aforementioned non-meteorological biases from tornado datasets. Some studies (Bruening et al. 2002, Verbout et al. 2004, Brooks and Carbin (website: http://www.spc.noaa.gov/wcm/adj.html), have used linear regression techniques to adjust yearly tornado reports for non-meteorological inflation, while Doswell et al. (2006) adjusted his ranking system by detrending only those variables that showed the most evident secular trends (e.g., the number of tornadoes, the number of strong tornadoes, the number of violent tornadoes, and the number of tornadoes with tracks greater than 80 km). Brooks et al. (2003) and Doswell (2007) partially addressed the problem by using only the later, more reliable parts of the database (1980-1999 and 1970-2002, respectively), when more robust reporting and surveying

procedures were in place. Despite these approaches, each study indicates considerable uncertainty due to inaccuracies in the tornado dataset when attempting to detrend the data, even in the latter years of the dataset (Verbout et al. 2006).

Since the 1950s, many have attempted to define U.S. tornado outbreaks using objective criteria that can be consistently applied across all tornado outbreaks. Flora (1953, pp. 207-213) listed outbreaks during the period 1880-1952, and Wolford (1960, p. 40) detailed notable outbreaks between the years of 1916-1958. Both authors offered subjective, non-meteorological definitions for their tornado outbreaks, focusing on 1) outbreaks that resulted in extensive property damage and/or a large number of deaths and 2) tornado counts ranging from 3 to 72 for each event.

Pautz (1969) refined the concept of U.S. tornado outbreaks to include three categories: small (6-10 tornadoes), moderate (11-20 tornadoes), and large (greater than 20 tornadoes). This minimum tornado count criterion became a benchmark for the tornado outbreak definition used in the current study. Galway (1975, 1977) used similar outbreak definitions to those listed by Pautz (1969), but also mentioned that an “in-house” tornado outbreak definition of five or more tornadoes occurring during the lifecycle of a given weather system was used by the Severe Local Storms unit of the National Severe Storms Forecast Center in Kansas City, Missouri.

Galway (1977) created a climatology of U.S. outbreaks of ten or more tornadoes occurring between 1880 and 1975 (i.e., not the same as the

above ‘in-house’ definition). Included in this climatology were three types of outbreaks: 1) “local” outbreaks in which tornadoes were confined to a seven hour period and a 10,000 square mile region; 2) “progressive” outbreaks that generally move from west to east; and 3) “line” outbreaks of tornadoes that form on an axis (generally north/south) and have very little eastward progression. This work was the first in which classes of outbreaks were defined using spatial criteria rather than simple tornado counts.

More recently, Doswell et al. (2006) established a flexible ranking system for gauging tornado outbreaks. To create their ranking index, they included variables such as path length, Fujita (or F) scale rating (Fujita 1971), numbers of strong and violent tornadoes, and numbers of long-track tornadoes. As described above, this approach also included detrending of tornado data to remove the aforementioned non-meteorological biases inherent within the individual variables in the dataset.

There are several impact factors that stress the importance of the concept of tornado outbreaks, as opposed to simple counts of individual tornadoes, despite the above biases in tornado reporting. Galway (1977) found that 73% of tornado deaths between 1952 and 1973 were associated with outbreaks of 10 or more tornadoes. He also stated that 97.9% of such tornado outbreaks occurring between 1870 and 1949 were associated with tornado deaths, while 43.1% of those outbreaks resulted in fatalities between 1950 and 1975. The aforementioned Tri-State Tornado of 1925 was actually part of a larger outbreak of tornadoes that were responsible for

nearly 100 additional fatalities in Kentucky, Tennessee, and Indiana on the same day (Burgess et al. 2006). Hundreds of fatalities resulted from additional historic outbreaks, including the Deep South (Louisiana and Mississippi) outbreak of April 1908, the Tupelo, Mississippi, to Gainesville, Georgia, tornado outbreak of April 1936, and other outbreaks described by Flora (1953, pp. 208-213) and Grazulis (1993, pp. 34-38). More recently, most of the killer tornadoes of the 2011 season were associated with outbreaks (e.g., Carolinas on April 15; Tuscaloosa/Birmingham and Hackleburg, Alabama, on April 27; Joplin, Missouri, on May 22; El Reno, Oklahoma, on May 24), as were many of the most significant tornadoes during the 2000-2010 period (e.g., Veterans Day, 2002, outbreak from Mississippi to Ohio; May 2003 tornado outbreaks from the central and southern Great Plains to the eastern seaboard; Super Tuesday outbreak of 2008, including Arkansas, Kentucky, Tennessee, Mississippi, and Alabama).

Thus, the “six or more tornadoes in the continental U.S. east of the Rocky Mountains” criterion for tornado outbreaks is consistent with Pautz (1969), has been used extensively in Cook and Schaefer (2008), and will be relied on heavily for gauging tornado outbreaks in this study. The general use of ‘tornado outbreak day’ criterion for categorizing tornado events is not unique (Pautz 1969, Galway 1975, Galway 1977, Brooks et al. 2003, Schneider et al. 2004) and is more stable than simple tornado counts with regard to secular tornado reporting trends (Cook and Schaefer 2008),

especially since the 1980s (Brooks et al. 2003). In addition to its simplicity and stability, usage of this definition helps in identifying days with a synoptic-scale pattern conducive for tornado events over a relatively large area without the strict use of more detailed meteorological criteria (a key goal of this study).

1.3 Atmospheric conditions associated with tornado outbreaks

a. Historical Perspective

As soon as American society began to understand the peril associated with tornado outbreaks, many attempts were aimed at increasing understanding of the surrounding synoptic and mesoscale environments associated with these events. In documented tornado events of the 1800s, weather observers often associated tornado events with low barometric pressure and warm, generally stormy conditions (Finley 1884, 1888; Ludlum 1970, pp. 86-87 and throughout book). In the immediate vicinity of tornadoes, observers frequently recorded heavy rain and damaging hail, along with lightning, thunder, and a low roar (Ludlum 1970, pp. 86-87 and throughout book). More specific to the Natchez, Mississippi, tornado of May 7, 1840, in the hours antecedent to and concurrent with the tornado, weather observers noted low local barometric pressure, rainy and stormy conditions in Arkansas, and warm, windy conditions over southeastern Louisiana. Observers also indicated a cold frontal passage and

unseasonably cool conditions in the region the day following the tornado event (Ludlum 1970 pp. 86-89).

Attempts to identify synoptic weather patterns associated with individual tornado occurrences first began with pioneer J.P. Finley, under the auspices of the Army Signal Corps (Galway 1985, Grice et al. 1999, Corfidi 1999). Between 1883 and 1887, J.P. Finley began addressing the forecast problem by organizing a network of approximately 2000 tornado observers east of the Rocky Mountains to report tornadic activity and concurrent weather conditions. Using these data, Finley developed a set of maps and guidelines to describe tornado-producing weather patterns (Finley 1888, Galway 1985, Galway 1992) that focused on key quantities such as those now termed dry-air intrusions, cold-air intrusions, frontal boundaries, and inland surges of tropical-maritime air from the Gulf of Mexico. The fruits of Finley's work resulted in the first experimental tornado forecasts in 1884, in which meteorological conditions were determined to be 'favorable' or 'unfavorable' for tornado occurrence for 18 districts in the continental U.S. (Murphy 1996). However, the belief that a public tornado forecast would create panic and do more harm than good prompted a ban on the use of the word "tornado" in official products beginning around 1886 (Galway 1992, Corfidi 1999). This led to a "dark age" (Corfidi 1999) in tornado forecasting and research that persisted until the World War II era, when the protection of critical infrastructure from severe weather became paramount to war

activities and produced a resurgence in tornado research and forecast-related activity (Grice et al. 1999, Corfidi 1999).

During World War II, as military specialists recognized the need for forecasts of tornado outbreaks, Showalter and Fulks (1943) led the U.S. Weather Bureau in an effort to compile information on tornado formation (Schaefer 1986, Galway 1992). They identified several important surface indicators for tornado development, including pronounced horizontal wind shear, convergence or frontal activity, potentially statically unstable air, and surface cyclogenesis. Furthermore, they used upper air observations of temperature, moisture, wind direction, and wind speed near tornado occurrences to identify the following tropospheric features that contributed to tornado outbreaks (as summarized by Schaefer 1986): “1) a relatively dry layer superposing a relatively moist layer, with both being at least convectively neutral but both possibly being convectively unstable; 2) the upper layer has a lower wet bulb potential temperature and there must be vertical wind shear; 3) the two layers are separated by a temperature inversion; 4) forcing and/or lifting of the lower air mass must take place; and 5) thunderstorms must be occurring.”

In March 1948, E. J. Fawbush and R. C. Miller used the combination of the above ingredients to create the first successful tornado forecast (Grice et al. 1999, Corfidi 1999). They employed surface and tropospheric analyses to issue a “tornado alert” for Tinker Air Force Base, Oklahoma, when they recognized that the developing atmospheric conditions were

similar to the situation associated with a tornado that struck the base a few days earlier. When a tornado hit the base again on that day -- thus verifying their tornado forecast -- it had far reaching impact by garnering the attention of the meteorological and defense communities. That impact, in turn, led to the establishment in 1952 of a special severe weather unit of the Weather Bureau-Army-Navy (WBAN) Analysis group in Washington DC (Corfidi 1999). This unit, dedicated to the forecasting of severe storms and tornadoes, subsequently was renamed the Severe Local Storm Warning Center (SELS) in 1953 and moved to Kansas City, Missouri, in 1954. Later, it was renamed named the National Severe Storms Forecast Center in 1966, and was given it's current name, the Storm Prediction Center (SPC), 14 months before moving to its present location in Norman, Oklahoma, in 1997 (Galway 1992, Grice et al. 1999, Corfidi 1999).

b. Modern Era

Efforts to further understand atmospheric conditions favorable for tornado outbreaks have continued from that March day in 1948 through today. The continuing work of Fawbush and Miller through the early 1970s, along with growing operational experience of forecasters at the newly formed SELS, led to the 1953 development of a 'checklist' of conditions on which to base severe thunderstorm and tornado forecasts (Figure 1.1). This checklist included several parameters considered important for organized severe thunderstorm activity -- the Showalter Stability Index (Showalter 1953)

measuring static stability from thermodynamic profiles; the presence of a moist boundary layer beneath a dry, elevated mixed layer above ~8000 feet AGL; convective instability above the moisture inversion; low-level (~5000 feet AGL) warm advection; upper-level (~16,000 feet) cold advection; steep moisture gradient on the west side of a low-level moist axis; strong surface wind convergence and cyclonic shear; and a lifting mechanism, such as a front or 'pressure-jump' line. The use of this 'ingredients-based' approach (a term coined by Doswell et al. 1996) for tornado forecasting -- some elements of which are still in use today -- enabled forecasters to achieve some early success in their tornado predictions in a time where other scientists considered their efforts primitive and even futile (Galway 1985, 1992; Schaefer 1986). One example of an early success was the issuance of the first public tornado watch by WBAN on March 21, 1952, in anticipation of a tornado outbreak that occurred across Arkansas, Tennessee, Kentucky, and Mississippi.

The identification of these basic atmospheric ingredients for individual tornadogenesis provided a launching point for further efforts by scientists to understand environments associated with the larger-scale tornado outbreaks defined above. Researchers identified features such as the 'loaded-gun'

Check List of Criteria
for Severe Local Storm and Tornado Forecasting
WBAS Kansas City - 1953

		YES	NO
	Vertical Structure		
1.	"Typical" airmass structure - moisy surface layer at least 3000 but less than 8000 feet thick with mean mixing ratio 8g/kg or more and R.H. 65% or more, overrun by deep dry layer with R.H. dropping off abrubtly to 50% or less above moisture inversion.	___	___
2.	Conditional and convective instability above moisture inversion.	___	___
3.	Showalter Stability Index -5°C or lower.	___	___
4.	Level of Free Convection (LFC) 650 mb or greater.	___	___
5.	Strong positive area on sounding.	___	___
	Upper Air Conditions		
6.	Low level (5,000') southerly axis of maximum winds 35 knots or over, with 850 mb moist tongue.	___	___
7.	700 mb dry tongue (R.H. less than 50%).	___	___
8.	Upper level (16,000') westerly axis of maximum winds 35 knots or over.	___	___
9.	Warm air advection below the LFC.	___	___
10.	Cold air advection above above LFC.	___	___
	Surface Conditions		
11.	Dew point ridge from the south, 55°F or greater, with steep gradient on the western side.	___	___
12.	Strong convergence - cyclonic wind shear.	___	___
13.	Lifting mechanism - front, instability line, semi-micro High or Pressure Jump line.	___	___

REMARKS:

FORECASTER_____TIME_____DATE_____195__

Figure 1.1: Checklist of criteria for severe local storm and tornado forecasting (Galway 1992)

soundings (Carr 1952, Danielson 1975) in which the superposition of a divergent jet stream aloft and low-level convergence induced by a low-level jet stream (Beebe and Bates 1955, McNulty 1978) provided an environment that facilitated the ascent of a convectively unstable air mass to the level of free convection. Researchers also found that tornado formation was aided by surface drylines (Rhea 1966, Schaefer 1974), topographical features (e.g., coastline, mountains; Hales 1985), backing surface winds (Sasaki and Tegtmeier 1974, Maddox et al. 1980), and outflow boundaries/warm fronts (Maddox et al. 1980).

With continued advances in data measurement and assimilation capabilities, real-time communication and display of weather observations, and improved computing resources, researchers and forecasters have made advances in identifying environments and atmospheric variables associated with tornado outbreaks. Schaefer and Doswell (1984) used empirical orthogonal function analysis to create composites of atmospheric conditions associated with 'progressive' tornado outbreaks, events Galway (1977) defined to involve "an outbreak that progresses (advances) generally from west to east with time". Using conditions associated with two winter and twelve spring tornado outbreaks that struck the central and southern Great Plains (Kansas, Oklahoma, and Texas) from 1950 to 1968, they found three characteristic types of 500 hPa flow patterns responsible for progressive tornado outbreaks: 1) southwest flow aloft events; 2) northwest

flow aloft events, and 3) a less often observed ‘cut-off’ low event in the southwestern U.S.

In an updated version of the approach in Schaefer and Doswell (1984), Mercer et al. (2011) analyzed synoptic-scale patterns using principal components analysis of reanalysis data to develop composite patterns for the top 50 tornado outbreaks from 1970 to 2003 in the continental U.S. Comparison was made with composites from the top 50 nontornadic severe weather outbreaks (i.e., < 6 tornadoes), as ranked by Doswell et al. (2006). Those composites reveal that atmospheric environments in the vicinity of U.S. tornado outbreaks have a strong low- and mid-tropospheric trough, a surface low pressure area, and high vertical shear, static instability, and storm relative environmental helicity. Also, there is stronger mid-level vorticity and vertical shear present in tornado outbreaks compared to nontornadic outbreaks.

Both of the above studies examined large-scale synoptic patterns and identified and/or reestablished traits common to tornado outbreaks, despite the use of different outbreak subsets. Their findings, along with those from other key research (McNulty 1978, Weisman and Klemp 1984, Johns and Doswell 1992), have identified four main categories of synoptic-scale ingredients that are conducive to tornado outbreaks (and even severe thunderstorm outbreaks): 1) moisture availability, usually from low-level warm advection of maritime tropical air masses originating from the Gulf of Mexico; 2) a lifting mechanism, in the form of a surface front and/or upper

tropospheric quasi-geostrophic forcing and related geopotential height perturbations; 3) static instability, resulting from cold-air advection aloft, warm-air advection near the surface, and/or surface solar insolation; and 4) vertical shear, involving changing of direction and/or speed of wind with height. While each of the above ingredients alone is unlikely to result in a tornado outbreak, elements from many of them are present in most tornado outbreaks.

1.4 Tornado climatologies and other methods of tornado analysis

Tornado climatologies that document long-term behavior of tornado activity have played an integral role in understanding tornado environments and providing background information to support forecasters, since the earliest days of tornado forecasting in the late 1800s. Initially during the 1880s, J.P. Finley progressively developed a climatology of U.S. tornadoes through annual updating and used it concurrently as a baseline for his experimental tornado predictions (Corfidi 1999). Thom (1963) calculated tornado probabilities based on frequency distributions of tornado path width and length in Iowa, Kansas, and surrounding areas using data that spanned 1916-1962. Pautz (1969) developed a tornado climatology for the continental U.S. based on documented tornado occurrence per square mile from 1955-1967, while Galway (1977) divided the continental U.S. into five geographical regions and calculated monthly tornado frequencies for those regions using two separate time periods (1870-1949 and 1950-1975). Kelly

et al. (1978) developed a tornado climatology for the continental U.S. using a database that contained cross-referenced tornado reports between 1950-1976 while eliminating doubtful reports. This same Kelly et al. (1978) database was used by Schaefer et al. (1986) to generate a statistical tornado hazard probability model to examine hazard-potential in local areas by using totals for 1° and 2° latitude/longitude grid boxes.

Further refinement and improvement of tornado climatologies continued with Doswell and Burgess (1988), who investigated the inhomogeneities and other inconsistencies in various tornado datasets based on tornado ratings and path length. More updated tornado climatologies and risk assessments subsequently have been developed by Brooks et al. (2003), Ramsdell and Rishel (2007), Brooks (2011, http://www.nssl.noaa.gov/users/brooks/public_html/tornado), and others. These most recent climatologies have been based on the NOAA/NWS/NCEP SPC Severe Weather database (Schaefer and Edwards 1999), although the NCDC tornado database (http://www.ncdc.noaa.gov/) also is available for use. These datasets are mostly similar and described in detail in Chapter 2. Both were compiled using tornado track data (start point, end point, maximum path width, F-scale/EF-scale rating, and time of occurrence) gathered from local Weather Service Forecast Office (WSFO) use of public reports and damage surveys.

The approaches used to analyze tornado databases to produce the above climatologies have had varied time and space dimensions, including:

1) national counts for each year during 1955-1969 (Pautz 1969) and 1980-1999 (Brooks et al. 2003); 2) regional totals for individual years between 1883-1887 (Finley 1888), 1955-1969 (Pautz 1969), 1950-1975 (Galway 1977), 1950-1988 (Marzban and Schaefer 2001), and 1951-2006 (Muñoz and Enfield 2011); 3) individual monthly counts for the years 1955-1969 (Pautz 1969); 4) state-by-state annual totals for the years 1955-1969 (Pautz 1969), 1953-1974 (Kessler and Lee 1976), 1916-1996 (Agee and Zurn-Birkhimer 1998), and 1950-2003 (Cook and Schaefer 2008); 5) annual totals of tornado days in the continental U.S. for each year during 1955-1969 (Pautz 1969), 1950-1975 (Galway 1977), and 1875-2003 (Schneider et al. 2004); 6) yearly counts for 1°, 2°, and 4° latitude/longitude grids for 1950-1976 (Kelly et al. 1978) and for a 1.25° grid for 1950-1992 (Bove 1998); and 7) average tornado spatial density per square mile/kilometer from 1950-1976 (Kelly et al. 1978) from 1950-1996 (Bove 1998), from 1980-1999 (Brooks et al. 2003), from the years of 1880-2005 (Ashley 2007).

1.5 El Niño-Southern Oscillation influences on U.S. tornadoes

Although much effort has been invested in understanding the regional atmospheric environment associated with U.S. tornado outbreaks for the area east of the Rocky Mountains, and developing climatologies of tornado occurrences and characteristics, there has been relatively little investigation of the relation of U.S. tornado outbreaks to the El Niño-Southern Oscillation (ENSO) phenomenon (Bjerknes 1969; Wyrtki 1975; Rasmusson and Carpenter 1982; Ropelewski and Halpert 1987; Peixoto

and Oort 1992, pp. 415-426; Federov and Philander 2000). ENSO is generally defined as a coupled atmospheric-oceanic phenomenon involving variability of the tropical Pacific low-level winds and resulting anomalous warming (or cooling) of tropical Pacific sea surface temperatures (SSTs) in a broad region that extends from the western coast of South America westward across the Pacific Ocean (to about 160°E), spanning the 10°N-10°S latitude belt.

The relationships between small-scale phenomena like tornadoes and much larger-scale phenomena (such as ENSO) centered thousands of kilometers away presently are unclear and apparently complex. However, the very large scientific and societal benefits that would result from a better understanding of these relationships suggest this is an area of worthwhile and meaningful research. There is scientific encouragement for pursuing this line of research, particularly due to the meaningful results identified in previous analyses of relationships between ENSO and U.S. tornado occurrence (e.g., Marzban and Schaefer 2001, Knowles and Pielke 2005, Cook and Schaefer 2008). While ENSO does not directly impact individual thunderstorms responsible for tornadogenesis (Cook and Schaefer 2008), it does modulate influences on the mean latitudinal position of the subtropical jet stream across North America (Lee and Galway 1956; Miller 1972; Rasmussen and Mo 1993; Cook and Schaefer 2008; Climate Prediction Center 2012, website: http://www.cpc.ncep.noaa.gov/products/analysis_monitoring/ensocycle/nawinter.shtml), which is

a key factor for development of tornado outbreaks (Schaefer 1986, Johns and Doswell 1992).

Although a number of studies have investigated the relationships between ENSO and U.S. tornadoes, they have yielded conflicting results to date. Some suggest that stronger tornadoes occur in the central and eastern parts of the United States during La Niña conditions (Bove 1998, Knowles and Pielke 2005), while others found that La Niña conditions simply do not have such an effect (Agee and Zurn-Birkhimer 1998, Schaefer and Tatom 1998). Hagemeyer (1998) concluded that more frequent and stronger tornadoes occur in Florida during El Niño, while Bove (1998) suggests that Florida experiences fewer tornadoes in both El Niño and La Niña phases. Meanwhile, some researchers claim that increases in tornado frequency occur in the mideastern and northeastern United States (Schaefer and Tatom 1998, Marzban and Schaefer 2001) and in northwestern Missouri (Browning 1998) during La Niña conditions, while Agee and Zurn-Birkimer (1998) noted increases in frequency of tornado activity throughout the eastern United States during La Niña. Some of these contradictory results undoubtedly arise from differences in analysis methods and study periods, with Agee and Zurn-Birkhimer (1998) examining tornado outbreaks back to 1884 and the Bove (1998) study beginning only in 1950.

1.6 Seasonal Tornado Forecasting

"Where's my seasonal tornado forecast?"
- President Barack Obama during the devastating tornado outbreaks of 2011

Interest in seasonal prediction of tornadoes has grown tremendously in recent years, particularly in response to the historic tornado outbreaks of 2011. In that year, numerous significant tornado outbreaks occurred across a rather large area of the U.S. east of the Rocky Mountains and were responsible for over 500 deaths, many thousands of injuries, and over $10 billion in damages (National Climatic Data Center 2011, National Oceanic and Atmospheric Administration 2014). These tornadoes had such a societal impact that even President Obama took note of the damage, mentioning the need for a seasonal tornado forecast. These tornadoes were record breaking in several aspects:

1) An EF5 tornado struck Joplin, Missouri on May 22, 2011, killing 158, injuring 1150+, demolishing structures in a large part of the center of the town, and accounting for $2.8 billion dollars in damage. Although this tornado was part of a regional outbreak of tornadoes that struck southwest Missouri, northeast Oklahoma, southeast Kansas, and northwest Arkansas, this single tornado broke a record as the deadliest tornado to strike anywhere in the U.S. since 1950.
2) Fifteen long-tracked EF4/5 tornadoes struck portions of the Deep South during the "Super Outbreak" of April 27, 2011. The

outbreak was responsible for tremendous loss of life (316 deaths, 238 of those in Alabama) and rivaled the most intense outbreaks ever recorded, including the Super Outbreak of April 3, 1974 (30 EF4/5 tornadoes) and the Palm Sunday Outbreak of April 11, 1965 (17 EF4 tornadoes).

3) Numerous high-impact tornadoes occurred in 2011 tornado outbreaks outside of the aforementioned episodes, including the EF2 that struck Jackson, Mississippi on April 15, 2011; EF3 that struck Raleigh, North Carolina and surrounding areas on April 16, 2011; EF4 that struck Saint Louis, Missouri on April 22, 2011; and the EF5 that struck areas near El Reno, Oklahoma on May 24, 2011.

The notion of a seasonal tornado forecast wasn't new then; in fact, a seasonal tornado forecast was attempted on an experimental basis by the NOAA NWS Storm Prediction Center (SPC) in October 2009. The forecast was valid for the upcoming winter season of 2010 and was circulated internally within the NOAA National Weather Service. The outlook was heavily based on the results of Cook and Schaefer (2008) and an excerpt from this outlook follows:

> "Even though tornadoes can occur anywhere and at any time during the year, <u>El Niño events have historically been associated with the development of cold season tornado activity along the southern U.S. near the Gulf Coast from</u>

Texas eastward to Florida. Central Florida has experienced the brunt of this activity over the years, with particularly deadly night time tornado activity occurring in February 1998 and February 2007. Other recent deadly cold season tornado outbreaks have affected parts of Georgia, Texas, and Mississippi during El Niño conditions." [emphasis added]

The outlook was actually quite a success despite the fact that it was the first of its kind. Two tornado outbreaks were observed in the winter of 2010 (Figures 1.2 and 1.3); the first across northeast Texas, Louisiana, and Mississippi on January 20, 2010 and the second in North Carolina, South Carolina, and Florida on March 28, 2010. Despite this early success, more refining and testing was needed to determine whether a reliable experimental tornado outlook could become an official National Weather Service product.

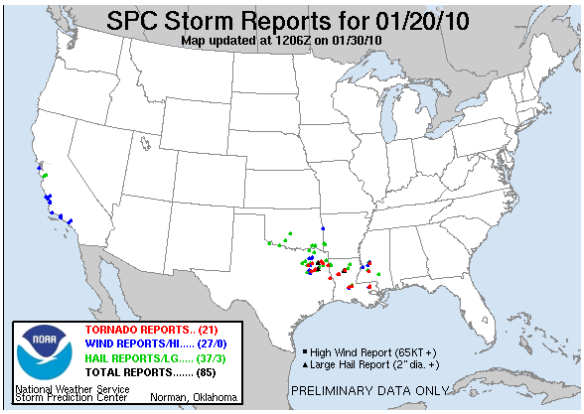

Figure 1.2: Storm reports from the January 20, 2010 tornado outbreak. Source: http://www.spc.noaa.gov/climo/reports/100120_rpts.html

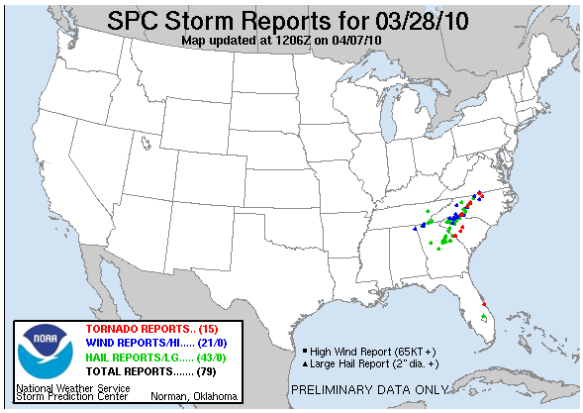

Figure 1.3: Storm reports from the March 28, 2010 tornado outbreak. Source: http://www.spc.noaa.gov/climo/reports/100328_rpts.html

Several studies addressing the seasonal tornado forecast problem have been published since 2011, focusing mainly on the impact of larger-scale climate drivers on spring (April and May) tornado outbreaks in the U.S. Muñoz and Enfield (2011) found an enhanced Intra-Americas Low-Level Jet stream during the cool phase of ENSO (La Niña), which resulted in an increased influx of moisture from warm water sources (i.e. Gulf of Mexico) and an increased occurrence of tornadoes in areas east of the Mississippi River. Lee et al. (2013) identified a preferred ENSO pattern that altered the mean configuration of the atmosphere in April and May to become more conducive for the development of tornado outbreaks east of the Rocky Mountains. Thompson and Roundy (2013) discussed potential for seasonal prediction of tornado outbreaks based on the Madden Julian Oscillation (MJO; Madden and Julian 1971) and argued that the MJO alters mass fields in a manner conducive for increased tornado activity in its second phase. Barrett and Gensini (2013) also found a different result than

Thompson and Roundy in their research of the MJO-tornado outbreak relationship; they identified an increased likelihood of those outbreaks in phases 6 and 8 in April and in phases 5 and 8 in May.

Although the aforementioned research gives credence to the potential of a seasonal prediction tool, there are weaknesses in each of the studies that need to be addressed before a reliable longer-term goal of a seasonal prediction scheme can be achieved:

1) None of the aforementioned research systematically identified each tornado outbreak for inclusion in a climatology. Lee et al. (2013) separated their data according to the ten positive Trans-Niño years, ten negative Trans-Niño years, and ten neutral Trans-Niño years for some of their analyses, effectively excluding about half of their available data for analysis. Barrett and Gensini (2013) only considered violent tornado outbreaks from 1990-2011 in a similar manner to that used in Cook and Schaefer (2008), although Cook and Schaefer focused the majority of their results on a much broader tornado outbreak day definition due to issues with maintaining appropriate sample sizes for analysis.
2) Each of the studies base their findings on monthly or seasonally averaged atmospheric conditions that shift as a function of ENSO/MJO, but do not go into depth regarding synoptic-scale atmospheric features associated with individual outbreaks (i.e., ., low-level jet streams, upper-level jet streams, surface cyclones,

geopotential height troughs, etc.). Some of these atmospheric features in individual outbreaks aren't represented in a monthly or seasonal atmospheric climatology.

3) Two of the studies (Muñoz and Enfield 2011, Lee et al. 2013) only used coarse indices for gauging tornado activity over broad regions, which prevented them from assessing distinct geographic shifts in tornado activity. In fact, the index Muñoz and Enfield 2011 did not assess tornadoes that occurred in the Great Plains region and only focused on tornadoes that occurred in the Southern and Midwestern U.S.

1.7 Goals and Objectives

The primary motivation for this study is to set the foundation for further development of a seasonal tornado prediction tool by: 1) gaining a better understanding of winter and early spring (January through April) tornado outbreaks in the U.S. east of the Rocky Mountains and 2) diagnosing the influence of El Niño/La Niña on synoptic-scale atmospheric features commonly associated with tornado outbreaks.

Cook and Schaefer (2008; hereafter referred to as CS08) began addressing this problem by identifying organized winter tornado activity and shifts in that activity based on ENSO phase. That study focused on January-March when ENSO-related teleconnections are strongest in the Northern Hemisphere (Rasmusson and Carpenter 1982, Ropelewski and

Halpert 1986). Using state-by-state analyses of tornadoes occurring on tornado days to help gauge ENSO-related shifts in tornado activity, CS08 found that stronger, longer-lived tornadoes occurred in tornado outbreaks during the cold and neutral phases of ENSO when compared to the warm ENSO phase.

Although CS08 provides a significant foundation, the current study will build on CS08 in several key respects. First, it will analyze newly derived gridded (1° latitude/longitude) tornado data instead of the state-by-state tornado counts used in CS08 and several other previous tornado-related studies (Pautz 1969, Agee and Zurn-Birkhimer 1998). The latter data do not facilitate uniform and objective analyses due to the varied and irregular shapes and sizes of U.S. states. Second, reanalysis data will be employed to examine the regional-to-synoptic-scale atmospheric characteristics and processes that produce tornado outbreaks, in contrast to the CS08 reliance on anecdotal evidence and speculation regarding the physical mechanisms at work. Third, intraseasonal variations in tornado activity will be investigated as a function of ENSO, whereas CS08 only identified seasonal ENSO relationships.

In addition to building upon CS08 in the above manner, the current study also will delve deeper into the temporal, spatial, and physical relationships between tornado outbreaks and ENSO. Specifically:

1) The study period will be extended from the traditional January-March winter period to include April. This extension will incorporate several additional historic tornado outbreaks (e.g., Palm Sunday Outbreak, April 11, 1965; Super Outbreak, April 3-4, 1974; Andover, Kansas, Outbreak, April 26, 1991)

2) A new tornado climatology will be created that investigates tornado outbreaks on a seasonal and intraseasonal basis. This climatology will be based on the above 1° gridded analyses of tornado occurrence, will treat individual tornado 'tracks' in addition to tornado start points, and will feature analyses of tornado 'destruction potential' (Thompson and Vescio 1998). In addition, reanalysis data will be used to generate a climatology of the atmospheric conditions that produce tornado outbreaks.

3) An 'atmospheric' climatology of synoptic-scale features associated with tornado outbreaks will be developed. This new climatology will provide deeper insights into the changes associated with individual sets of tornado outbreaks than monthly averages of atmospheric fields as provided in previous analyses (Muñoz and Enfield 2011; Lee et al. 2013).

2. DATA AND METHODOLOGY

As mentioned in Chapter 1, a primary goal of this work is to identify the influence of ENSO on U.S. tornado outbreaks east of the Rocky Mountains. Fundamental to this task is the development and understanding of basic climatologies of tornado outbreaks and the larger-scale atmospheric conditions that contribute to those outbreaks. These climatologies will help identify shifts in tornado outbreaks that may be influenced ENSO. The tornado climatologies must be based on appropriate datasets, such as the aforementioned NOAA/NWS/NCEP SPC Tornado/Severe Thunderstorm database (Schaefer et al. 1980, Schaefer and Edwards 1999). This chapter focuses on development of the required research-quality, gridded dataset of tornadoes derived from the SPC Tornado database. It also provides information on the use of the NCEP/NCAR Reanalysis Dataset (Kalnay et al. 1996) for analyzing tornado outbreaks and their concurrent larger-scale atmospheric conditions, respectively.

2.1 Physical Attributes of Tornado Outbreaks

a. Data Requirements, Uses, and Limitations

As noted in Chapter 1, two severe weather databases exist for U.S. tornado analysis: 1) the NCDC tornado database (http://www.ncdc.noaa.gov/) and 2) the NOAA/NWS/NCEP SPC Tornado/Severe Thunderstorm database (Schaefer et al. 1980, Schaefer and Edwards 1999). Both

datasets contain the following information from January 1950 through the present -- start and end points (latitude and longitude) of tornado tracks, Fujita scale (F-scale, Fujita 1971) and Enhanced Fujita scale (EF-scale, McDonald and Mehta 2006) ratings, start times (CST), path width, path length, number of fatalities, number of injuries, and state(s) in which each track occurred. These characteristics are established by local WSFOs and certified by NCDC before becoming an official part of each dataset.

Both datasets contain F-scale ratings of tornado damage from 1950 through January 31, 2007 and EF-scale ratings from February 1, 2007, to the present. The transition between F-scale and EF-scale occurred after a group led by the SPC and Texas Tech University submitted recommendations to the National Weather Service to change their tornado rating system (McDonald and Mehta 2006). While this transition involved wind speeds being revised downward from the F- to the EF-scale, the damage ratings were designed to maintain consistency before and after the transition. Thus, the same types of tornado damage that occurred after January 2007 receive the same F/EF-scale rating as if that damage had occurred previously. Because of this consistency, the term “F/EF-scale” is used in this study to cover the damage scale rating of all tornadoes in outbreak days regardless of when they occurred.

Despite similarities between the NCDC and NCEP/SPC tornado datasets, several key differences exist. Collectively, those differences suggest that the SPC database is the more consistent of the two and

therefore the most appropriate for this study. One problem with the NCDC database is that two months of relatively recent tornado data are missing (June and July 1993). Additionally, while NCDC's tornado database records various characteristics of tornadoes on a more detailed, county-by-county basis, temporal inconsistencies exist in that database because tornadoes that have occurred since the mid-1970s have been surveyed in much greater detail than for earlier periods. The result is a NCDC database in which some tornadoes contain greater spatial detail than others (G. Carbin 2012, personal communication). In contrast, the NCEP SPC database assigns only a maximum F/EF-scale rating and path width for each tornado track in its dataset, which eliminates the potential for the inconsistency found in the NCEP database. Given the above factors and the fact that recent U.S. tornado climatologies have exclusively used the SPC tornado database (Marzban and Schaefer 2001, Brooks et al. 2003, Verbout et al. 2006, Doswell et al. 2007, and others), exclusive use of the NCEP/SPC tornado database was deemed appropriate here.

Many limitations are present in any set of tornado records and must be addressed before the development of tornado climatologies and larger-scale analyses. Several authors (Doswell and Burgess 1988, Grazulis 1993, Brooks et al. 2003, Verbout et al. 2006, and others) have identified factors that contribute to inaccuracies in tornado reporting, including: 1) errors in reporting of time and location information, 2) changes in population and related population biases in tornado reporting, 3) evolution of the nature

of detailed storm surveys through time, 4) improved efforts toward collecting tornado damage information for warning verification, and 5) the subjective nature of damage scale (F/EF) ratings for tornadoes. Brooks et al. (2003) also state that tornadoes are a rare occurrence at any particular location. CS08 dealt with these limitations by qualitatively linking observed shifts in tornado activity to atmospheric teleconnections between ENSO and synoptic-scale features that are known contributors to tornado outbreaks (i.e., surface cyclone tracks, lower-tropospheric convergence anomalies, and shifts in the position of the jet stream). A similar, yet even more detailed approach compared to CS08 is employed here and discussed in greater detail in Section 2.2 and Chapter 4.

As mentioned in Chapter 1, the present study builds on the foundation of CS08. That study used a subset of the SPC tornado dataset that only included January through March 1950-2003 tornadoes that occurred on 'tornado outbreak days' that were defined (like here) as days in which six or more tornadoes occurred in a 24 hour period (0600 UTC – 0600 UTC), but for anywhere in the continental U.S. This tornado outbreak day criterion was used and alluded to in previous studies of tornado outbreaks (Pautz 1969; Galway 1975, 1977; Brooks et al. 2003; Schneider et al. 2004; Doswell et al. 2006). As indicated in Chapter 1, it was employed here because tornado outbreak days imply organization and influence by synoptic-scale atmospheric conditions (which here are assumed to be influenced by larger-scale climate system modes such as ENSO) and

because they exhibit less pronounced secular trends than total tornado counts as will be shown in Section 3.1.

CS08 limited its investigation to January-March tornado outbreak days because that part of winter accounted for the strongest teleconnections between El Niño/La Niña and Northern Hemispheric weather patterns (Horel and Wallace 1981, Ropelewski and Halpert 1987). April has been included in the present study to account for influences on tornado activity that persist beyond that period and also to incorporate several historic tornado outbreaks that resulted in extensive societal impacts (e.g., April 11, 1965 Palm Sunday outbreak; April 3, 1974 Super Outbreak).

b. Methods of Spatial Tornado Analyses

CS08 used national and state-by-state counts of tornadoes and computations of their destruction potential for outbreaks between 1950-2003, to gauge shifts in tornado frequency, strength, and location as a function of ENSO phase. This analysis will pursue wider synoptic and climate system associations and employ more objective methods of tornado analysis (i.e., gridded tornado counts, gridded tornado day counts, and gridded destruction potential computations) instead of depending on state-by-state analyses that are affected by varying and irregular state shapes and sizes. The graphical and statistical analyses of tornado data involved use of the Enthought Python Distribution v. 7.2 software (website:

http://enthought.com/products/epd.php). In cases where isoplething of gridded variables was employed, a Gaussian filter was applied spatially (in both latitude/longitude dimensions) to the data in the entire domain before isopleths were created. The bandwidth of the Gaussian filter was set to 1° which is consistent with Shafer and Doswell (2010) who subjectively identified this bandwidth to be helpful in discriminating between clusters of severe weather events across the continental U.S. Table 2.1 summarizes the tornado documentation developed from the above data, which is explained further and illustrated in subsequent sections.

Types of plots	**Variables measured**
Plots of tornado tracks	Location
Gridded tornado counts	Frequency, Location
Gridded 'tornado day' counts	Frequency, Location
Gridded destruction potential	Strength, Location

Table 2.1: Types of gridded analyses performed.

i. Plots of tornado tracks

Plots of tornado tracks were generated by tracing a straight line between the starting and ending points (latitude/longitude) for each tornado. In most instances, the lines were color coded to indicate F/EF-scale rating. For brief touchdowns that did not have a change in latitude and longitude, end points were extended by 0.01° (approximately 1 kilometer both southward in latitude and eastward in longitude) only to ensure that they could be seen visibly on plots. The maximum F/EF-scale rating along the

tornado track was assigned to the entire track, which is standard practice for all tornado ratings in the SPC Severe Weather Reports database (Schaefer and Edwards 1999). Figure 2.1 provides an example of tornado tracks that occurred on February 5, 2008. Locations of tornadoes that occurred on that day (including areas from Illinois and Indiana southward to Mississippi, Arkansas, and Texas) can be readily seen, including the large number in western Kentucky-Tennessee. In addition, the color-coding on this map helps quickly identify locations of stronger tornado occurrence.

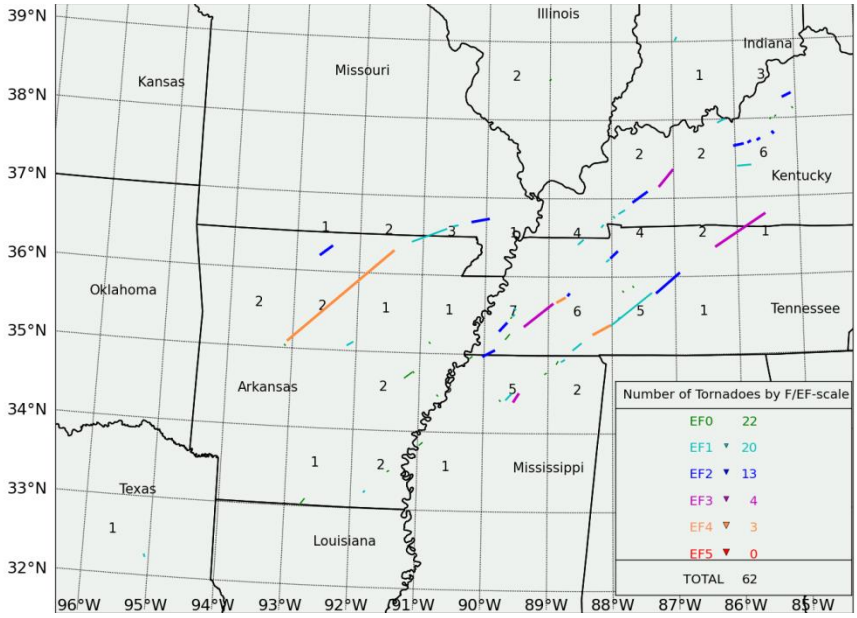

Figure 2.1: Example plot of tornado tracks (color coded by EF-scale rating) and resulting gridded tornado counts (discussed in Section 2.1.ii) for tornadoes occurring on February 5, 2008. The grid outlined is 1° latitude by 1° longitude and numbers represent the number of times a tornado impacted a grid cell.

ii. Gridded tornado counts

A simple process was used for generating gridded tornado counts (Figure 2.1). First, a basic 1° latitude by 1° longitude grid was set up across the entire continental U.S. east of the Rocky Mountains, with each cell bounded by parallels and meridians at each full degree of latitude and longitude. For all tornadoes with a path length of greater than one mile, a set of latitude/longitude points was calculated for each full mile of tornado track. A count was then kept for each time a tornado track initially touched down on the grid and then subsequently crossed a parallel or meridian. For tornadoes with path lengths of less than 1 mile (not to be confused with aforementioned tornado tracks whose beginning and end points did not exhibit a change in latitude/longitude), only the initial touchdown point was considered in the total because these tornadoes were assumed to not have crossed a grid cell. This 'one-mile' threshold for tornado path length was used because the path lengths in the SPC severe weather database are given in miles. (Note: tornadoes that contain path lengths of less than one mile do not necessarily imply that their starting and ending latitude/longitude points are the same.)

The database development process described above was repeated for all tornado tracks considered in the study. This process is an enhancement over other spatial analyses of tornadoes in that gridded counts incorporate entire tracks, not just initial touchdown points (e.g., Kelly et al. 1978, Bove et al. 1998, Brooks et al. 2003). This enhancement 1)

enables a more comprehensive spatial assessment of tornado locations across entire tracks, which is particularly helpful for longer-tracked tornadoes, and 2) also enables a more accurate assessment of potential impact in localized areas along the entire tornado track (see Destruction Potential Index, Section 2.1.b.iv). The totality of the data set created is documented in Figures 2.2-2.3 and climatological patterns in this data are identified and discussed in Section 3.1.

iii. Gridded tornado day counts

Gridded 'tornado day' counts were calculated in the same manner as the aforementioned gridded tornado counts, except that the tornado day counts represent the number of days at least one tornado occurred in a particular grid cell on a tornado outbreak day. This type of analysis is helpful for assessing the frequency of tornado outbreak occurrence in any location. The totality of this new dataset is documented in Figures 2.4 and 2.5, while associated climatological patterns will be identified and discussed in Section 3.1.

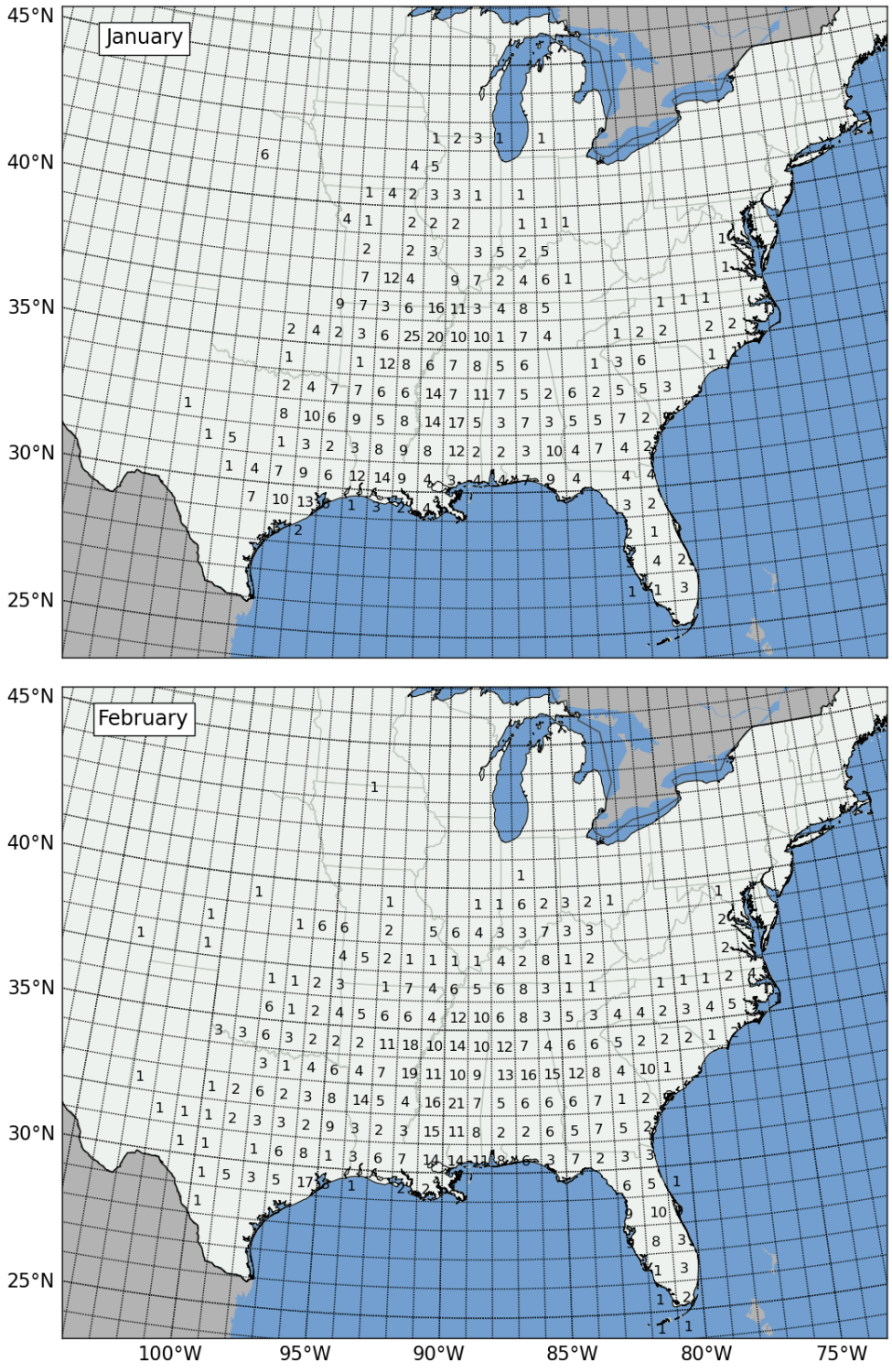

Figure 2.2: Gridded tornado counts for all January (top) and February (bottom) 1950-2010 tornado outbreaks in the study.

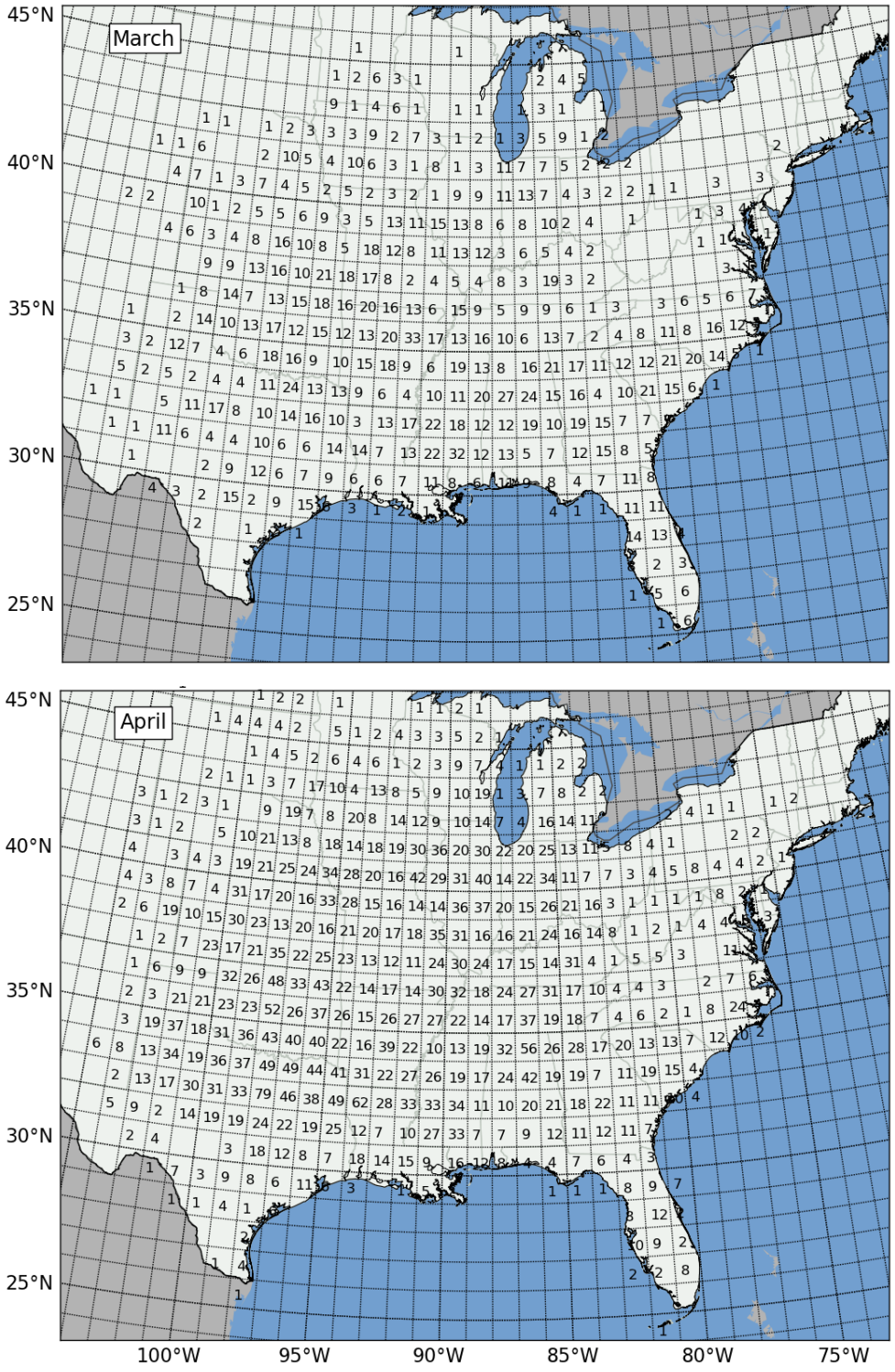

Figure 2.3: Gridded tornado counts for all March (top) and April (bottom) 1950-2010 tornado outbreaks in the study.

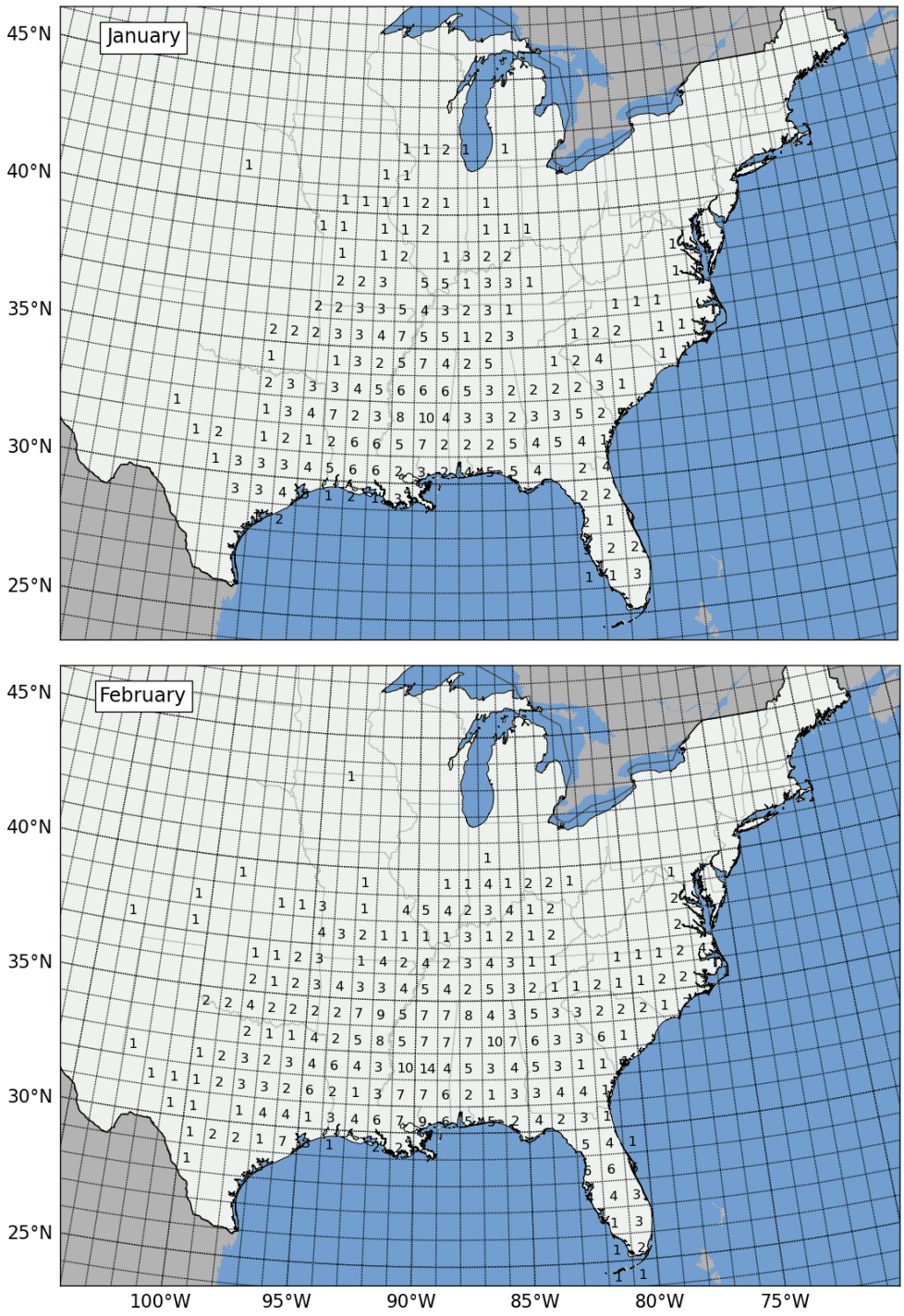

Figure 2.4: Gridded tornado day counts for all January (top) and February (bottom) 1950-2010 tornado outbreaks in the study.

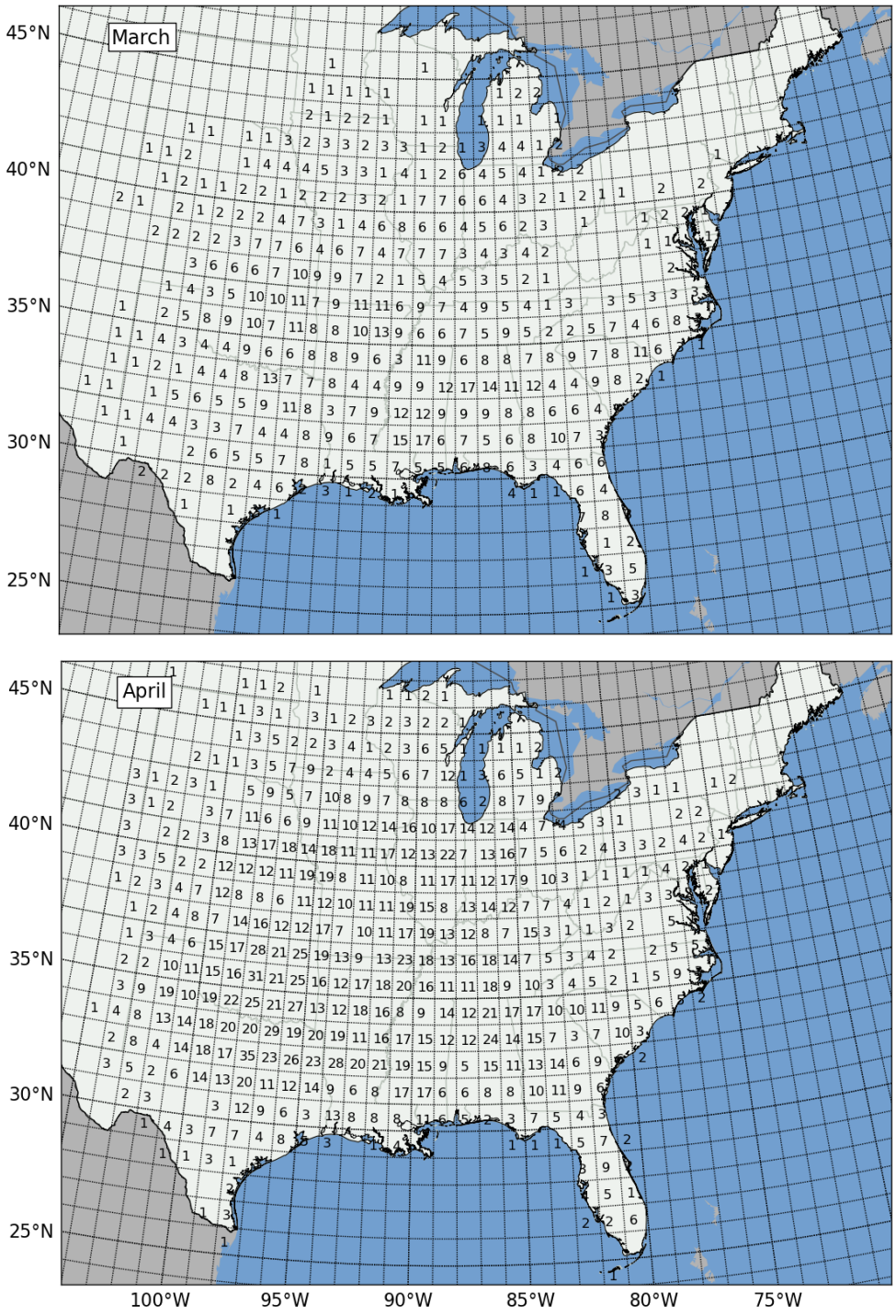

Figure 2.5: Gridded tornado day counts for all March (top) and April (bottom) 1950-2010 tornado outbreaks in the study.

iv. Gridded Destruction Potential Index

The destruction potential index (DPI; Thompson and Vescio 1998, Doswell et al. 2006) was used to combine the size, intensity, and longevity of tornado occurrence. The concept behind the DPI is that tornadoes having wider path widths, longer path lengths, and higher F/EF-scale rating possess a greater damage potential than weaker, narrower, and shorter-track tornadoes. The DPI attempts to quantify these differences in destruction potential, and is calculated using the following equation:

$$\mathrm{DPI} = \sum_{i=1}^{n} a_i \left(F_i + 1 \right) \qquad (2.1)$$

where a is the area (square miles) affected by the tornado track (path length multiplied by path width) and F is the F/EF-scale rating assigned to the entire track. This index is summed (Σ) across an entire subset of n tornadoes in a designated region, for which i represents each specific tornado. Because F/EF-scale ratings are unitless, the DPI is treated as a unitless index.

The application of DPI in this study has a similar purpose to that in CS08. In that study, the authors were able to use DPI to quantitatively determine whether stronger, longer-lived tornadoes occurred in various phases of ENSO. Additionally, state-by-state analyses in that study helped identify statistically significant regional shifts in DPI that could be tied to ENSO. In that study and the current one, the DPI was estimated in a coarse rather than more exact manner because of its sensitivity to small changes in

tornado track characteristics (e.g., intensity or path width) and also because of the pre-existing errors within the database discussed in Section 2.1.a.

For this study, gridded DPI values were calculated in essentially the same manner as the gridded tornado counts. The DPI was calculated for each full mile of each tornado track and then totaled for each 1° by 1° grid cell. For tracks of less than one mile in length, the DPI for the entire track was assigned to the cell of the initial touchdown point of the tornado. Although this gridded calculation method contains the potential for small DPI errors -- e.g., from treating tornado path lengths as multiples of one mile and tracks crossing into new grid cells between full-mile segments rather than at the beginning or end of a mile segment -- errors relative to DPI calculated here for individual, ungridded tracks were generally less than 2%. These errors were estimated by comparing DPI values for many individual tornadoes to gridded DPI values for those tornadoes using the aforementioned method. Figure 2.6 illustrates DPI estimates for the Super Tuesday tornado outbreak documented in Figure 2.1 and the totality of this gridded DPI dataset is documented in Figures 2.7 and 2.8.

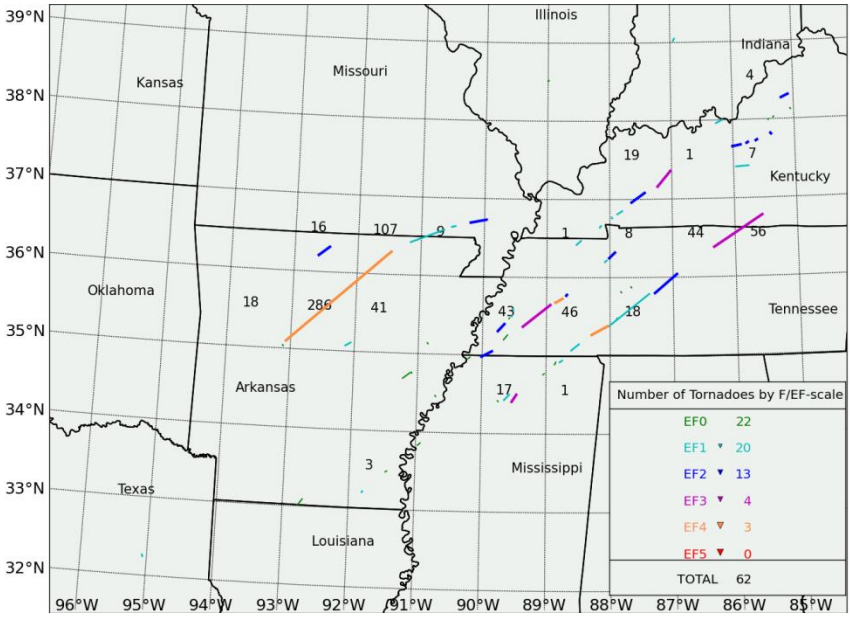

Figure 2.6: Example of gridded DPI calculation using tornadoes that occurred during the Super Tuesday tornado outbreak of February 5, 2008, for which the indicated tornado tracks are taken from Figure 2.1.

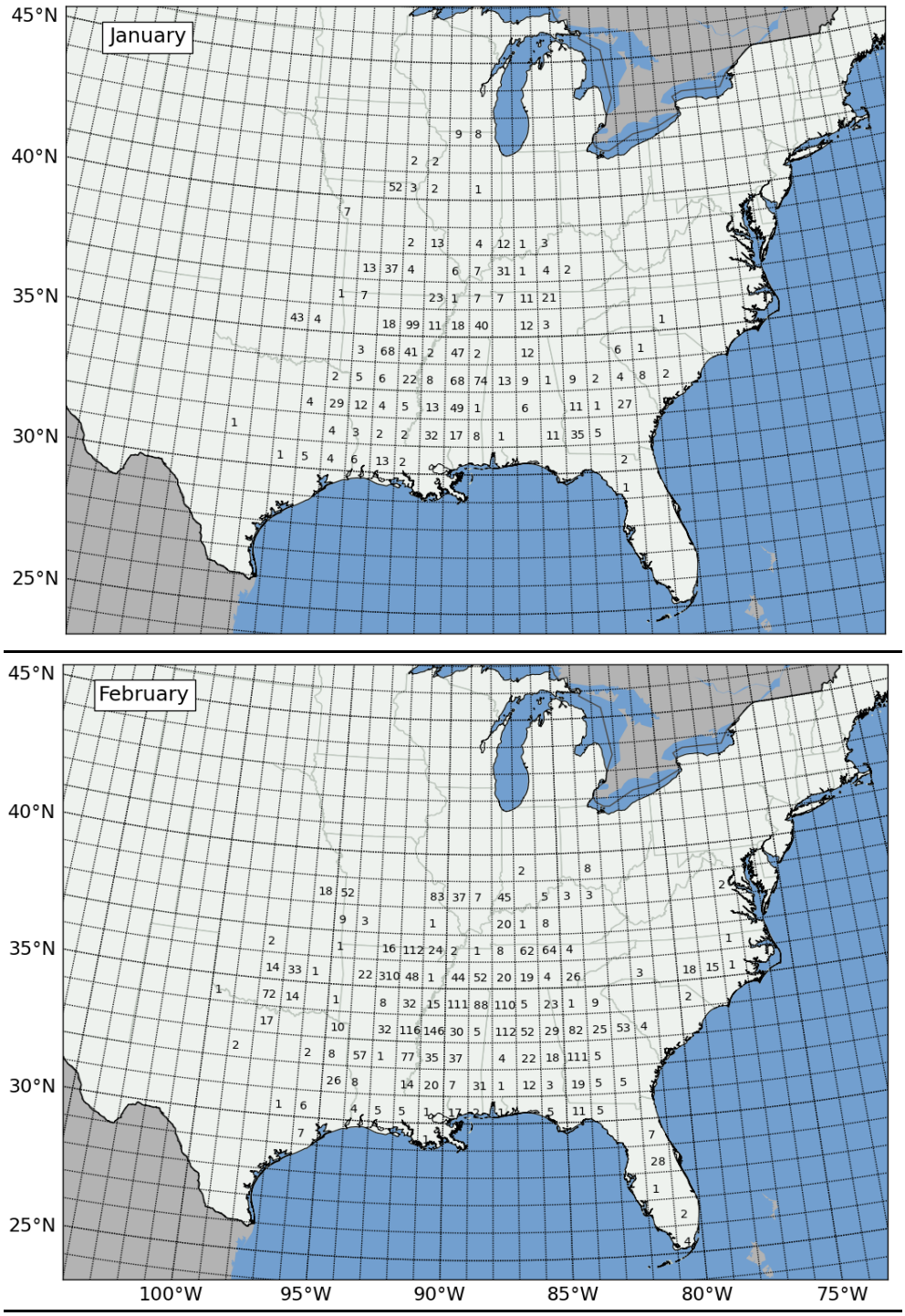

Figure 2.7: Gridded DPI for all January (top) and February (bottom) 1950-2010 tornado outbreaks in the study.

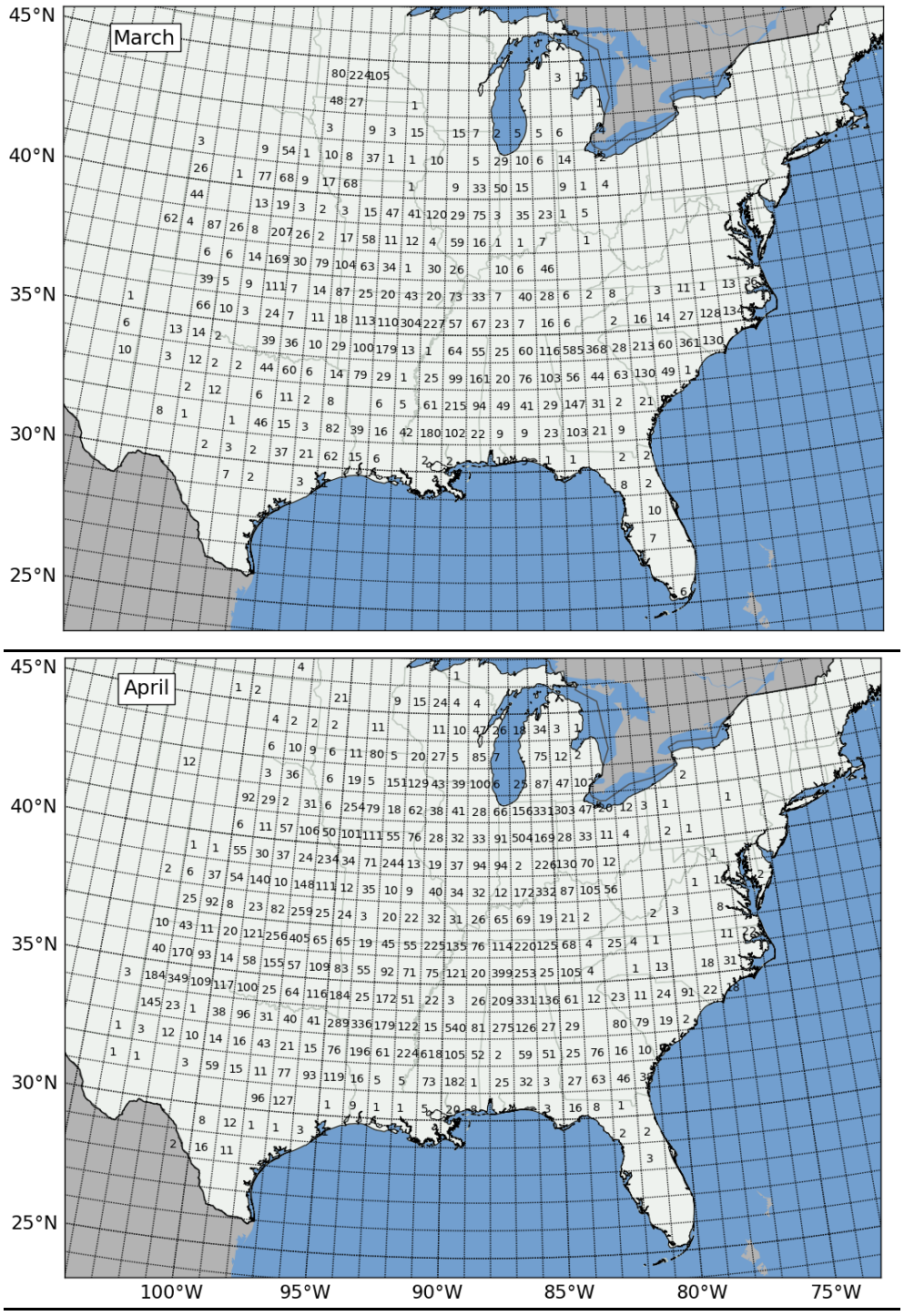

Figure 2.8: Gridded DPI for all March (top) and April (bottom) 1950-2010 tornado outbreaks in the study

c. Time Documentation

As mentioned in Chapter 1, non-meteorological trends in tornado data exist when examining the time-dimension of the tornado dataset. Evidence of this non-meteorological trend is found annual tornado counts and tornado-day counts found in Figure 2.9 and 2.10. Secular trends are obvious in these figures and it is quite certain that improved reporting procedures (among other factors discussed in Chapter 1) are contributing to the increases in annual tornado reports between 1950 and 2010.

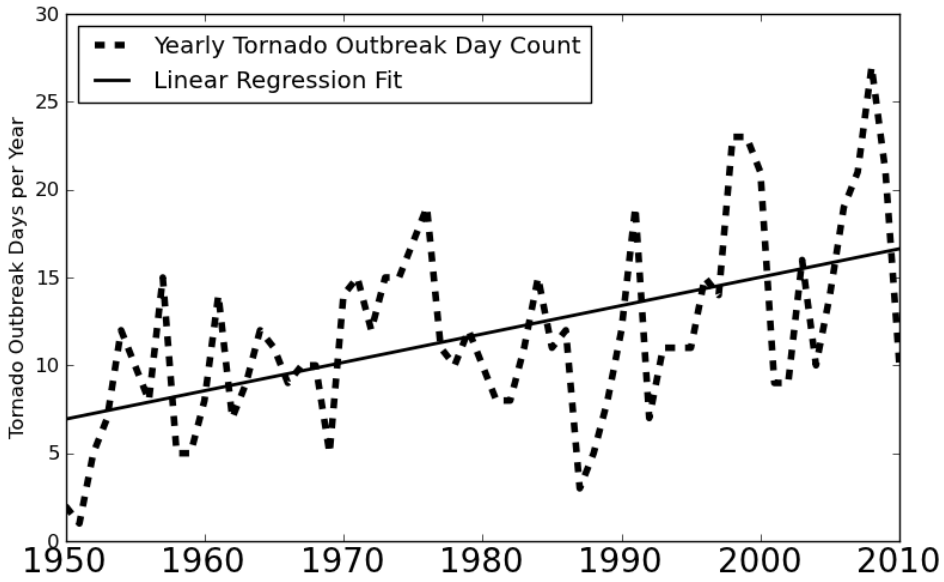

Figure 2.9: Yearly counts of January through April tornado outbreak days east of the Rocky Mountains from 1950 to 2010. Outbreak days increase by an average of 0.16 day per year ($r^2 = 0.28$) throughout the 61-year period.

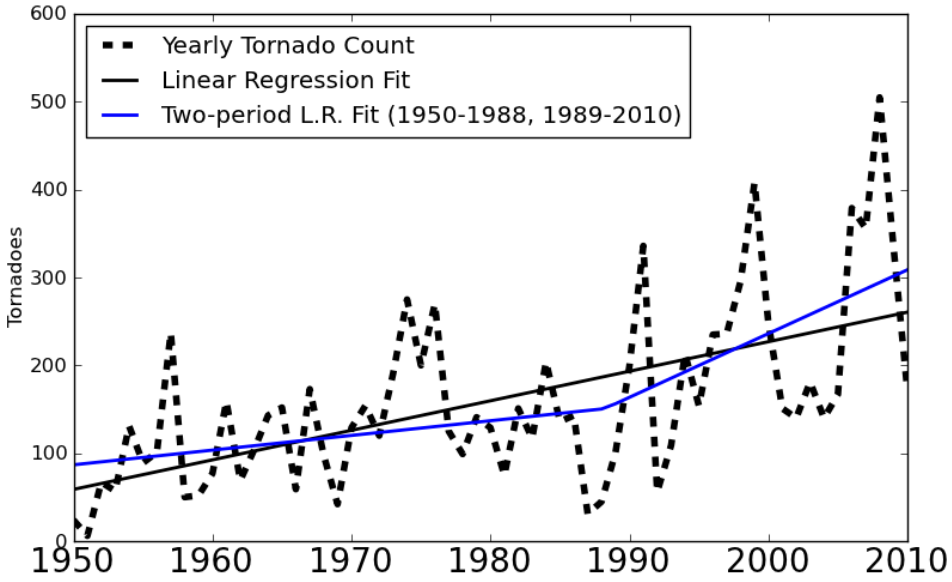

Figure 2.10: Yearly counts of tornadoes occurring on January through April tornado outbreak days east of the Rocky Mountains from 1950 to 2010. Yearly tornado counts increase on average by about 3.34 throughout the entire 61-year period ($r^2 = 0.34$). This increase, however, is less pronounced early in the period (1.67 increase in annual tornado counts from 1950-1988; $r^2 = 0.08$) and more pronounced from 1989-2010 (7.26 tornado per year increase; $r^2 = 0.17$).

The trends in this study identified in the above figures are somewhat different from those identified in other studies. Tornado outbreak frequency between January and April 1950-2010 increase by 0.16 day annually (Figure 2.9) and tornado counts in those outbreaks increase by about 3.34 tornadoes annually (Figure 2.10). These figures are not as large as those identified in Brooks et al. 2003 (hereafter referred to as BDK03), who found that tornado days increase by about 0.5 day per year and that tornado counts on those days increase by about 14 per year. Some of these differences arise from the time period of study (January 1955-December 1999 for BDK03, January-April 1950-2010 for the current study) and from

varied definitions of a tornado day (1 tornado in the continental U.S. in a 24-hour period in BDK03, 6 tornadoes in the continental U.S. in a 24-hour period in the current study). Identification of trends such as these are important for determining which sets of tornado statistics allow for comparison of outbreaks that may have occurred in various parts of the 61-year period of investigation. A more extensive discussion of trends associated with tornado data used for this study will be given in Chapter 3.

In addition to time series analyses of tornado outbreaks on an interannual basis, five 3° by 3° regions were selected for analysis of tornado outbreaks primarily on a seasonal basis (Figure 2.11). These are important for analysis of regional evolution of tornado activity and were chosen for the following reasons:

1) Arkansas due to statistically significant La Niña-related shifts in tornado outbreak activity, particularly in January (Section 4.1),
2) Northern Alabama due to the presence of DPI and tornado maxima there during April (Section 3.1 and 3.3),
3) Northern Texas due to the presence of tornado maxima in April (Section 3.1),
4) Northern Indiana due to the presence of a strong ENSO/tornado relationship identified in Cook and Schaefer (2008) and the presence of historic strong and violent tornado outbreaks in the area during April (e.g., April 3, 1974 and April 11, 1965), and

5) Northern Kansas and southern Nebraska due to the strong ENSO-relationship during March and April in that region (Sections 4.1 and 4.4).

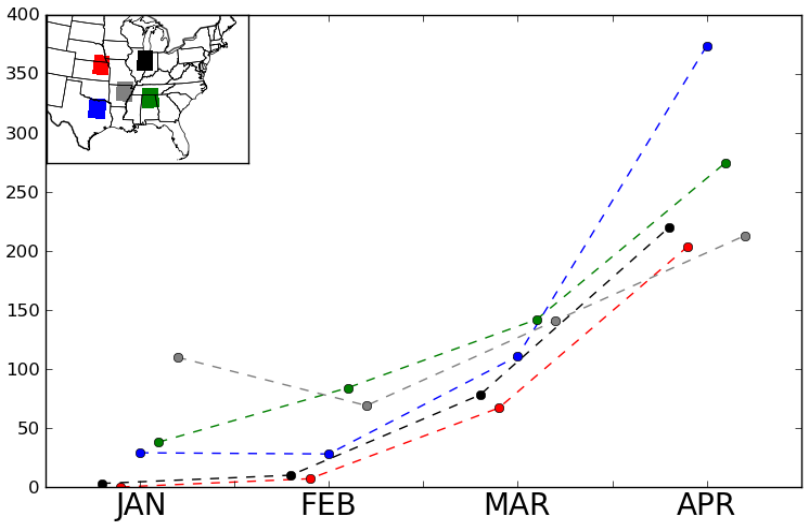

Figure 2.11: Monthly tornado counts in five 3° by 3° regions shown in inset. Lines and brackets are color-coded based on their respective region.

d. Statistical Techniques for Hypothesis Testing

As mentioned in CS08 and referred to in Dixon et al. (2011), it is often necessary and helpful to perform statistical tests to determine whether temporal and spatial shifts in tornado activity are significant. Bootstrap resampling (Efron and Tibshirani 1993, Dixon et al. 2011) was used to test shifts in tornado data for statistical significance. The bootstrap resampling technique involves taking a dataset containing *n* data points and resampling (or randomly selecting) from those data to recreate a new sample the same

size as the original dataset. This process is repeated a large number of times (5000 replications for the current study) to ensure a robust set of resampled replicates of the initial dataset for which inferences about the data can be made.

After the replicates are generated, bias-corrected, accelerated (BCa) confidence intervals (CI) were used based on the bootstrapped replicates. This method was chosen instead of empirical CIs because BCa CIs are second-order accurate, meaning that their standard error goes to zero at a rate faster than empirical CIs. The bias-correction factor is computed as the proportion of the bootstrap replicates that are less than the original data estimate. The acceleration factor represents a rate of change in the bootstrap statistic's standard error. In contrast, empirical CIs that are not bias-corrected or accelerated assume that the standard error of the bootstrap statistic is the same for all values of their true statistic, which is not always true.

Once BCa CIs are calculated for respective statistics, classes of data can be compared to determine whether changes in tornado activity in the current study are statistically significant. This technique was used by Dixon et al. (2011) to examine the possibility of a separate tornado alley in the southern U.S. apart from other regions of the country. Applications of this technique will be used in subsequent chapters.

2.2 Analyses of Atmospheric Features Associated with Tornado Outbreaks

CS08 demonstrated the importance of taking into account the underlying synoptic-scale atmospheric factors that contribute to observed shifts in tornado activity. CS08 did not complete an independent analysis of those synoptic-scale atmospheric features, but rather drew upon refereed literature to establish linkages between El Niño/La Niña and North America weather. That refereed literature focused on broader, longer-term (30-90 day) averages of weather conditions instead of synoptic-scale atmospheric features that were in place on the days of the outbreaks. Thus, even though those longer-term linkages did incorporate atmospheric conditions on days concurrent with tornado outbreaks, the overwhelming majority of the linkages developed and referenced in those studies were based on atmospheric conditions on days in which no tornadoes were reported. In spite of this limitation, ENSO-related shifts in the atmospheric environment across North America were plausibly associated with identified shifts in tornado activity, encouraging continued and advancing analysis in this area of emerging research.

The current study builds on the aforementioned limitation in CS08 by creating a more 'outbreak-focused' analysis of the synoptic-scale atmospheric factors associated with tornado outbreaks. Section 3.2 will discuss the synoptic-scale atmospheric factors considered for this study and identification of those features using atmospheric variables such as

temperature, geopotential height, relative humidity, and wind. Aspects of the data used for this study and methods of analysis of synoptic-scale features will be discussed in Section 2.2.b and preceded by a review of synoptic-scale atmospheric features associated with tornado outbreaks (Section 2.2.a).

a. Review of synoptic-scale atmospheric features associated with tornado outbreaks

As mentioned in Chapter 1, key research from several studies (McNulty 1978, Weisman and Klemp 1984, Johns and Doswell 1992) have identified four main categories of atmospheric 'ingredients' present in the majority of tornado outbreaks: 1) moisture availability, 2) lifting mechanism, 3) static instability, and 4) vertical shear. During tornado outbreaks, four types of synoptic-scale atmospheric features usually interact to provide the aforementioned ingredients: a) surface cyclones, b) low-level jet streams, c) mid- and upper-tropospheric jet streams, and d) mid- and upper-tropospheric shortwaves. For this study, the investigation will remain focused on the four aforementioned synoptic-scale atmospheric features, as opposed to smaller-scale features (i.e., outflow boundaries, sea-breeze boundaries, etc.), for two reasons: i.) the influence of ENSO is most likely linked to large-scale atmospheric features and diminishes significantly on smaller scales, ii.) tornado outbreaks in winter are more closely linked to synoptic-scale processes than in other seasons (CS08).

i. Surface Cyclones

Surface cyclones were recognized fairly early in the existence of tornado forecasting and pattern recognition as a key element of tornado outbreaks (Finley 1884, Finley 1888, Schaefer 1986) and play an important role in most tornado outbreaks with few exceptions. They aid in development of moisture and static instability by drawing warm, humid air masses from warmer source regions to the south (typically the Gulf of Mexico or the Gulf Stream) that effectively becoming a moisture source for updrafts in convective storms. The aid in the development of synoptic-scale lifting by fostering development of synoptic-scale lifting mechanisms through the development of frontal circulations (boundaries between air masses of varied origin) and drylines (Schaefer 1974, Parsons et al. 2000) and aid in development of low-level shear through development of subgeostrophic and convergent wind flow toward areas of surface low pressure centers due to surface friction.

Because of the nature of surface cyclones and accompanying surface fronts, the movement of surface cyclones can determine where tornado development occurs (Galway and Pearson 1981). Often, a 'warm sector' of the surface cyclone (Finley 1884, 1888; Miller 1972; Schaefer 1986) will denote the location most favorable for tornadogenesis. It is usually bounded by the positioning of frontal boundaries to the north and west, which separate warm, unstable air from more stable (cooler and/or drier) air.

ii. Low-level jets

In the simplest sense, a low-level jet is defined as a low-level maxima in wind speed, usually in the lowest few kilometers of the atmosphere (Blackadar 1957, Stensrud 1996). In the U.S., LLJs are most commonly observed as a southerly jet over the Great Plains and often aid in development of moisture and instability in tornado outbreak regions due to rapid transport of air originating from maritime origins (i.e., the Gulf of Mexico) northward because of their south-to-north orientation. They enhance vertical wind shear (Uccelini and Johnson 1979, Mead and Thompson 2011) which aid in development of severe thunderstorm and tornado outbreaks and also foster velocity and moisture convergence on the 'nose' of the jet (Maddox et al. 1980, Zhong et al. 1996) which can also serves as a lifting mechanism for severe convection and tornadoes. Newton (1967) and Barnes and Newton (1983) depict low-level jets in their diagrams of classic tornado-producing and severe thunderstorm producing patterns.

iii. Mid- and upper-tropospheric features associated with tornado outbreaks

Mid- and upper-tropospheric features, namely geopotential height troughs and polar/subtropical jet streams existing between 700 – 200 hPa, or 3000 – 11000m ASL, have been identified as key components of severe weather and tornado outbreaks. These features are normally identified via the analysis of geopotential heights, temperature, moisture, and wind fields

on constant pressure surfaces and contribute to the development of shear, lift, moisture, and instability in the following ways:

1) They result in temperature advection (also known as a ‘cold wind aloft’) which can foster the development of severe convection when the jet is oriented atop an axis of low-level instability (Schaefer 1986)

2) They result in dry air advection aloft and the development of elevated mixed layers (EMLs; Carlson et al. 1983, Lanicci and Warner 1991) because the air being advected by the jet stream is of continental origin. While not present in every tornado outbreak, the EML is a critical part of many tornado outbreaks because it acts as a ‘lid’ to cap widespread deep convective overturning, often resulting in increased destabilization through solar absorption and advection processes. The EML can also act to keep individual convective storms isolated, which can foster supercell development and more efficient tornado production if other atmospheric factors (i.e., shear, moisture) are supportive.

3) The vertical circulations associated with jet streams themselves (Cahir 1971) can foster development of severe convection. The regions of rising motion associated with the left exit and right entrance regions of the jet aid tornado development in environments otherwise supportive of severe storms (McNulty 1978, Uccellini and

Johnson 1979) although Schaefer (1986) states that rising motion can occur in essentially any portion of a jet stream.

4) Winds in the mid- and upper-troposphere are faster than those in the lower-troposphere due to decreased effects of friction at higher altitudes. Additionally, the direction of geostrophic flow at higher altitudes can be different from the actual flow at low-levels, which contributes to directional vertical shear. Although these factors alone do not dictate tornado outbreak occurrence, speed and directional vertical shear are important factors for tornado outbreaks. (Weisman and Klemp 1984, Johns and Doswell 1992)

b. Methods for analyzing synoptic-scale conditions associated with tornado outbreaks

As mentioned previously, it is important to analyze synoptic-scale atmospheric conditions associated with tornado outbreaks to further establish any spatial shifts in tornado activity and establish possible physical causation for those shifts. To address this challenge, composites of synoptic-scale conditions associated with tornado outbreaks were created by identifying and grouping outbreaks containing similar spatial anomalies of various synoptic-scale atmospheric features associated with tornado outbreaks. Along with compositing of atmospheric variables in place across the continental U.S. during the outbreaks, the character of tornadoes (location, frequency, strength) during the outbreaks was assessed to help

identify trends of tornado outbreak activity and ultimately assess potential influences of ENSO on the synoptic-scale atmospheric features contributing to the outbreaks.

i. NCEP/NCAR Reanalysis Dataset

The NCEP/NCAR Reanalysis Dataset (Kalnay et al. 1996) was used for in the construction of composites of synoptic scale atmospheric conditions. This global dataset is defined on a 2.5° longitude by 2.5° latitude grid with 17 vertical levels. The domain used within this dataset encompasses the continental United States in a region bound by 130°W, 67.5°W, 25°N, and 50°N. (Figure 2.12). By defining a domain of this size, aforementioned synoptic-scale features that contribute to tornado outbreaks (discussed in this section) can be readily identified.

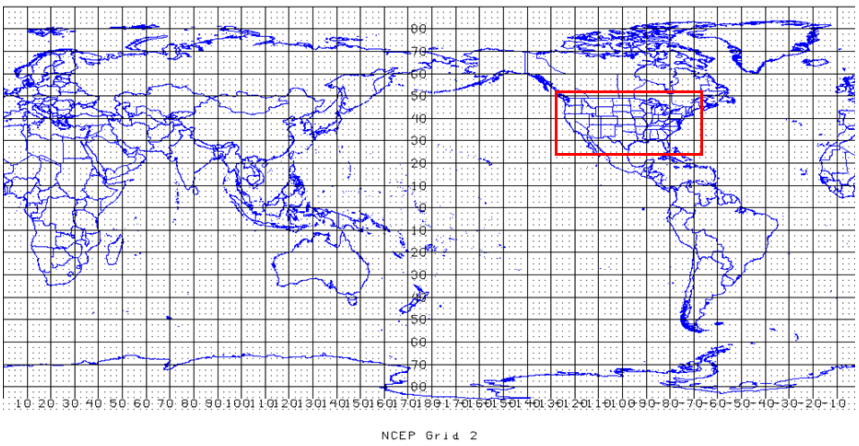

Figure 2.12: Domain used for NCEP/NCAR Reanalysis Data. Red rectangle encloses subdomain used for the current study. Figure from http://www.nco.ncep.noaa.gov/pmb/docs/on388/tableb.html

This domain is comparatively smaller than that of Mercer (2008) and Mercer et al. (2011), who needed to include larger surrounding areas of the

Pacific and Atlantic Oceans to alleviate potential boundary condition problems for numerical modeling. The domain is larger than that used by Schaefer and Doswell (1984), who studied only a few tornado cases from the Great Plains, whereas the current study includes tornado outbreaks that occur from the western Great Plains to as far east as North Carolina and Florida.

Five variables were used in the creation of the atmospheric composites (geopotential height/sea-level pressure, temperature, relative humidity, U-component wind, and V-component wind) at five different atmospheric levels (300 hPa, 500 hPa, 700 hPa, 850 hPa, and surface) to identify the important synoptic-scale atmospheric features that contribute to the outbreaks being studied. Additionally, composites of lifted index and precipitable water were created for comparison across outbreaks to compare the presence of statically unstable warm sectors and the presence of moisture across outbreak areas. Kalnay et al. (1996, Tables 3 and 4) gave reliability ratings for the variables available in the Reanalysis dataset. They gave geopotential height, temperature, U-component wind, and V-component wind the highest “A” rating because they were considered to be among the most reliable variables in the dataset. Relative Humidity, Lifted Index, and Precipitable Water were given “B” ratings because, although observational data directly affect the value of the variable, the model used to create the reanalysis variable also has a very strong influence. Kalnay et al. (1996) recommend that variables given a “B” designation be used with

some caution. Hence, more focus will be placed on variables that received an “A” reliability designation.

Reanalysis data for each of the outbreaks were available four times per day at 00 UTC, 06 UTC, 12 UTC, and 18 UTC. To determine the appropriate time of day for the present analyses, an average of the start times for each tornado on a tornado outbreak day was calculated. The Reanalysis time closest to the average of the start times of the individual tornadoes was used for the set of atmospheric conditions representative of the tornado outbreak day. For example, since the average start time of each tornado in the April 3, 1974, tornado outbreak was approximately 1720 CDT (2320 UTC), the 00 UTC 4 April 1974 Reanalysis data were deemed most representative of atmospheric conditions associated with that tornado outbreak. Figure 2.13 shows a climatology of the average start times of the tornadoes occurring on tornado days during the study period (January-April 1950-2010). Most of the average tornado start times per outbreak occurred between 12-19 CDT (18-01 UTC) time frame with a distinct peak 16-19 CDT peak. As a result, most outbreaks required use of 00 UTC Reanalysis as an appropriate representation of the atmospheric conditions associated with concurrent tornado outbreaks. This finding is somewhat consistent with Mercer (2008), who found it appropriate that analyses for 00 UTC on the day following the tornado outbreak day would provide good representations of the atmospheric conditions in place during the respective tornado outbreaks in his study.

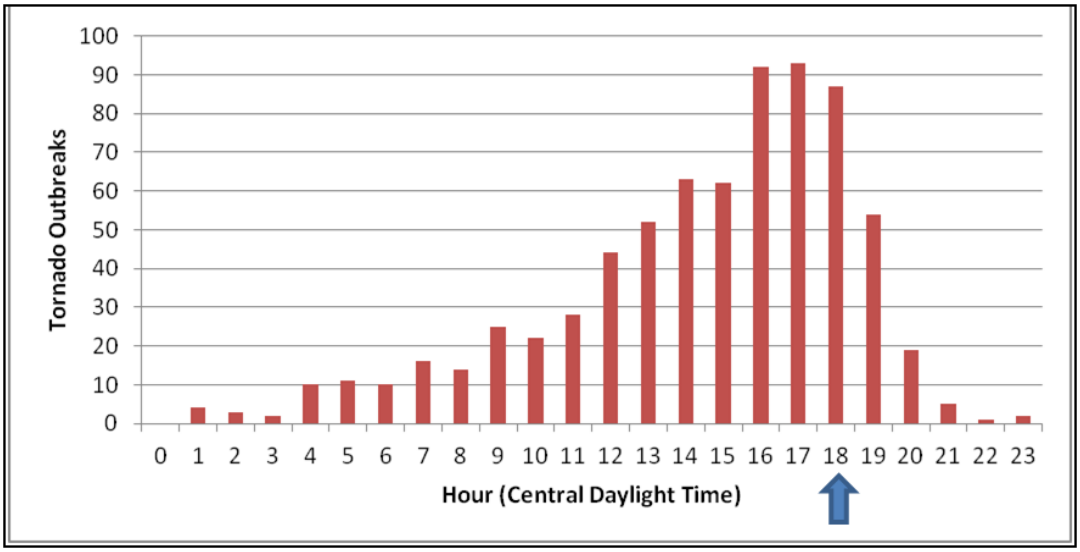

Figure 2.13: Histogram illustrating average start times of tornadoes on each outbreak day.

ii. Composite Methodology

S-mode PCA (Richman 1986) was used to create composites of synoptic-scale atmospheric conditions associated with tornado outbreaks and analyze their intraseasonal shifts, their shifts in relation to ENSO, and their resultant impact on tornado outbreak activity. This approach was used because it helped to identify spatial anomalies (i.e., groups of gridpoints that vary similarly in the domain outlined in Figure 2.12) of a particular variable being analyzed (Richman 1986) and also provided an objective mechanism for compositing multiple events containing similar spatial anomalies. Although the current PCA methodology used in this study was adapted from preceding studies that performed PCA on sea surface temperatures in the

Pacific Ocean (Montroy 2006) and atmospheric variables discriminating between types of severe weather outbreaks (Mercer 2008), the current study is the first of its kind to create a climatology of synoptic-scale atmospheric features associated with tornado outbreaks during the January-April time frame. Figure 2.14 outlines the five-step process used in this study for creating composites of synoptic-scale atmospheric conditions.

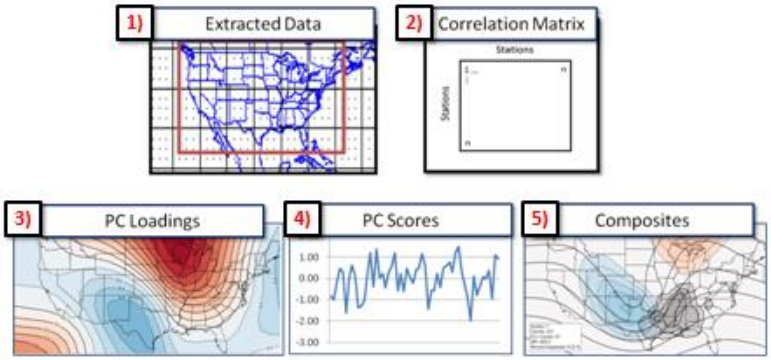

Figure 2.14: Outline of the five-step process used to conduct PCA on specified atmospheric variables

The "extracted data" referred to in Figure 2.14 and used for this study simply consists of varied subsets of the Reanalysis data described in Section 2.2.b.i from each tornado outbreak day. The criteria for these subsets were chosen based on the specified goal of the analysis. For instance, creation of the climatology of synoptic-scale atmospheric conditions in Chapter 3 requires the application of PCA to individual atmospheric variables (outlined in Table 2.2) from monthly subsets of outbreaks (e.g., 500 hPa geopotential heights on January tornado outbreak days compared to 500 hPa geopotential heights on February tornado

outbreak days, then compared to 500 hPa geopotential heights on March tornado outbreak days, and finally to 500 hPa geopotential heights on April tornado outbreak days). Key differences (and similarities) between the composites from those four subsets were then analyzed to identify systematic differences in outbreaks with progression from January through April. A similar approach is used in Chapter 4, with subsets of data from tornado outbreaks selected based on their time of occurrence and also the phase of ENSO to determine any possible influences from those larger scale factors on subsequent tornado outbreaks. Again, these linkages help further establish the relationship between ENSO and tornado outbreaks compared to statistical analyses of tornado counts (Cook and Schaefer 2008).

After appropriate data subsets were chosen, unrotated principal component (UPC) loadings were derived by 1) creating a standardized anomaly matrix by standardizing the data subset chosen for PCA (subtracting the data subset mean and dividing by the standard deviation) and then 2) calculating an inter-grid cell correlation matrix based on the newly created standardized anomaly matrix. The UPCs were derived from the inter-grid cell correlation matrix in an S-mode sense (Richman 1986, Montroy 2006) and were essential in identifying groups of grid cells that vary similarly.

Orthogonal rotation using the Varimax criterion (Kaiser 1958) was used to better capture the characteristic patterns of variance in the data

subset. This rotation scheme enhances the physical interpretability of principal components by 1) maximizing interstation variances, thus further regionalizing areas of relatively large loading magnitudes and 2) removal of domain shape dependence (Richman and Lamb 1985). This approach is also consistent with previous studies (Richman and Lamb 1985, Richman 1986, Montroy 2006) that have illustrated the benefit of Varimax rotation of principal components.

Synoptic-scale Atmospheric Features of Interest	Atmospheric Variable Used to Identify Features	Contribution toward Tornado Outbreaks
Upper-tropospheric Jet Stream	300 hPa ϕ, U Wind, V Wind	Lifting Mechanism, Shear
Surface Cyclones	Sea Level Pressure, U Wind, V Wind	Lifting Mechanism, Shear
Lower-tropospheric Jet Stream (LLJ)	850 hPa ϕ, U Wind, V Wind	Lifting Mechanism, Shear
Static Instability	Lifted Index	Instability
Moisture	Precipitable Water	Moisture

Table 2.2: Synoptic-scale atmospheric features of interest and variables used to identify them. PC analyses are conducted on the atmospheric variables for multiple subsets of outbreaks to determine the presence and character of the four ingredients and their associated synoptic-scale atmospheric features. Wind fields (shown in red) are derived from results of PC analyses of geopotential height (as described in subsequent paragraphs).

Determining the optimal number of PCs to retain and rotate was a key aspect to optimal application of PCA to data subsets. This determination was accomplished through 1) use of the 'point teleconnection pattern' method described in Richman and Lamb (1985) and Richman (1986) and 2) visual inspection of Varimax-rotated PC (VRPC) loading patterns. These methods both maximize how well the VRPCs represent the input data and remove loading patterns that are less representative of the

input data subset. These loading patterns essentially represent groups of gridcells that covary similarly and are maximized in locations where groups of gridpoints are most strongly correlated.

The application of the point teleconnection pattern method involves the use of a congruence coefficient, which is the result of correlating spatial loadings from each VRPC with the row/column of the parent correlation matrix that corresponds to the maximum loading. Richman (1986) indicated that congruence coefficients greater than |0.92| are indicative of a "good" match between loadings and the parent correlation matrix. VRPCs containing congruence coefficients less than |0.92| were truncated from the analysis.

Another asset to visual inspection of VRPC loadings is to ensure that multiple dominant signals are not retained within the same PC. This phenomenon is exemplified in Figures 2.15.ii, 2.15.iv, and 2.15.v. In Figure 2.15.ii, a large area of negative loadings is located across the eastern one-third of the domain. When an additional PC is retained and rotated, this area of negative loadings is separated into two centers of action, the first across the far southeastern portion of the domain (Figure 2.15.iv) and the second centered across the northeastern U.S. (Figure 2.15.v). This is helpful because it ensures that Varimax rotation is helping to capture the patterns of maximum variance in the dataset and then properly separating those patterns across PCs that explain the most variance.

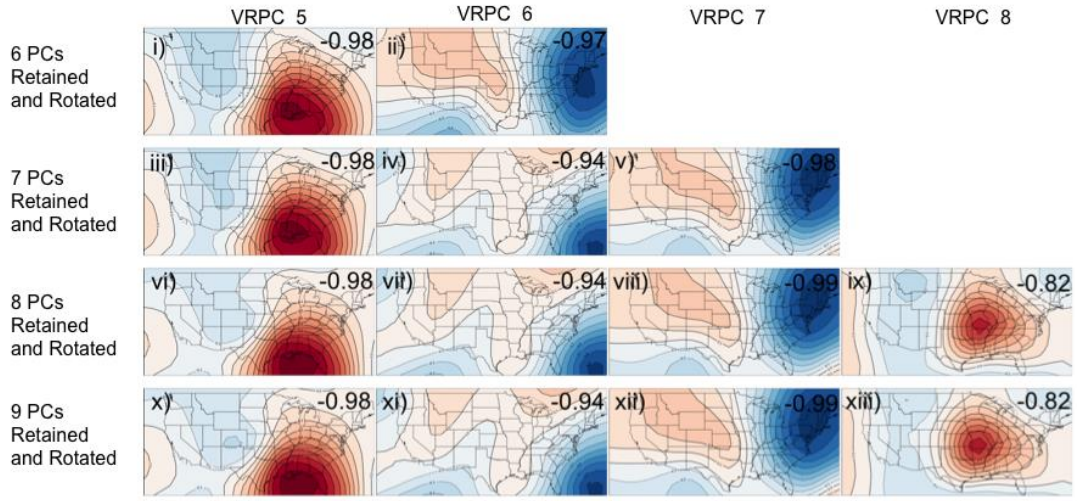

Figure 2.15: January 500 hPa geopotential height VRPC loading patterns and congruence coefficients (in upper right) when 6-9 UPCs were retained and rotated. Congruence coefficient magnitudes dropped below |0.92| in VRPCs whenever eight or more UPCs were retained and rotated, indicating that retaining and rotating seven UPCs was optimal for this example.

Richman and Lamb (1985) indicated that PC score time series relating VRPC loading patterns to standardized anomalies of individual events provide a basis for case studies of individual events. In that particular study, composites were created based on mean fields of groups of individual events that met or exceeded a subjectively-chosen minimum PC score of 1.0. Although several objective measures of determining an appropriate minimum threshold for PC score were investigated, the process for choosing this threshold ultimately relied on visual inspection of individual events and their standardized anomalies compared to VRPC loadings to ensure that events were a suitable match for compositing with similar cases. The minimum PC score threshold also ensured that the magnitude of any spatial anomalies of individual events were consistent with local maxima in

VRPC loading patterns. Larger magnitudes of PC scores indicate a stronger match between individual events and VRPC loading patterns.

An example of composited 500 hPa geopotential height fields for January tornado outbreaks that match VRPC1 (based on minimum PC score and correlation coefficient thresholds) is shown in Figure 2.16. In this example, contours represent the mean geopotential height field for all included events and shaded regions represent departure of the composite from the mean geopotential height field in all outbreaks in the entire month of January. (Note: In composites of relative humidity and precipitable water in subsequent chapters, shaded regions will not indicate departures from a mean, but will instead represent the magnitude of the respective variable being composited.) Hatched regions indicate locations where tornadoes occurred during corresponding outbreaks.

Although the magnitudes and locations of loadings were important for the spatial analyses of atmospheric variables in this study, the signs of the loadings are arbitrary. Because of this, both positive and negative values of loadings should be considered for creation of composites. This is done by simply creating composites of tornado outbreaks with principal component scores less than or equal to -1.0. Figure 2.17 shows composites in cases where the signs of loadings are opposite of those in Figure 2.16. For simpler naming conventions, the first set of composites containing outbreaks with positive principal component scores are labeled with a + (e.g., January PC1 + in Figure 2.16) and composites of outbreaks with

negative principal component scores are labeled with a - (i.e., January PC1 - in Figure 2.17).

The result of these efforts is a series of composites that outline the dominant patterns of certain atmospheric variables during tornado outbreaks in January-April. These dominant patterns describe much of the variance in atmospheric features associated with subsets of tornado outbreaks. These composites ultimately provide the ability to determine important shifts in atmospheric features associated with outbreaks in time (Chapter 3) and as a function of ENSO (Chapter 4). In addition, they help determine which synoptic-scale atmospheric patterns contribute to stronger outbreaks (gauged by higher tornado counts, higher significant tornado counts, and higher DPI).

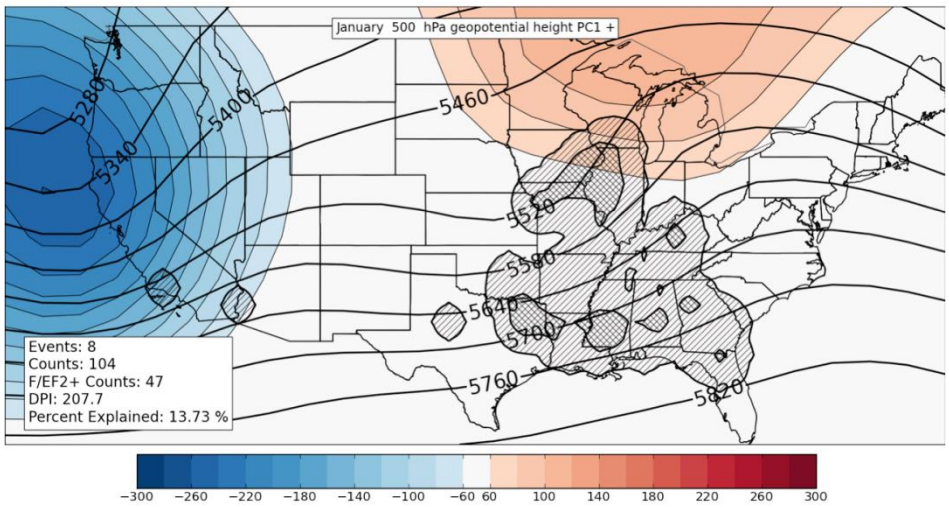

Figure 2.16: Example composite of January 500 hPa geopotential heights in tornado outbreaks containing VRPC scores greater than 1 (black contours). Shaded regions in blue (red) indicate where composited mean height fields are below (above) average of the mean January 500 hPA geopotential height field for all January tornado outbreaks in the entire dataset. Tiers of hatched areas indicate relative concentrations of tornado activity that are counted on a 1° latitude/longitude grid in a manner similar to that outlined in Section 2.1.b.iii. A Gaussian filter with bandwidth = 1° was applied to the data before hatching.

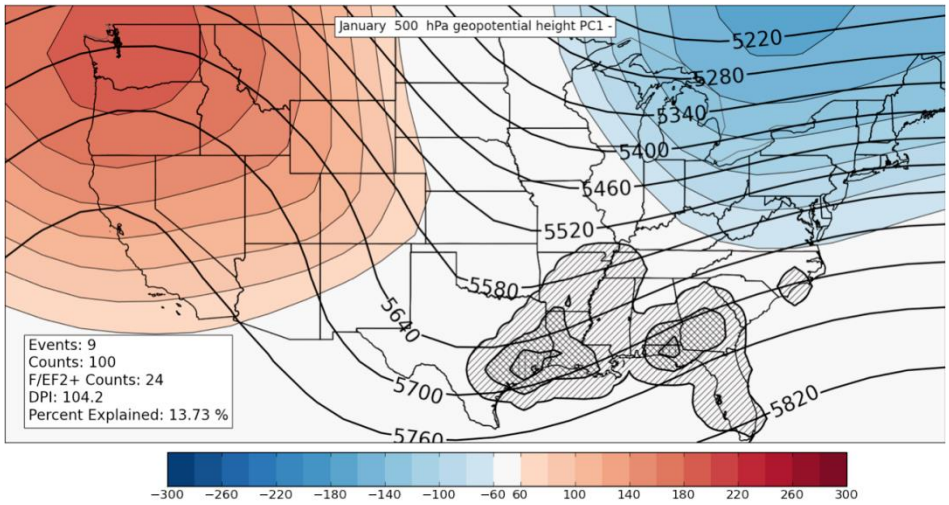

Figure 2.17: As in Figure 2.16, except composites are for events that have VRPC 1 scores less than -1.

3. JANUARY-APRIL TORNADO OUTBREAK CLIMATOLOGY

As alluded to in Chapters 1 and 2, tornado climatologies have served as an important part of understanding tornado outbreaks since the earliest documented efforts by J.P. Finley in the 1880s. The identification of climatological trends in tornado outbreaks from January-April 1950-2010 is especially important for this work because 1) it will help separate robust meteorological signals from non-meteorological biases in the tornado dataset and 2) identification of relatively neutral trends in the data is helpful for comparing outbreaks across various parts of the dataset (e.g., outbreaks in the 1950s vs. outbreaks in the 2000s) and will be pursued here. Analysis of synoptic-scale atmospheric conditions associated with the outbreaks will further establish the meteorological signals and help separate them from non-meteorological biases. These tasks are paramount to subsequent work on gauging the influence of large-scale climate system modes on tornado outbreaks, because the small sample sizes make it difficult to identify robust, statistically significant trends in tornado data.

Sections 3.1-3.3 discuss interannual and interdecadal trends in the location, frequency, and strength of tornadoes in tornado outbreaks. Section 3.4 discusses a new atmospheric climatology of the synoptic-scale atmospheric conditions associated with tornado outbreaks and their connections to the trends identified in the physical tornado climatology described in Sections 3.1-3.3. Section 3.5 concludes the chapter and briefly

discusses the application of techniques and concepts of this chapter to the relationship between ENSO and tornado outbreaks.

3.1 Tornado Location

a. Average Seasonal Patterns

Initial results from this study are in agreement with past tornado climatologies (e.g. Pautz 1969; Galway 1977; Brooks et al. 2003, referred hereafter as BDK03; Verbout et al. 2006) that indicate a general increase in tornado occurrence in outbreaks from winter into early spring. In a few of the analyses in this chapter, the occurrence date of each of these outbreaks was categorized into seven overlapping ~30 day periods defined for this study in Table 3.1 and these overlapping periods are used extensively in creation of the climatology.

Time period	Abbreviation	Dates
January	J	Jan 1 - Jan 31
Mid-January to Mid-February	J16	Jan 16-Feb 15
February	F	Feb 1 - Feb 29
Mid-February to Mid-March	F16	Feb 16 - Mar 15
March	M	Mar 1 - Mar 31
Mid-March to Mid-April	M16	Mar 16 - Apr 15
April	A	Apr 1 - Apr 30

Table 3.1: Definition of time periods used in study.

Maxima in tornado activity occur in the south central United States during the four-month study period (Figure 3.1). January and February appear to be quite similar, with most frequent tornado occurrences in an area from northeastern Arkansas southward to central Mississippi. Although the maximum frequency of tornadoes remains in northeastern Arkansas in March, the general pattern indicates an increase in tornado outbreak activity into the early spring from March through April and a distinct westward expansion of tornado occurrence into the southern Great Plains is also noted. Local maxima occur in northern Texas and northern Alabama beginning in mid-March (M16). By the end of the four-month period of study, the area most prone to tornado outbreaks has shifted westward to northeastern Texas and southern Oklahoma.

It is important to note that tornado occurrence is certainly not limited to the south-central and southeastern U.S. during the winter and early spring (Figure 3.1). Tornadoes have occurred further north of these areas in each monthly and mid-monthly period. Strong and even violent tornadoes in tornado outbreaks have occurred in these areas in January (e.g., F3 in southern Wisconsin on January 7, 2008), February (e.g., F4 near Saint Louis, Missouri on February 10, 1959), March (e.g., F5 near Hesston, Kansas on March 13, 1990), and April (e.g., F5 near Xenia, Ohio on April 3, 1974). April appears to be the month with most frequent tornado outbreak occurrence in these areas, although Figure 3.1 suggests that

tornadoes can occur in a large area east of the Rocky Mountains regardless of month of occurrence.

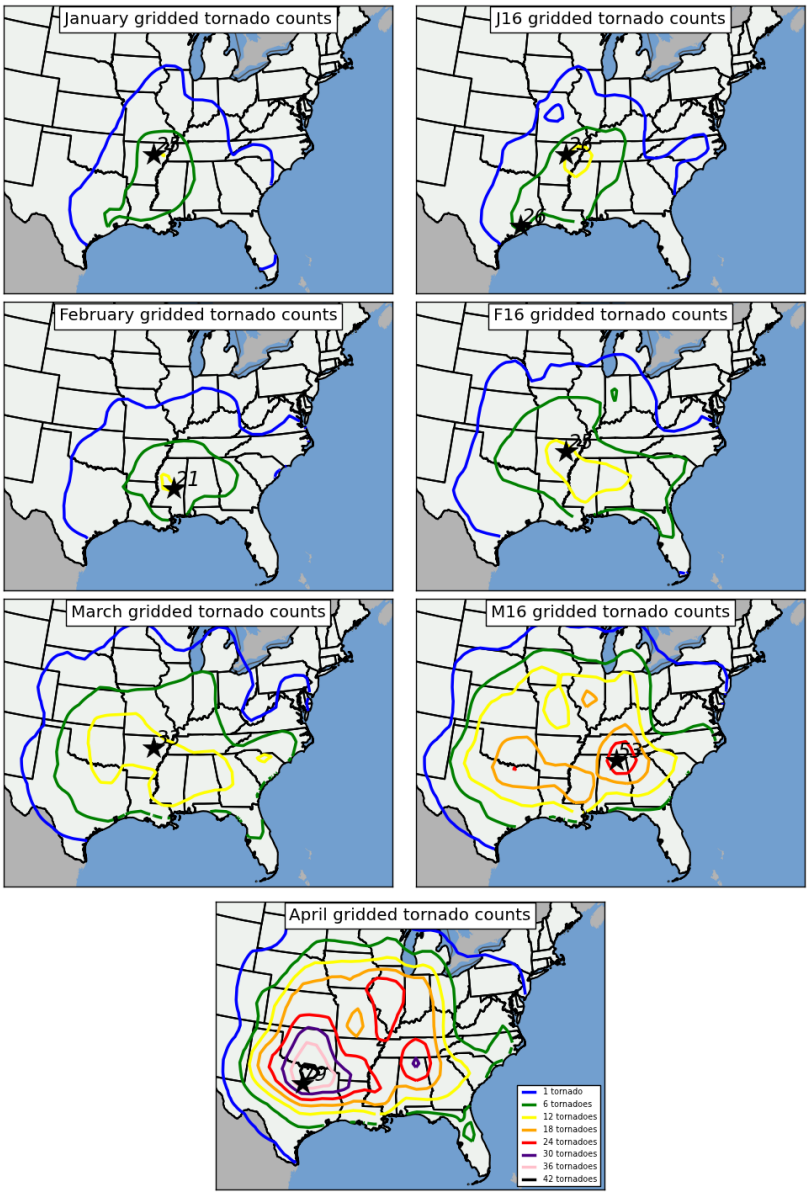

Figure 3.1: Contour plots representing the number of times tornadoes in tornado outbreaks occurred in grid boxes in each mid-month to mid-month period during 1950-2010. Star and associated number indicates location and number of maximum tornado occurrences on the grid. As mentioned in Section 2.1.b, a Gaussian filter with bandwidth = 1° was applied to the data before isoplething.

Statistical tests on the monthly gridded tornado data indicate that the seasonal variability of tornadoes occurring in outbreaks vary in different parts of the U.S. east of the Rocky Mountains. Figure 3.2 shows BCa CIs (discussed in Section 2.1.d) for tornado counts occurring in five separate regions of the study domain calculated using the bootstrap resampling methodology outlined in Section 2.1.d. Mid-South, Florida, southern Georgia, and areas immediately along the Gulf Coast do not exhibit as strong of seasonality in tornado data that regions outside of these areas do. Figure 3.2 also shows that seasonal dependence of tornado data is strongest in Northern Texas (as indicated by the most aggressive increase throughout the four month period) and least in the Mid-South region, where January tornadoes do not appear to be statistically different from April tornadoes based on the BCa CI.

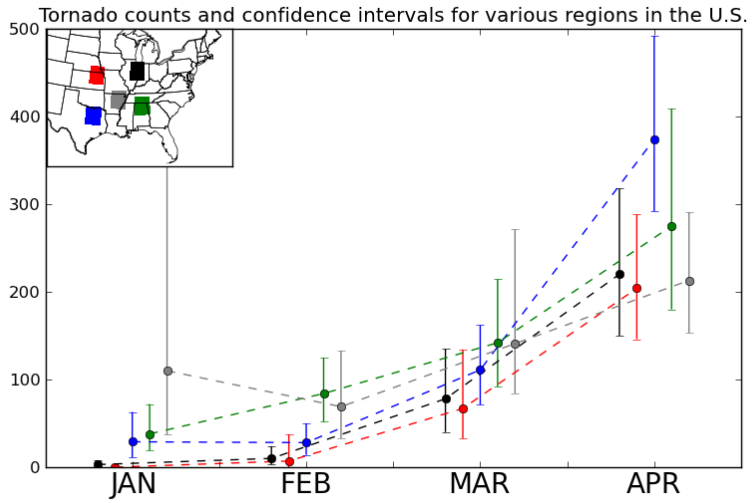

Figure 3.2: Monthly tornado counts (dashed lines) and 95% BCa CIs around the sum of monthly tornado counts (brackets) in five 3° by 3° regions shown in inset. Lines and brackets are color-coded based on their respective region.

b. Decadal Trends

Rather intriguing similarities and differences in locations of tornado maxima are observed on an interdecadal basis (Figures 3.3 and 3.4). Maxima in tornado activity are located across the southern tier of the U.S. in all decades, but increases in activity are noted in the 1960s across the Midwestern U.S. An overall decrease in tornado activity is noted in the 1980s, while maxima extend across the southern and southeastern U.S. in the 2000s. Although these general trends have been observed in decadal tornado analyses including all months (January through December), no reason for this relative decrease has ever been provided (Brooks 2012, personal communication).

Interdecadal trends in F/EF2 and stronger tornadoes in outbreaks and location of F2+ tornado maxima (Figure 3.4) exhibit important similarities and a few differences from interdecadal trends of all tornadoes occurring in outbreaks. Rather than showing a uniform increase in tornado counts across all decades, the 1980s and 2000s appear to be relatively quiet, while 1970s and 1990s are relatively active, particularly across the southern U.S. Maxima in decadal counts of F/EF2+ tornadoes are not always consistent with maxima in decadal counts of all tornadoes in outbreaks during these decades as well, with maxima of decadal tornado counts in northeastern Oklahoma in the 1980s and Mississippi in the 2000s quite different from maxima in decadal F/EF2+ tornado counts in northern Louisiana in the 1980s and southwestern Missouri in the 2000s.

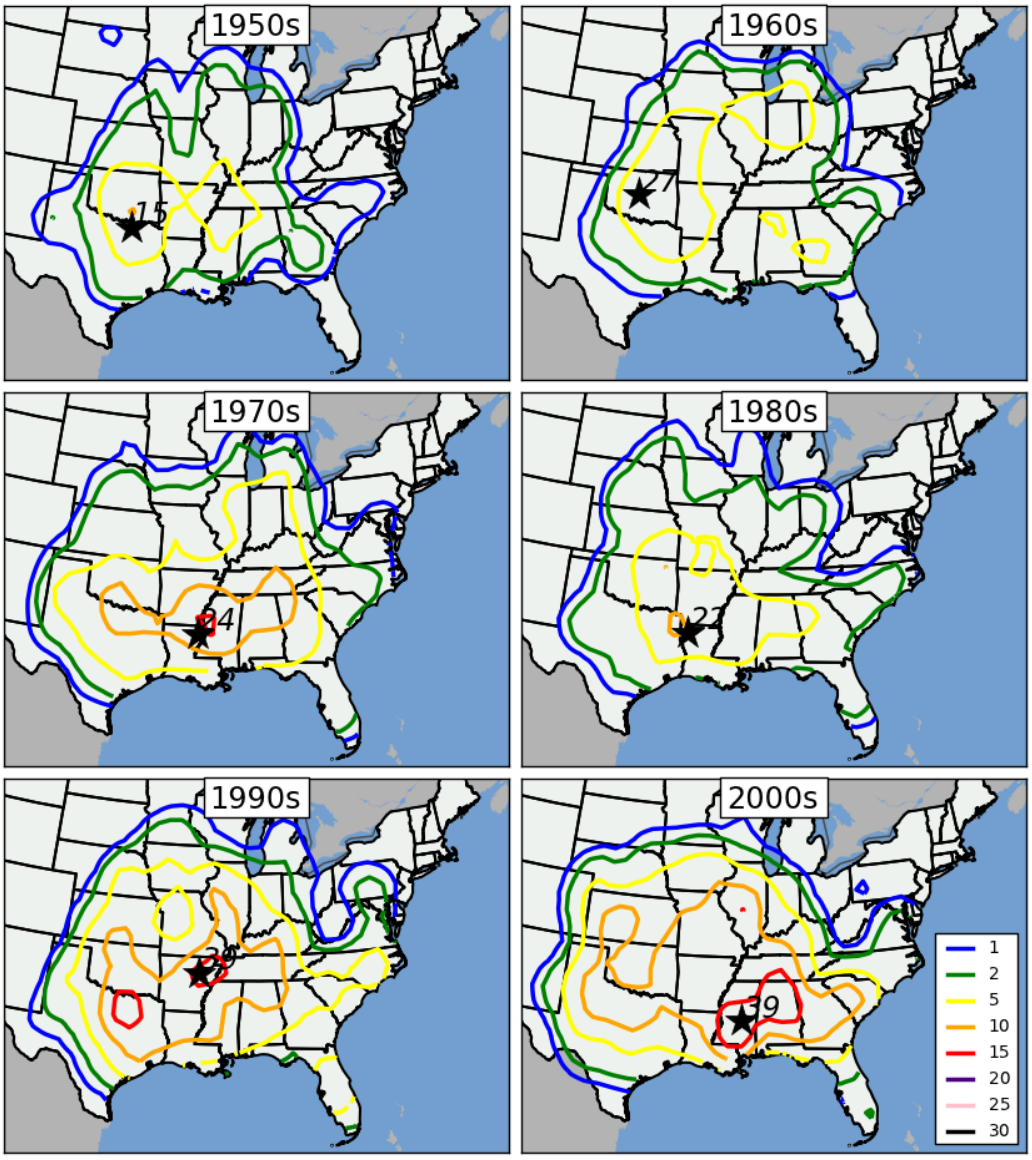

Figure 3.3: Decadal depiction of tornado counts for all January-April tornado outbreaks for the following periods: 1950-1959 (upper left), 1960-1969 (upper right), 1970-1979 (middle left), 1980-1989 (middle right), 1990-1999 (lower left), and 2000-2009 (lower right). Star and associated number indicates location and number of maximum tornado occurrences on the grid. As mentioned in Section 2.1.b, a Gaussian filter with bandwidth = 1° was applied to the data before isoplething.

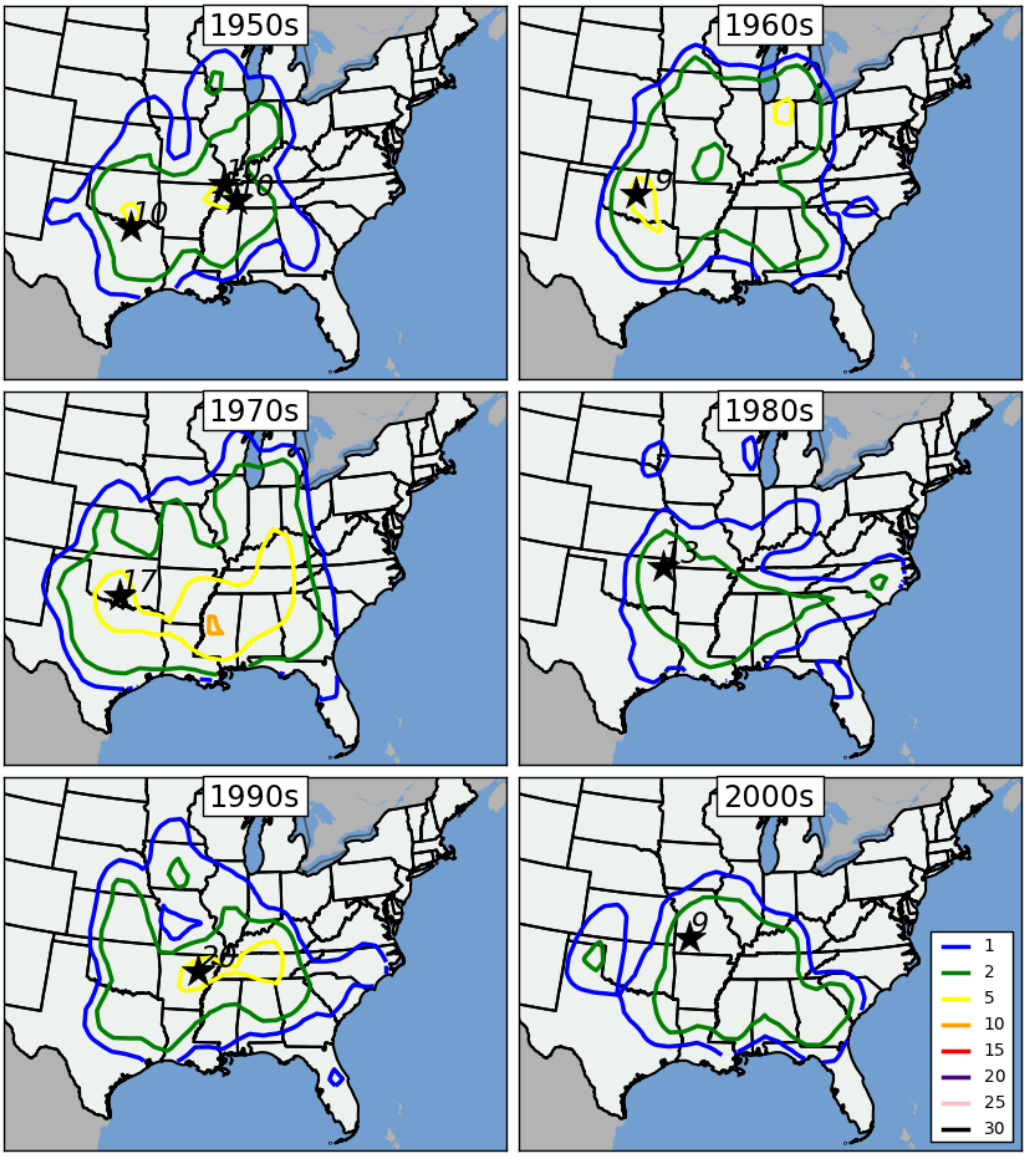

Figure 3.4: Decadal depiction of F/EF2+ tornado counts for all January-April tornado outbreaks for the following periods: 1950-1959 (upper left), 1960-1969 (upper right), 1970-1979 (middle left), 1980-1989 (middle right), 1990-1999 (lower left), and 2000-2009 (lower right). Star and associated number indicates location and number of maximum tornado occurrences on the grid. As mentioned in Section 2.1.b, a Gaussian filter with bandwidth = 1° was applied to the data before isoplething.

\Many of these differences in location of maxima between these two plots have not been identified before. The opposing trends in tornado counts compared to decreasing counts of F/EF2+ tornadoes in the 2000s, however,

is likely explained by an increase of reporting of F0 and F1 tornadoes, some of which may have been rated higher in past decades (Brooks 2011, http://www.nssl.noaa.gov/users/brooks/public_html/tornado). The decrease in F/EF2+ tornado occurrence with time is also discussed in Section 3.2.

3.2 Tornado Outbreak Frequency

a. Average Seasonal Trends

Initial results from this study are in agreement with past tornado climatologies (e.g. Pautz 1969; Galway 1977; BDK03; Verbout et al. 2006) that indicate a general increase in tornado occurrence in outbreaks from winter into early spring. 9746 tornadoes occurred in the 717 January through April tornado outbreaks (i.e., days with 6 or more tornadoes in a 24 hour period across the CONUS east of the Rocky Mountains). A nearly seven-fold increase in tornadoes occurring in outbreaks is observed between January (793) and April (5576; Table 3.2). Much of this increase occurs in the warm season: an increase of only 99 tornadoes occurs between January and February, compared to an increase of 3103 tornadoes between March and April.

Similar trends of increasing tornado activity are observed in counts of tornado outbreak days, counts of strong tornadoes (rated F/EF2 or greater; also referred to as 'significant' tornadoes), and counts of violent tornadoes (rated F/EF4 or greater). Only 56 tornado outbreaks were observed in January (~0.9 outbreak per year), with progressively increasing numbers of tornado outbreaks through the cold season of the year peaking at 390

outbreaks (~6.4 outbreaks per year) in April. On average, ~11.8 outbreaks can be expected per year during the January – April period.

	J	J16	F	F16	M	M16	A	JFMA Total
Tornadoes on outbreak days	793	863	892	1527	2485	3819	5576	9746
Tornado outbreaks	56	64	83	122	188	271	390	717
Tornadoes rated F/EF2 or greater	229	276	305	547	807	1198	1652	2993
Tornadoes rated F/EF4 or greater	10	17	17	33	60	118	152	239

Table 3.2: Intraseasonal evolution of January-April 1950-2010 tornado frequency in outbreaks(as defined in Chapter 1) east of the Rocky Mountains. Periods used to bin tornado data are monthly or mid-month to mid-month and therefore overlap. Each period indicates monthly bins of tornado data and dates may overlap. For instance, "J" indicates tornadoes occurring in the month of January while "J16" reflects tornadoes occurring between mid-January and mid-February.

Although both strong and violent tornadoes exhibit a similar trend to tornado counts and tornado outbreak frequency through the season, the sample sizes for these events is much smaller. Violent tornadoes are a rare occurrence; only 239 tornadoes in the dataset (~2.4% of all tornadoes that occur in tornado outbreaks) are rated F/EF4 or stronger. April is the most active month for strong (~27 per year) and violent (~2.5 per year) tornado occurrence, although these phenomena can occur in all months.

Even though tornado outbreaks tend to be more frequent toward April, tornadoes associated with individual outbreaks early in the four month period (January-February) can be just as widespread and numerous as those occurring later in the four month period (April). In any of the 30 day

periods, an average of about 13 tornadoes (~4 rated F2 or greater) occur in each outbreak although a drop to less than 11 tornadoes per outbreak is observed in February (Table 3.3). This statistically significant drop is due to more February outbreaks occurring in earlier decades (1950-1990) of the study period when underreporting of events was much more prevalent. A trend toward increasing violent tornadoes as time progresses toward the warm season is noted (0.18 per outbreak in January compared to 0.39 in April), although it is difficult to place an emphasis on this trend given the rarity of violent tornado occurrence in any part of the dataset. This important finding suggests that although winter outbreaks are less frequent than early spring ones, they can contain just as many tornadoes and be just as impactful.

	J	J16	F	F16	M	M16	A
Number of tornadoes per outbreak	14.16	13.48	10.75	12.52	13.22	14.09	14.3
Number of strong tornadoes per outbreak (≥F/EF2)	4.09	4.31	3.67	4.48	4.29	4.42	4.23
Number of violent tornadoes per outbreak (≥F/EF4)	0.18	0.27	0.20	0.27	0.32	0.44	0.39

Table 3.3: Averages of 1) tornadoes per outbreak, 2) strong tornadoes (rated F/EF2 or greater) per outbreak, and 3) violent tornadoes (rated F/EF4 or greater) per outbreak for the entire continental U.S. east of the Rocky Mountains.

b. Interannual Trends

Analyses of interannual trends in tornado outbreak day frequency suggest that non-meteorological influences on tornado data (e.g., population biases, reporting errors, and changes in verification efforts through time), while not completely absent, may not be as prevalent in the tornado outbreak dataset used for this study compared to datasets used in other studies. Tornado outbreak day frequency between January and April 1950-2010 increase by 0.16 day annually (Figure 3.5) and tornado counts in those outbreaks increase by about 3.34 tornadoes annually (Figure 3.6). These figures are not as large as those identified in BDK03, who found that tornado days from January 1955 to December 1999 increase by about 0.5 day per year and that tornado counts on those days increase by about 14 per year. Some of these differences arise from the time period of study and exclusion of tornadoes that occur from May to December and from varied definitions of a tornado day (1 tornado in the continental U.S. in a 24-hour period in BDK03, 6 tornadoes in the continental U.S. east of the Rocky Mountains in a 24-hour period in the current study). A possible explanation for the less pronounced trends in the current study is discussed by CS08, who state that underreporting of tornadoes is not as likely when high-impact tornado outbreaks are occurring.

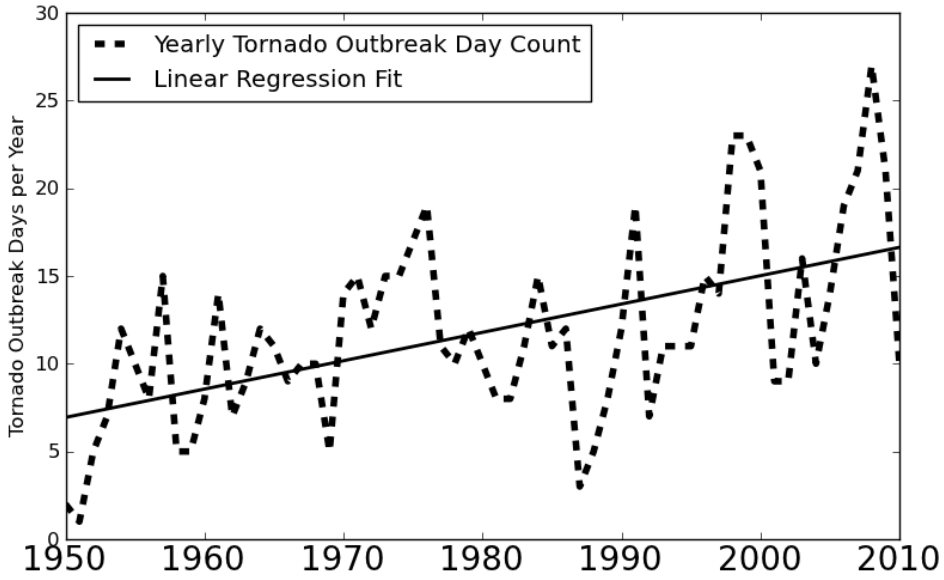

Figure 3.5: Yearly counts of January through April tornado outbreak days from 1950 to 2010 throughout the entire study region (r^2 = 0.28).

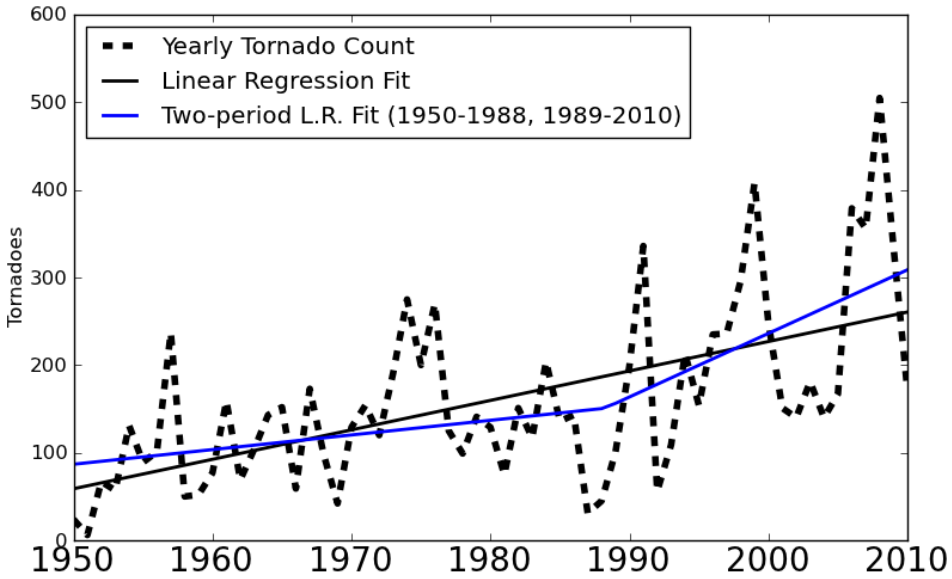

Figure 3.6: Yearly counts of tornadoes occurring on January through April tornado outbreak days from 1950 to 2010. Yearly tornado counts increase on average by about 3.34 throughout the entire 61-year period (r^2 = 0.34). This increase, however, is less pronounced early in the period (1.67 increase in annual tornado counts from 1950-1988; r^2 = 0.08) and more pronounced from 1989-2010 (7.26 tornado per year increase; r^2 = 0.17).

The nearly neutral trend in the annual number of strong (F/EF2+) tornadoes occurring in outbreaks suggests that this variable may be even more suitable for comparison of outbreaks across earlier and later periods in the dataset (Figure 3.7). Only a slight decrease in F/EF2+ tornadoes is observed (-0.24 per year) and although linear regression trends suggest 40-60 F/EF2+ tornadoes occurring in outbreaks can be expected in a given year from January-April 1950-2010, many years fall outside of this range and relatively active peaks are readily identified through peaks in 1956, 1974, 1990, 1999, and 2009. As mentioned previously, identification of neutral or nearly neutral trends in tornado activity across varying time periods in the dataset is helpful for making comparisons between tornado outbreaks in earlier versus later periods.

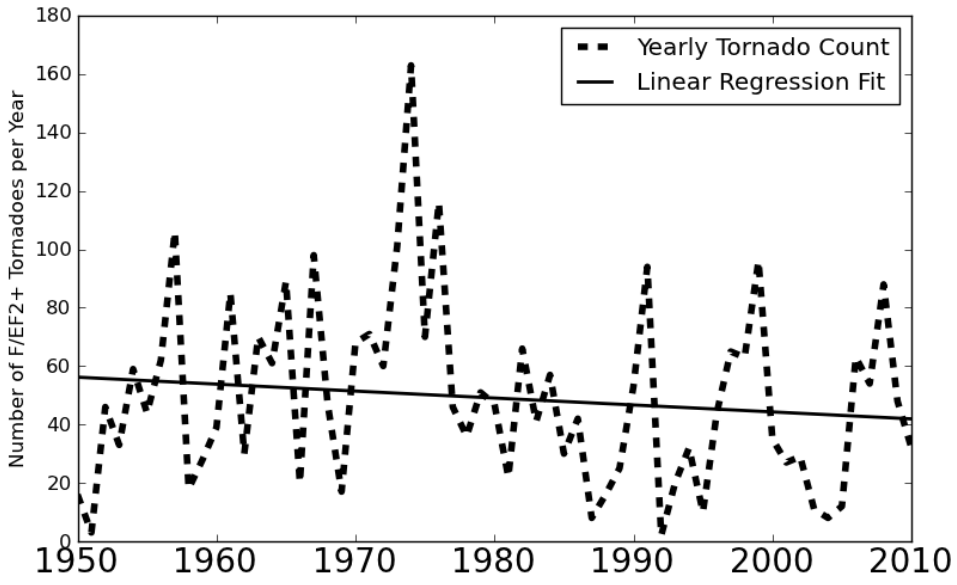

Figure 3.7: Yearly counts of tornadoes rated F/EF2+ that occur in January - April tornado outbreaks from 1950-2010 (r^2 = 0.017).

3.3 Tornado Strength

a. Intraseasonal Trends

As mentioned in Chapter 2, gridded DPI values are used to evaluate tornado destruction potential (an index combining strength and area affected by tornadoes) on a grid. Although DPI helps to readily identify locations of stronger, longer-tracked tornado activity, readers are referred to Chapter 2 for cautions regarding its interpretation and use for gridded analyses. Monthly evolution of DPI (shown in Figure 3.8) exhibits a similar shift to tornado counts shown in Figure 3.5 and also shows that the largest values exist across the south-central region in January and expand eastward into western Georgia in February. By March, greatest DPI values can be found in the southern states from Arkansas eastward to the Carolinas, although some increases are also noted in the Great Plains. The most dramatic northward and westward shifts can be found in the "M16" and April periods, where relative maxima in DPI can be found in the Texas Panhandle, southern Kansas and northern Oklahoma, and along an axis from southern Arkansas through Central Mississippi, central Tennessee, and northward through Indiana. The fact that larger DPI exists in early spring than in winter months is most likely tied to a subtle increase in the number of strong (F/EF2+) and violent (F/EF4+) tornadoes east of the Rocky Mountains (discussed in Section 3.2).

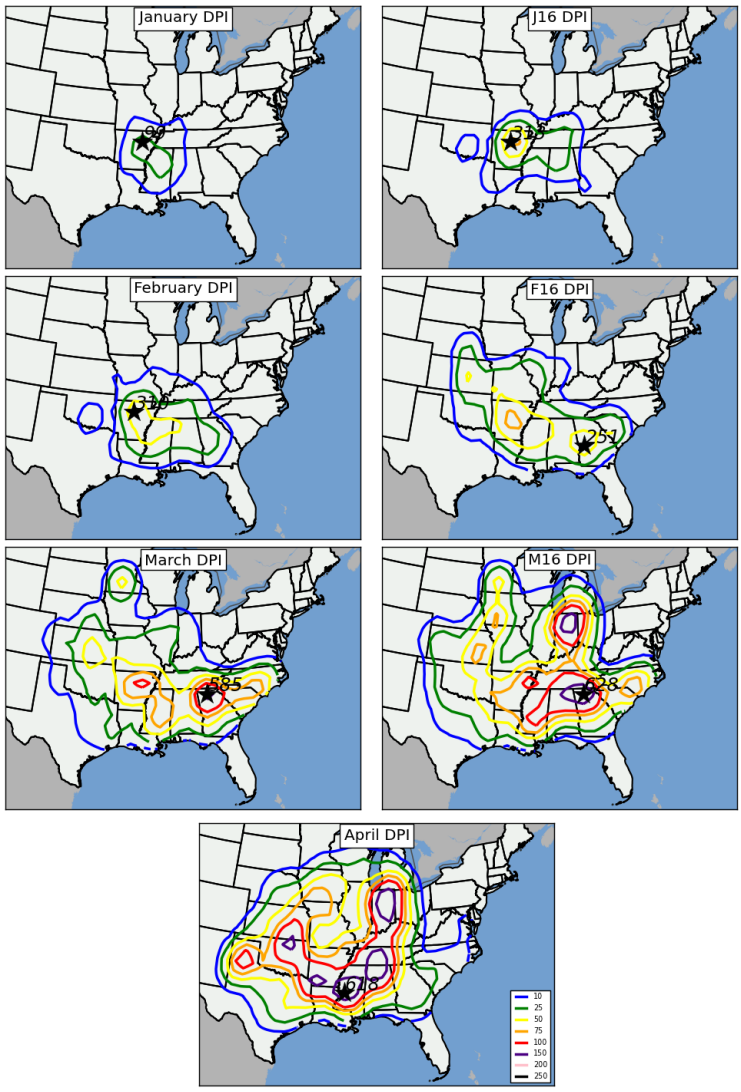

Figure 3.8: Contour plots representing gridded DPI in tornado outbreaks in each mid-month to mid-month period during 1950-2010. Star and associated number indicates location and number of maximum DPI on the grid. As mentioned in Section 2.1.b, a Gaussian filter with bandwidth = 1° was applied to the data before isoplething.

A comparison of trends in the evolution of DPI (Figure 3.8) and monthly and mid-monthly tornado counts (Figure 3.1) suggests that weaker, brief tornadoes are more common in the Great Plains than in locations farther to the east in an axis from Mississippi to Indiana, especially in the March-April time period. Maxima in tornado counts and DPI are in similar

areas of the Mid-South in January and February, but diverge in March as DPI increases drastically over northern Georgia, but tornado count maxima begin a westward shift toward the Plains. By April, the greatest tornado counts can be found in southern Oklahoma and northern Texas, which are quite different from the aforementioned DPI maxima which stretch from central Mississippi northeastward to Indiana and in northeastern Oklahoma and southwest Arkansas. Figure 3.9 also highlights these differences in regional values of DPI and include an axis of higher DPI per tornado in the same aforementioned areas (central Mississippi northeastward to Indiana).

As mentioned earlier, a distinct benefit of conducting a spatial analysis of DPI is that it readily identifies regions impacted by particularly powerful outbreaks featuring long-tracked, strong tornadoes. Table 3.4 shows particular outbreaks that have a large impact on regions of DPI maxima shown in Figure 3.8. The outbreaks outlined in Table 3.4 indicated where local maxima in gridded DPI values were impacted by at least one particularly intense tornado outbreak where DPI values greater than 200 occurred in a tornado outbreak day. A major drawback to DPI analyses such as these, however, is that in some cases, one strong, long-tracked tornado can heavily influence the DPI maximum in a particular area (e.g., southern Minnesota on March 29, 1998, Table 3.4) while in other instances numerous strong and/or violent tornadoes can increase the DPI across two or more outbreaks (Indiana on April 11, 1965 and April 3, 1974). This leads to some complications of analyzing gridded DPI values and necessitates

comparison of DPI to tornado counts to discern where stronger tornadoes are occurring in a climatological sense. Figure 3.9 illustrates gridded DPI values for grids containing five or more tornadoes to help remove outliers in DPI produced by only one or two tornadoes. Comparing Figure 3.9 to Figure 3.8 further reinforces the aforementioned observations that 1) DPI maxima do not necessarily coincide with tornado count maxima and that 2) on average, DPI values per tornado are higher from Indiana southward to central Mississippi than they are across the southern Great Plains, indicating a higher frequency of more impactful and damaging tornadoes across areas east of regions typically referred to as 'Tornado Alley' across the Great Plains.

Date	Location	DPI
January 21, 1999	AR, MS, TN, LA, MO, IL	249.71
February 5, 2008	AR, MS, TN, KY, MO, IN	768.83
February 21, 1971	LA, MS, AR, TN	255.31
March 28, 1984	NC, SC, GA, AL	945.73
March 13, 1990	KS, OK	673.91
March 1, 1997	AR, TN, MS, KY	474.33
March 29, 1998	MN, WI	460.75
April 11, 1965	IA, IN, WI, IL, MI, OH	1175.35
April 17, 1970	TX, NM	644.97
April 3, 1974	IL, IN, MI, OH, KY, TN, AL, MS, GA, NC	2384.08
April 2, 1982	AR, OK, TX, LA, MS, TN, MO, IL, IA	293.6
April 26, 1991	KS, OK, TX, NE, MO, IA	634.4
April 24, 2010	TX, MS, AL, GA, TN, KY	1585.13

Table 3.4: Selected tornado outbreak days that contributed strongly to gridded DPI quantities in Figure 3.5.

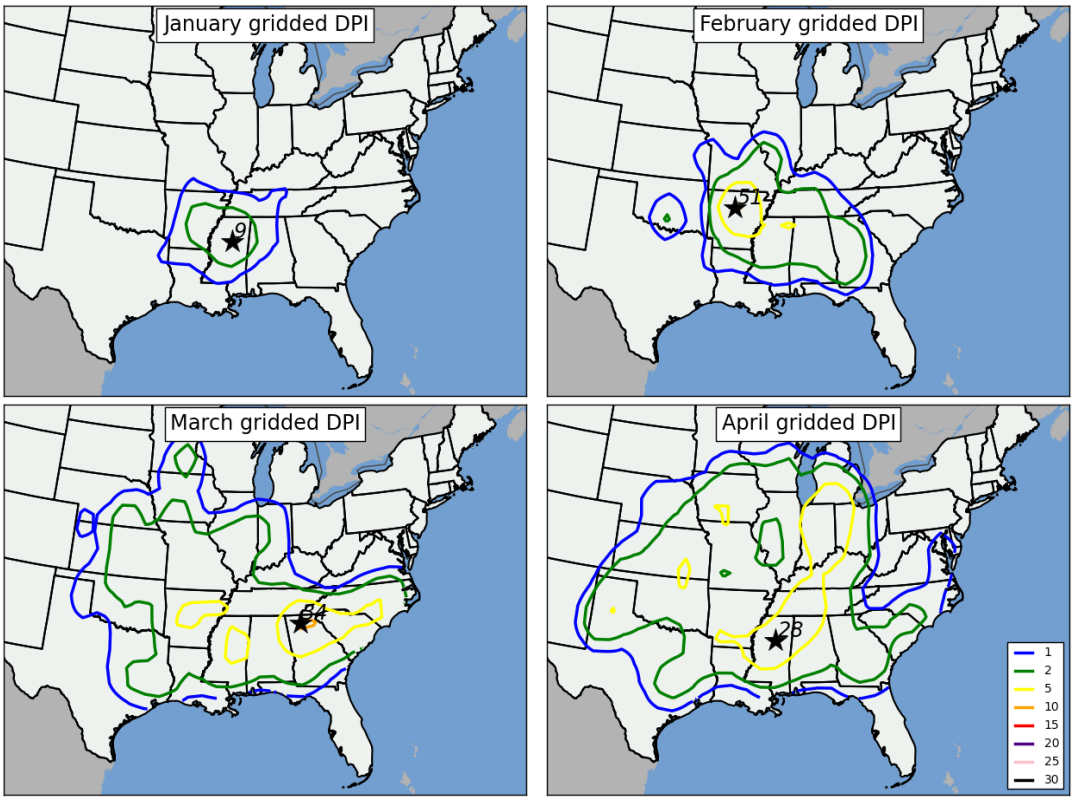

Figure 3.9: Contour plots showing monthly average DPI per tornado for each grid box containing five or more tornadoes. Star and associated number indicates location and number of maximum tornado occurrences on the grid. As mentioned in Section 2.1.b, a Gaussian filter with bandwidth = 1° was applied to the data before isoplething.

Seasonal trends in DPI suggest that stronger tornadoes with longer path lengths occur in early spring than in winter (Table 3.5), although much of this increase is attributed to large DPI values associated with violent tornadoes. The average DPI per tornado outbreak more than doubles between January (24.8) and mid-March to mid-April (60.3) while the average DPI per tornado also doubles from 1.8 to 3.8 in that time period. The total DPI in each monthly or midmonth-to-midmonth period exhibits a dramatic seasonal increase; however, this is not an unexpected result given the fact that both tornado frequency and tornado outbreak frequency also

increase during the season (Table 3.2). Given the fact that the frequency of strong tornadoes in the four-month period is relatively constant and the fact that the frequency of violent tornadoes shows an increase (Table 3.3), the increase in DPI per tornado and DPI per tornado outbreak can be attributed mostly to the increases in violent tornadoes (rated F4 or F5), which account for nearly 40% of the total DPI in all outbreaks despite only accounting for 2.4% of all tornado events in the dataset!

	J	J16	F	F16	M	M16	A
Total DPI	1389	2324	3243	5814	10503	16342	21163
Average total DPI per tornado outbreak	24.8	36.3	39.1	47.7	55.9	60.3	54.3
Average DPI per tornado in tornado outbreak	1.75	2.69	3.64	3.81	4.23	4.28	3.80
Average total Path Length(mi.) per tornado outbreak	68.1	71.0	66.2	85.8	77.7	82.5	78.4
Number of outbreaks with DPI above 25	14	18	27	43	61	88	119
Number of outbreaks with DPI above 50	9	12	16	26	38	55	76

Table 3.5: Seasonal evolution of DPI in tornado outbreaks east of the Rocky Mountains. Monthly and midmonth-to-midmonth definitions are consistent with those in Table 3.1.

Bias-corrected, accelerated confidence intervals (BCa CIs) calculated for DPI in five 3° by 3° regions across the U.S. (Figure 3.10) provide further detail regarding seasonality in localized areas with slightly different trends than in regional tornado counts. DPI is much higher in April in northern Alabama, despite tornado maximum residing in northern Texas at that same time (Figure 3.10). In January and February, however, DPI is much higher in the south central and northern Alabama regions compared to other

regions, while not much increase in DPI is noted at all between January and April in the south central region compared to other regions (especially northern Alabama). A key question is raised when investigating these diagrams: is DPI difference between northern Alabama and other regions meteorologically driven?

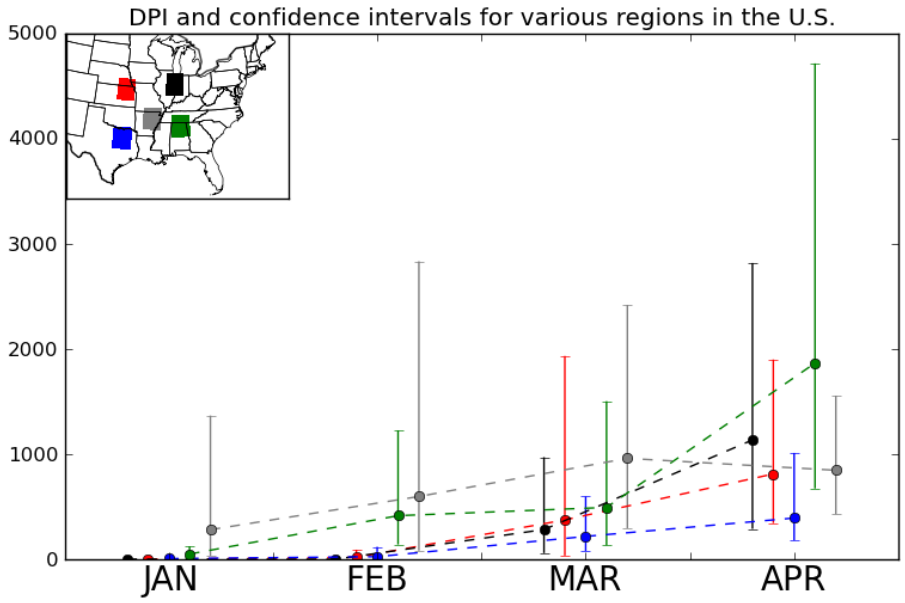

Figure 3.10: Monthly total DPI (dashed lines) and 95% BCa CIs around the sum of monthly tornado counts (brackets) in five 3° by 3° regions shown in inset. Lines and brackets are color-coded based on their respective region.

b. Interannual Trends

A more stable trend in tornado intensity and area impacted through time compared to tornado counts in outbreaks and tornado outbreak frequency is observed based on interannual DPI counts in tornado outbreaks (c.f.,Figs. 3.5 and 3.6). Although a positive trend in time is

identified in DPI (increase of 6.91 per year), much of this increase can be attributed to relatively large values in DPI in the last three years of the dataset (2008-2010). Removing these years yields a neutral trend from 1950-2007 (increase of only 2.15 per year, Figure 3.12). Because of the heavy weighting of DPI toward long-tracked, strong tornadoes, years with many intense tornado outbreaks (i.e., 1974, 2008) are readily apparent. Although meteorological reasons for the differences between the relatively stable trends identified in Figures 3.11 and 3.12 compared to Figures 3.5 and 3.6 may exist, these differences are more likely influenced by several artifacts of the database, including 1) decreased average path lengths due improved surveying of individual storms and enhanced efforts by the National Weather Service for detailed information about tornado paths during later parts of the period and 2) decreases in ratings due to greater scrutiny of tornado damage compared to tornadoes that occurred earlier in the period of study.

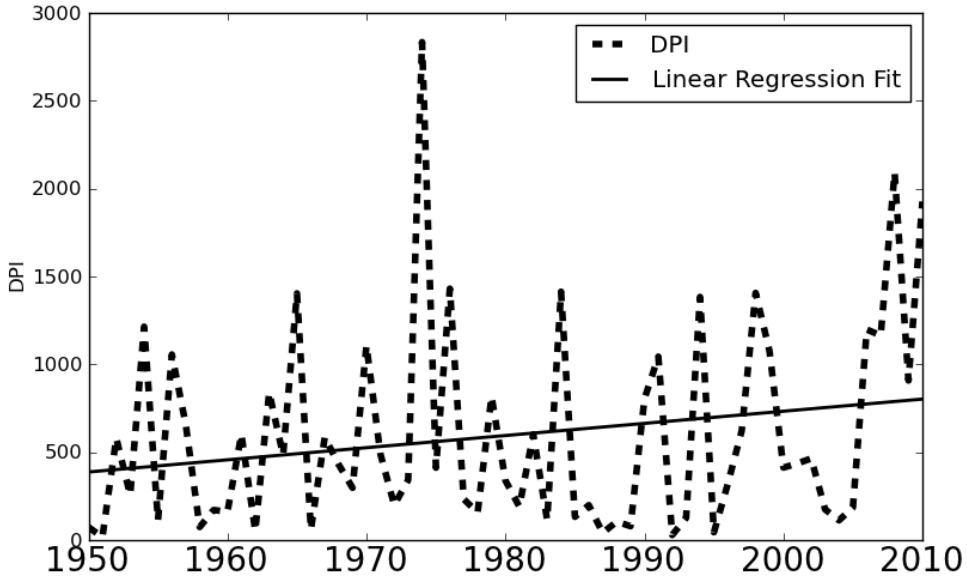

Figure 3.11: Yearly DPI for all January through April tornadoes occurring in tornado outbreaks from 1950-2010 (r^2 = 0.04).

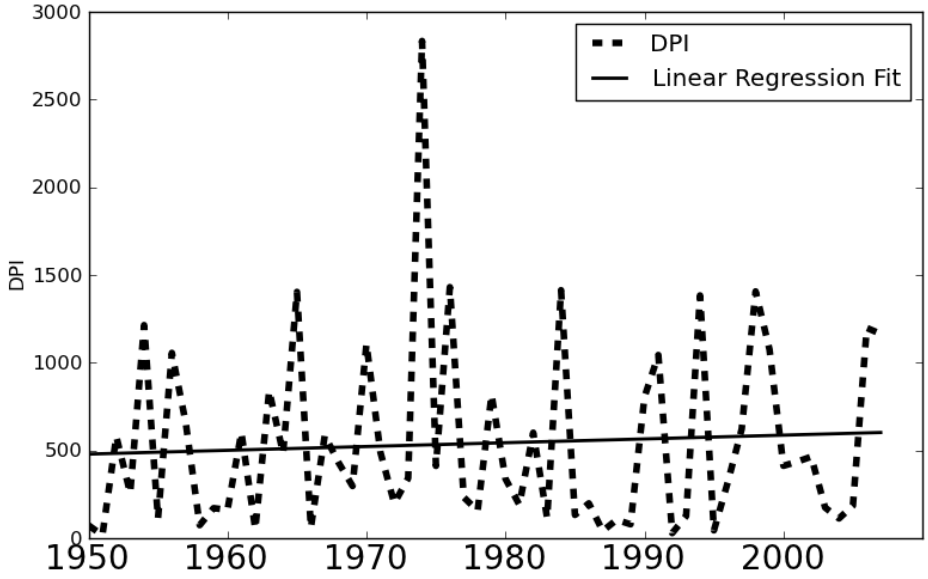

Figure 3.12: Yearly DPI for all January through April tornadoes occurring in tornado outbreaks from 1950-2010 (r^2 = 0.004).

3.4 An Atmospheric Tornado Outbreak Climatology

As with any tornado climatology, uncertainties and weaknesses related to accuracy in tornado reporting (first introduced in Section 1.2 and described fully in Section 2.1) will remain. Despite these weaknesses, meaningful results can be derived from conducting physical tornado climatologies. Related studies on concurrent atmospheric conditions that corroborate with results from physical tornado climatologies can also be particularly beneficial. Two key results were identified through the physical tornado climatology presented in Sections 3.1-3.3 that will be used throughout the remainder of the dissertation: 1) Drastic increases in tornado activity from January through April have been discussed, with a westward and northward shift of tornado maxima from the Lower Mississippi Valley into the Southern Great Plains during that time period, and 2) Several metrics for gauging synoptic-scale atmospheric patterns more conducive for tornado outbreaks were developed, including average number of tornadoes, significant tornadoes (rated F/EF2 or greater), DPI, and cumulative path length per tornado outbreak. Although the aforementioned metrics for differentiating tornado outbreaks have been used before (Pautz 1969, Galway 1977, BDK03, Verbout et al. 2006, Doswell et al. 2006), spatial analyses of DPI have never been accomplished before. Furthermore, the creation of a PCA-based atmospheric climatology of synoptic-scale featureas associated with individual tornado outbreaks has never been documented before in the scientific literature.

The focus of the following synoptic-scale atmospheric climatology revolves around the relationships between those synoptic-scale atmospheric features related to tornado activity (discussed in Section 2.2), their behavior and seasonal evolution, and also their relationship to the physical tornado climatology outlined in Sections 3.1-3.3 of this Chapter.

a. Surface cyclones

Surface cyclones were analyzed using the S-mode PCA methodology outlined in Section 2.2.b.ii on sea-level pressure (SLP) extracted from Reanalysis data concurrent to tornado outbreak times. Resulting composite maps indicate that many of the outbreaks that occur in the four month period are accompanied by a surface cyclone, usually positioned to the north and/or west of locations of tornado activity (Figures 3.13 through 3.16). These surface cyclones varied in position across a large part of the country, stretching from the Upper Midwest and Great Lakes regions (January PC2+, January PC5+, January PC6+, January PC7-), Mid-Mississippi Valley (January PC7+, January PC1-, and January PC6-), Southern Great Plains (January PC1+, January PC3+), and southeastern U.S. (January PC3-). The varied location of surface cyclones support the observation in the physical climatology that tornadoes can occur in northern portions of the study domain (east of the Rocky Mountains), well displaced from the southern tier of the U.S. at any time during the four-month period of study.

A gradual westward movement of surface cyclones during tornado outbreaks is also observed during the period (Figures 3.13 through 3.16). In April, a greater proportion of the SLP composites contain surface cyclones positioned in the southern (April PC3-, April PC5-) and central Great Plains (April PC2+, April PC3+, April PC4+, April PC6+, April PC4-, and April PC7-). Two of the composites contain surface cyclones positioned even farther west (northeastern Colorado, southwestern Nebraska in April PC1-) and north (western Wisconsin and southeastern Minnesota in April PC5+) than any of the aforementioned surface cyclones indicated in the Great Plains. In comparison, only two SLP composites of January tornado outbreaks indicated surface cyclones in the southern Great Plains region (January PC1+, January PC3+). This observation is consistent with findings in the physical climatology (Section 3.1) that indicate a westward expansion in tornado occurrence with progression toward mid-March and April.

In each of the months in the study, deep surface cyclones are observed across the western U.S. far removed from tornado activity east of the Rocky Mountains (e.g., January PC6+, Figure 3.13). Often times, these deep surface cyclones were associated with much weaker surface cyclones over the central U.S. in proximity of tornado activity. These types of patterns are also reflected in geopotential height fields as discussed in Section 3.4.c.

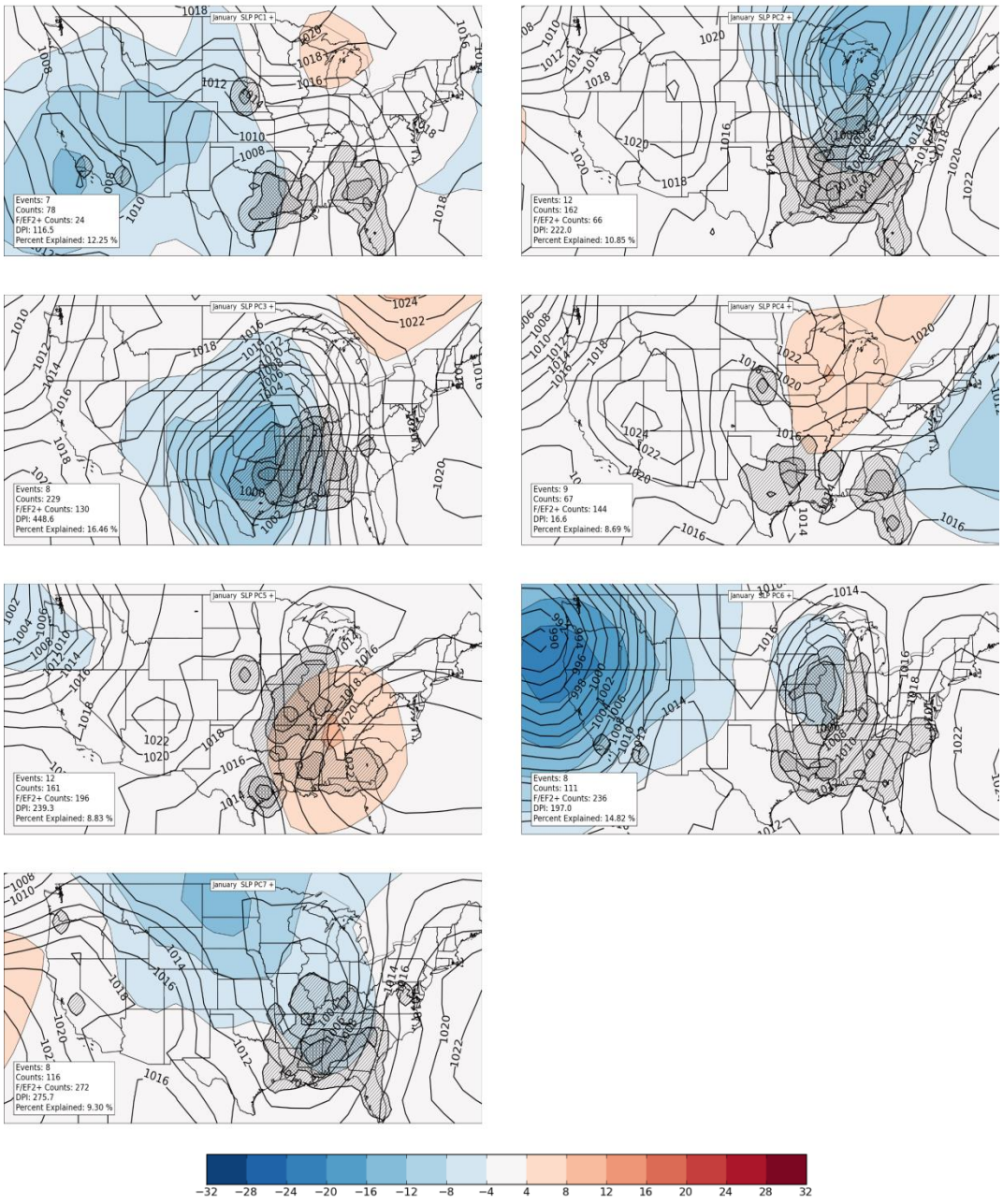

Figure 3.13: Composites of January SLP in tornado outbreaks containing VRPC scores greater than or equal to 1 (black contours, units in kilopascals). Shaded regions in blue (red) indicate where composited mean SLP fields are below (above) average of the mean January SLP field for all January tornado outbreaks in the entire dataset. Tiers of hatched areas indicate relative concentrations of tornado activity that are counted on a 1° latitude/longitude grid in a manner similar to that outlined in Section 2.1.b.iii. A Gaussian filter with bandwidth = 1° was applied to the data before hatching.

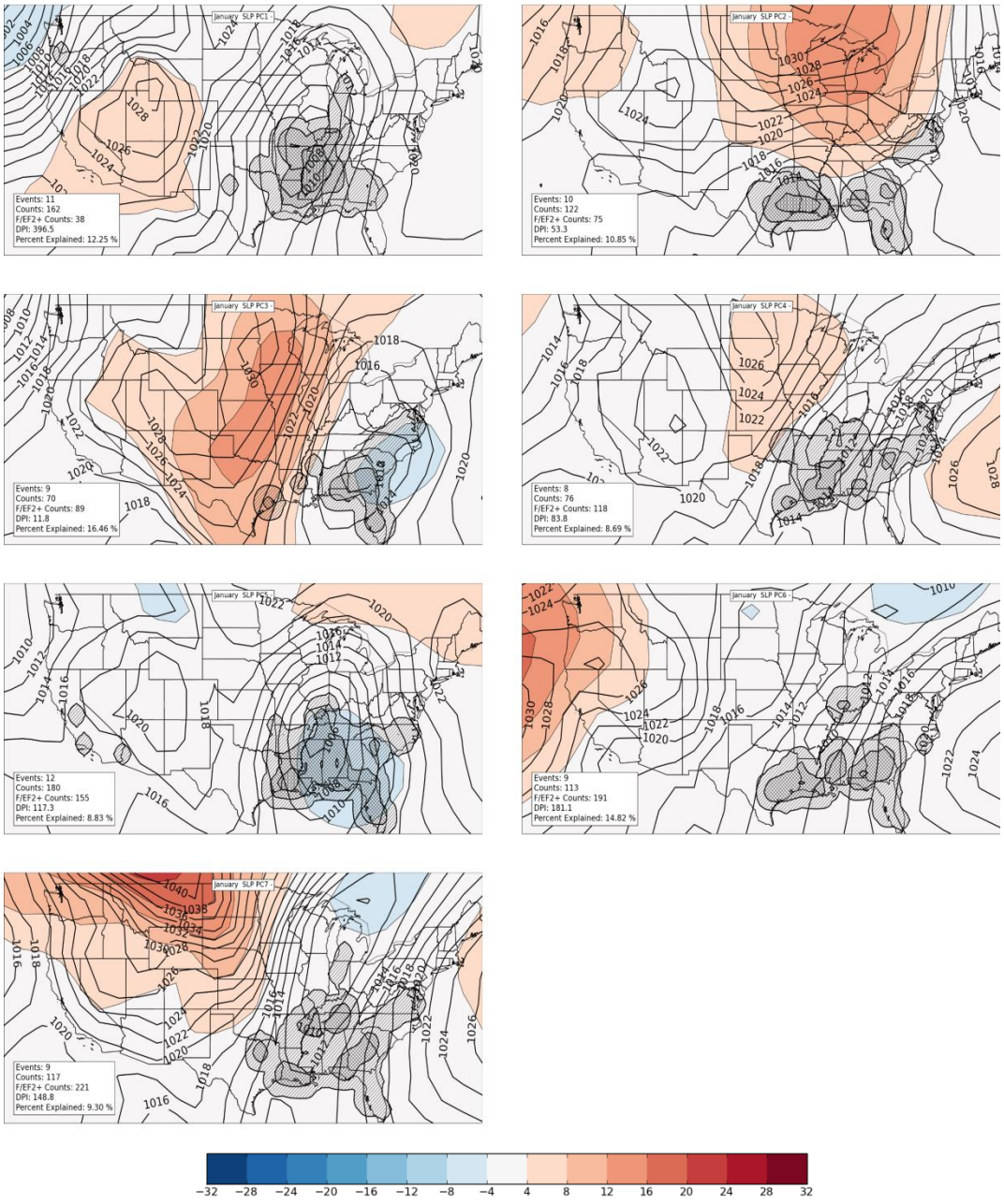

Figure 3.14: As in Figure 3.13, except for events with VRPC scores less than or equal to -1.

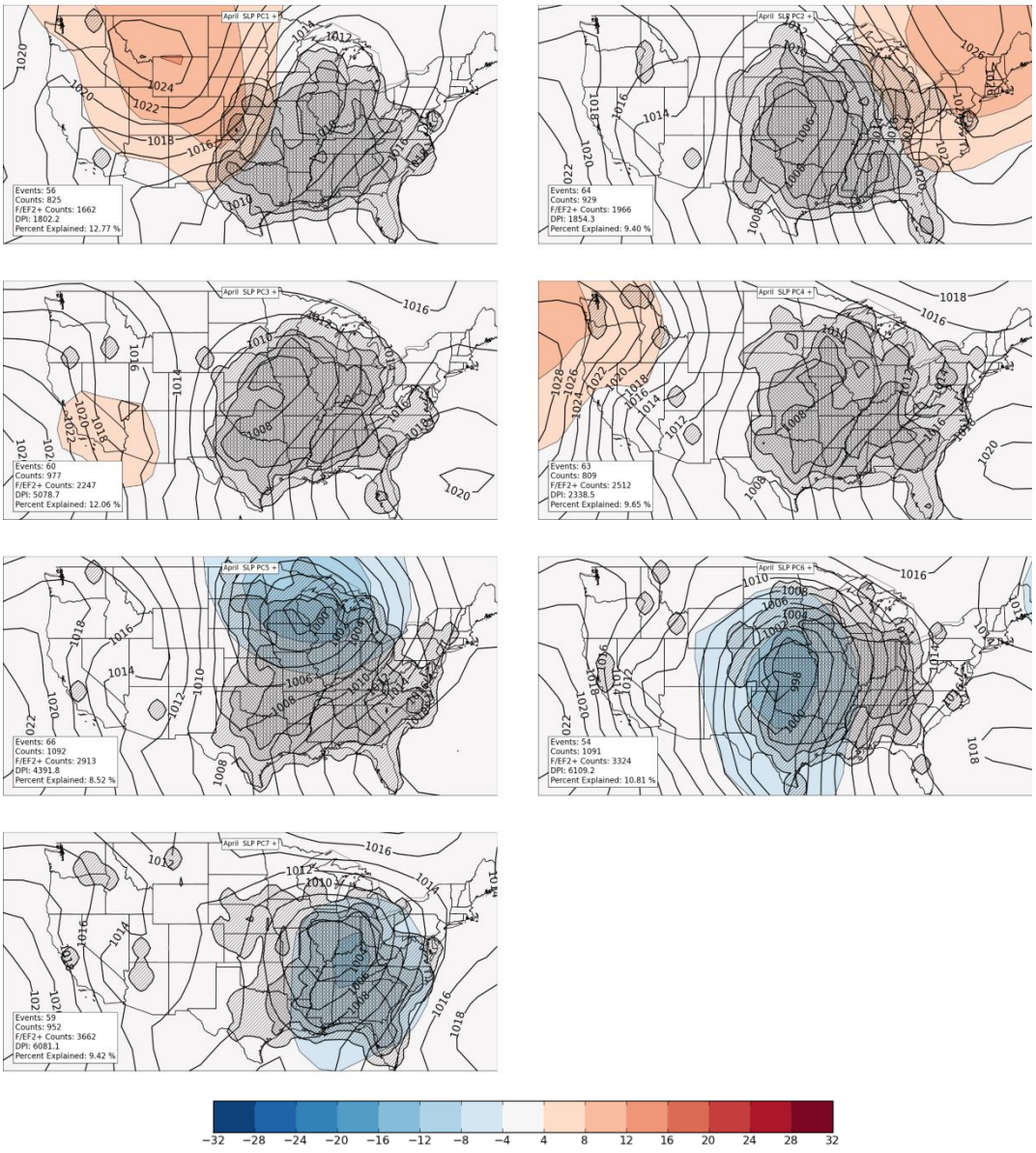

Figure 3.15: Composites of April SLP in tornado outbreaks containing VRPC scores greater than or equal to 1 (black contours, units in kilopascals). Shaded regions in blue (red) indicate where composited mean SLP fields are below (above) average of the mean April SLP field for all April tornado outbreaks in the entire dataset. Tiers of hatched areas indicate relative concentrations of tornado activity that are counted on a 1° latitude/longitude grid in a manner similar to that outlined in Section 2.1.b.iii. A Gaussian filter with bandwidth = 1° was applied to the data before hatching.

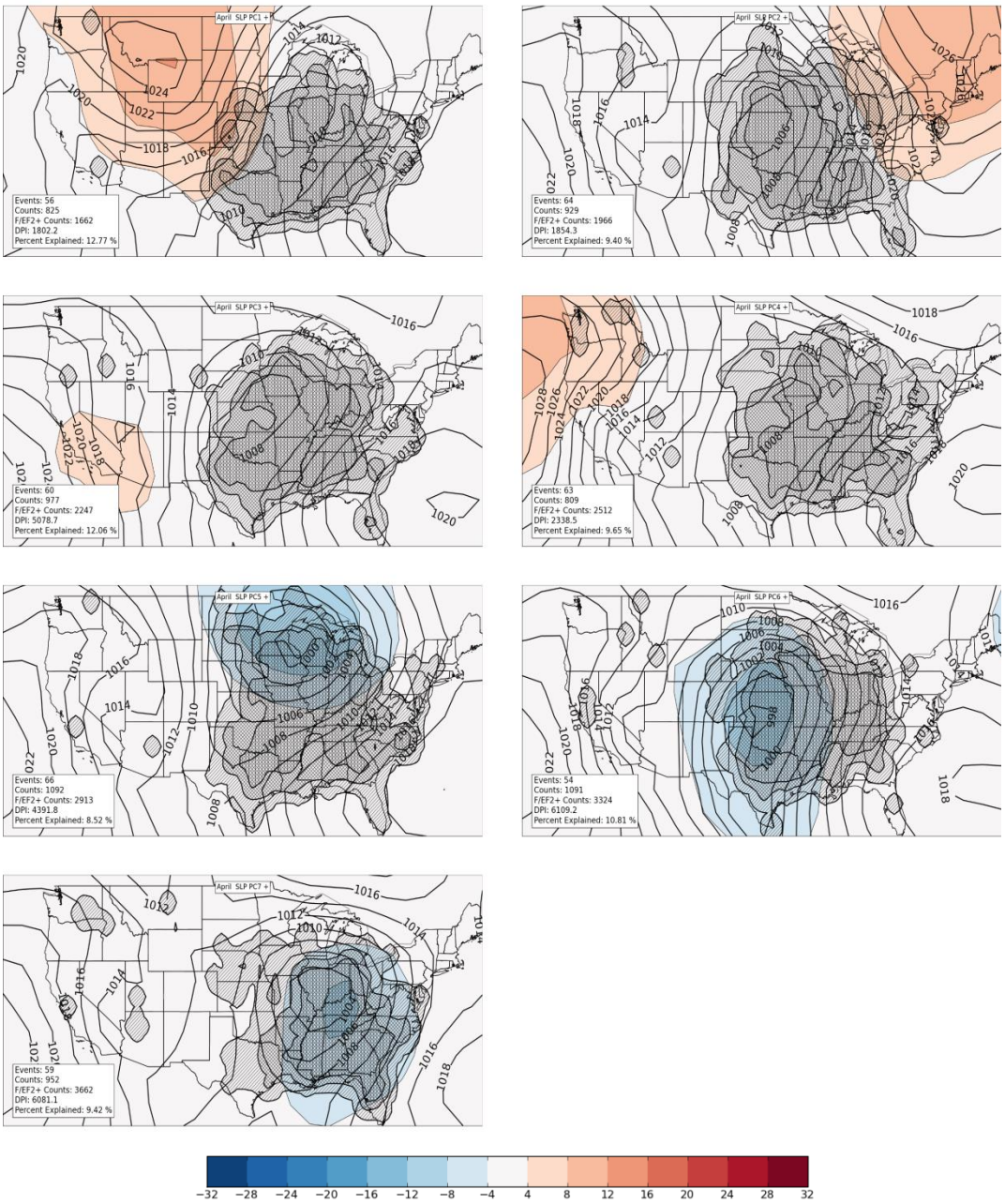

Figure 3.16: As in Figure 3.15, except for events with VRPC scores less than or equal to -1.

To further illustrate the material in Figures 3.13-3.16 in a condensed manner, plots of the location of minimum SLP in each composite were combined and plotted as shown in Figure 3.17. Tornado activity from events used to create each composite was also tallied on a one degree by one degree grid (as described in Section 2.1.b.ii) and contours plotted to indicate relative concentrations of tornado counts. These plots help succinctly describe spatial shifts in locations of atmospheric features related to tornado outbreaks on an intraseasonal basis (this section) and later as a function of ENSO (Section 4.4). Plots similar to these will be used to further assess spatial transitions within the atmospheric tornado outbreak climatology.

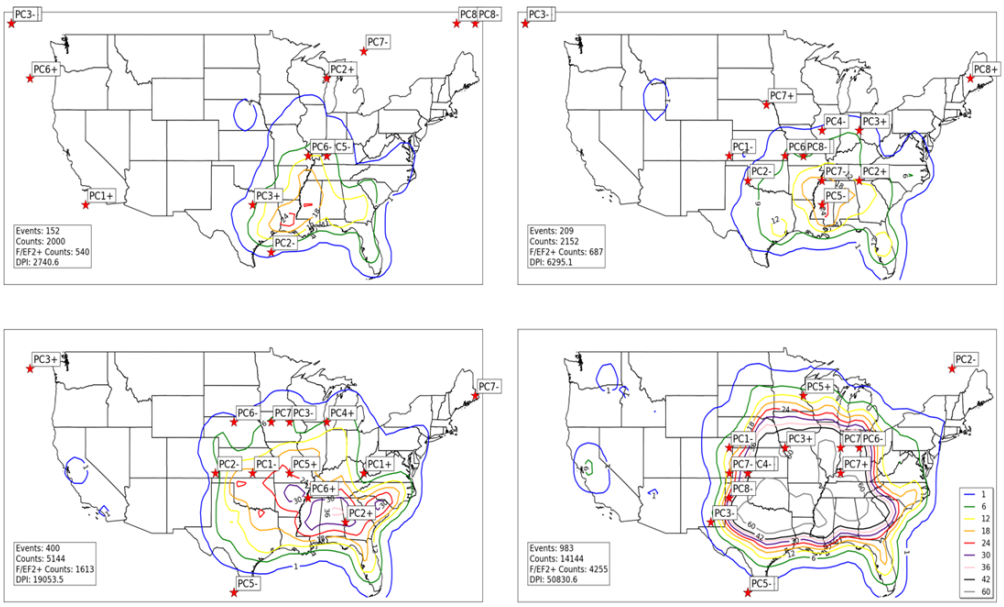

Figure 3.17: Locations of minimum SLP (noted by red stars) for all January tornado outbreak SLP composites (upper left), all February tornado outbreak SLP composites (upper right), all March tornado outbreak SLP composites (lower left), and all April tornado outbreak SLP composites (lower right). Contours represent concentrations of tornado activity concurrent with events used to create composites. Tornado counts are on a 1° by 1° grid as described in Section 2. 1.b.ii.

b. Low-level Jets

Low-level jet streams were analyzed using the S-mode PCA methodology outlined in Section 2.2.b.ii on 850 hPa geopotential height fields extracted from Reanalysis data concurrent to outbreak times. After individual events were grouped into composites using the procedure explained in Section 2.2, 850 hPa V-component wind fields from those same individual events were grouped and composited to analyze position of low-level jet axes. 850 hPa V-component wind fields were deemed sufficient for analysis given the climatological orientation of the low-level jet stream from south to north near tornado outbreak regions east of the Rocky Mountains (Blackadar 1957, Bonner and Paegle 1970, Uccelini and Johnson 1979, Maddox et al. 1980, Stensrud 1996, Mead and Thompson 2011, Weaver et al. 2012).

Generally, 850 hPa V-component wind maxima are concentrated in the southern and eastern parts of the U.S., just north of the Gulf of Mexico, with a westward trend in position of low-level jet axes with progression from January through April illustrated in Figure 3.18. Maxima in V-component wind during tornado outbreaks are observed mainly in the southeastern U.S. in January, but begin to increase in concentration to the west of those regions in February, March, and April. These are not unexpected results; low-level jet streams are responsible for transporting warm, moist lower-tropospheric air from maritime tropical sources into inland regions nearer tornado outbreaks (Section 2.2). The westward expansion of these low-

level jet streams is coincident with the westward migration of tornado maxima in the March-April time frame.

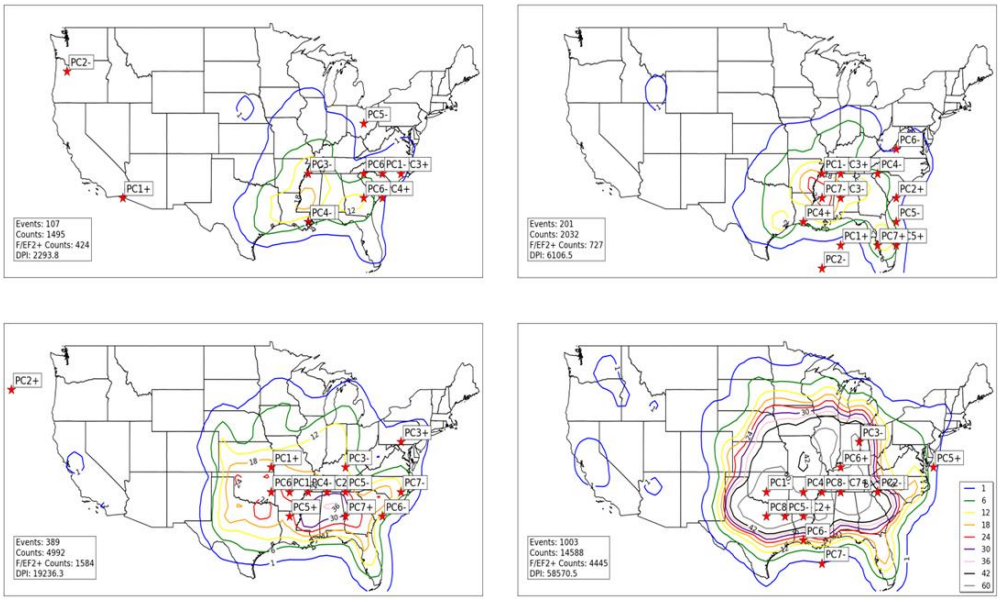

Figure 3.18: As in Figure 3.17, except red stars represent locations of maximum 850 hPa V-component wind in composites of 850 hPa geopotential height.

c. Mid- and upper-tropospheric geopotential height anomalies

As mentioned in Section 2.2.a.iii, geopotential height troughs and polar/subtropical jet streams existing between 700 – 200 hPa are noted as key synoptic-scale atmospheric features that influence tornado outbreaks. For identification of these atmospheric features, S-mode PCA was conducted on 300 hPa geopotential heights extracted from Reanalyses concurrent with tornado outbreak days and monthly tornado outbreak composites were created in a manner consistent with Sections 2.2.b.ii, 3.4.a, and 3.4.b. Due to the presence of geostrophic balance at all layers of

the atmosphere above the planetary boundary layer and the similarity of results from PCA of all layers from 700 hPa – 200 hPa, 300 hPa geopotential heights were deemed appropriate for this aspect of study.

Results from the composites verify that geopotential height troughs are present in many of the outbreaks in this study and that they usually exist adjacent to and northwest of locations of tornado activity (Figures 3.19-3.22). These height troughs vary widely in amplitude and can be rather weak on average (January PC2+, January PC7+, January PC4+, March PC7-, March PC4+) or large (January PC1+, January PC4-, March PC1+, March PC4+). The presence of troughs to the west of the locations of tornado occurrence results in southwesterly flow at the mid- and upper-troposphere nearer the tornado locations, which is a common occurrence in many tornado outbreaks (Schaefer and Doswell 1981, Barnes and Newton 1983).

Locations of geopotential height anomalies influence locations of tornado occurrence in outbreaks (Figures 3.19-3.22). January PC1+, February PC2+ (not shown), March PC7+, and April PC1- (not shown) contain a large area of negative anomalous geopotential heights in the northeastern U.S. In geopotential height patterns such as these, tornadoes tend to occur across the southern tier of the U.S. east of the Rocky Mountains and are also reduced in number farther north in Ohio and Pennsylvania. Another persistent pattern of height anomalies across each of the four months of study exhibits a strong geopotential height anomaly in

the far northwestern U.S. and adjacent areas of the Pacific Ocean and a lower-amplitude geopotential height trough in the central U.S. (January PC2-, February PC5- (not shown), March PC5+, April PC5+ [not shown]). Tornadoes in these types of geopotential height patterns tend to occur in the central and southern U.S. from Illinois southward to the Lower Mississippi Valley and eastern portions of the southern Great Plains (a surface reflection of this type of pattern is identified in PCA of SLP in Section 3.4.a). Generally, large areas of negative geopotential height anomalies across the intermountain western U.S. foster tornado outbreak development across the central and southern Great Plains (April PC4-, not shown), sometimes extending further east into the Lower and Middle Mississippi Valley (January PC8-, March PC8-).

Generally, locations of maximum negative geopotential height anomalies do not appear to change substantially during the January through April time period for most of the study domain (Figure 3.23). One exception to this appears to be over the south central region of the U.S.; several negative geopotential height anomalies are positioned across the south central U.S. from January through March (January PC8-, PC5-; February PC3-, PC5+, PC2-, PC6+, PC4-; March PC6+, PC4+, PC1-), but a noticeable absence of negative height anomalies are located in the same region in April (except for April PC6-). Although this finding supports the westward and northward migration of tornado count maxima discussed in Section 3.1.a, the overall similarity of large-scale patterns in outbreaks

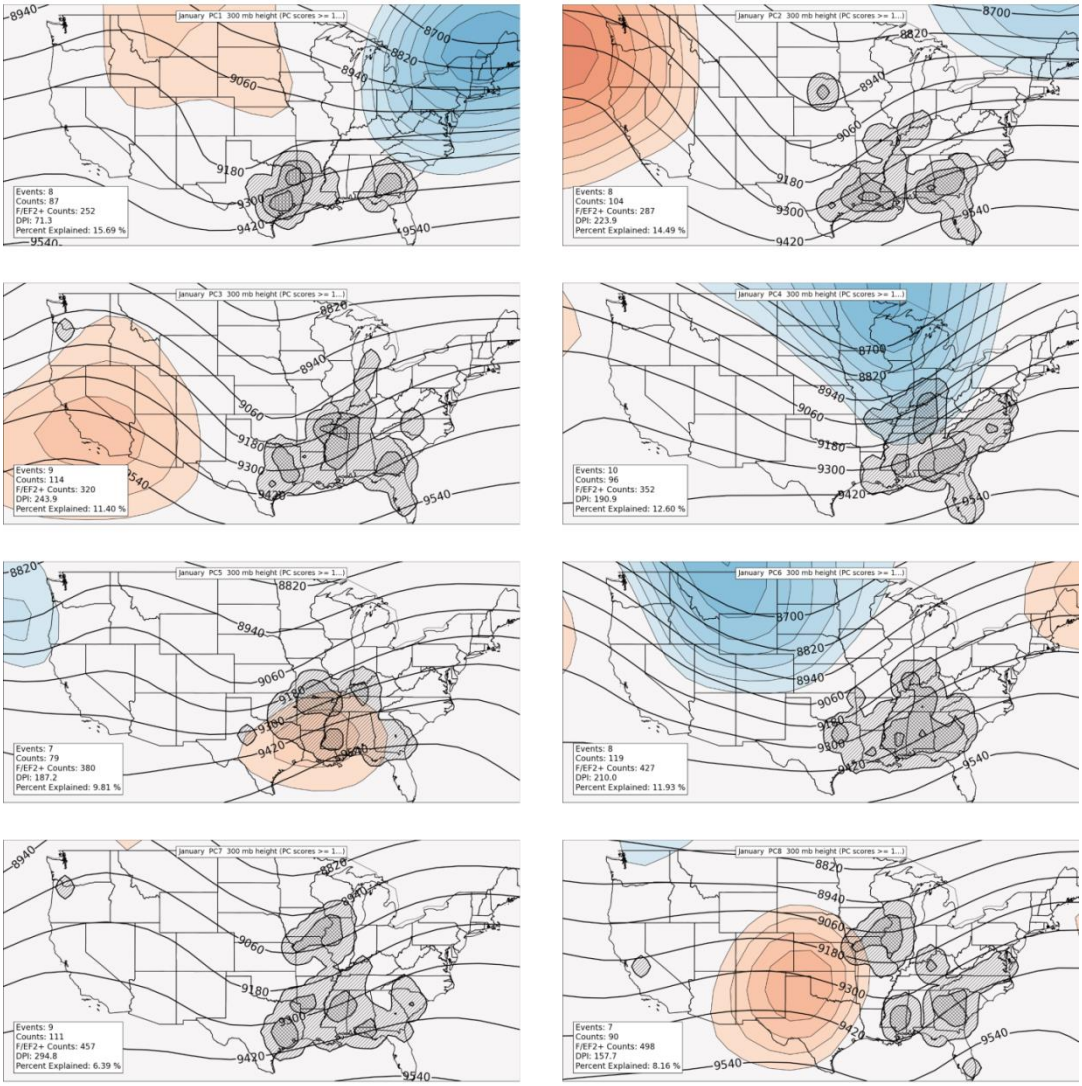

Figure 3.19: Composites of January 300 hPa geopotential heights in tornado outbreaks containing VRPC scores greater than or equal to 1 (black contours). Shaded regions in blue (red) indicate where composited mean height fields are below (above) average of the mean January 300 hPA geopotential height field for all January tornado outbreaks in the entire dataset. Tiers of hatched areas indicate relative concentrations of tornado activity that are counted on a 1° latitude/longitude grid in a manner similar to that outlined in Section 2.1.b.iii. A Gaussian filter with bandwidth = 1° was applied to the data before hatching.

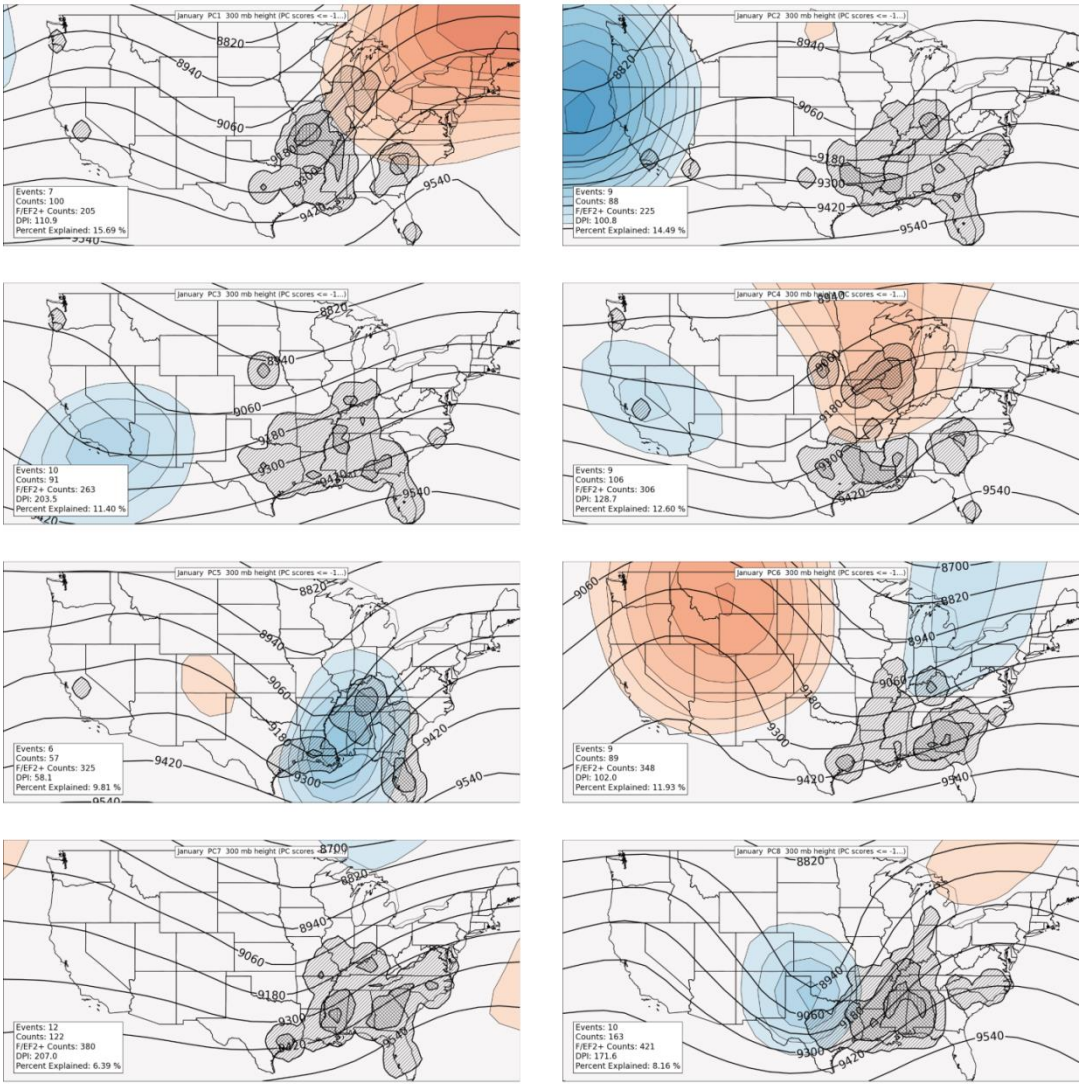

Figure 3.20: As in Figure 3.19, except for events with VRPC scores less than or equal to -1.

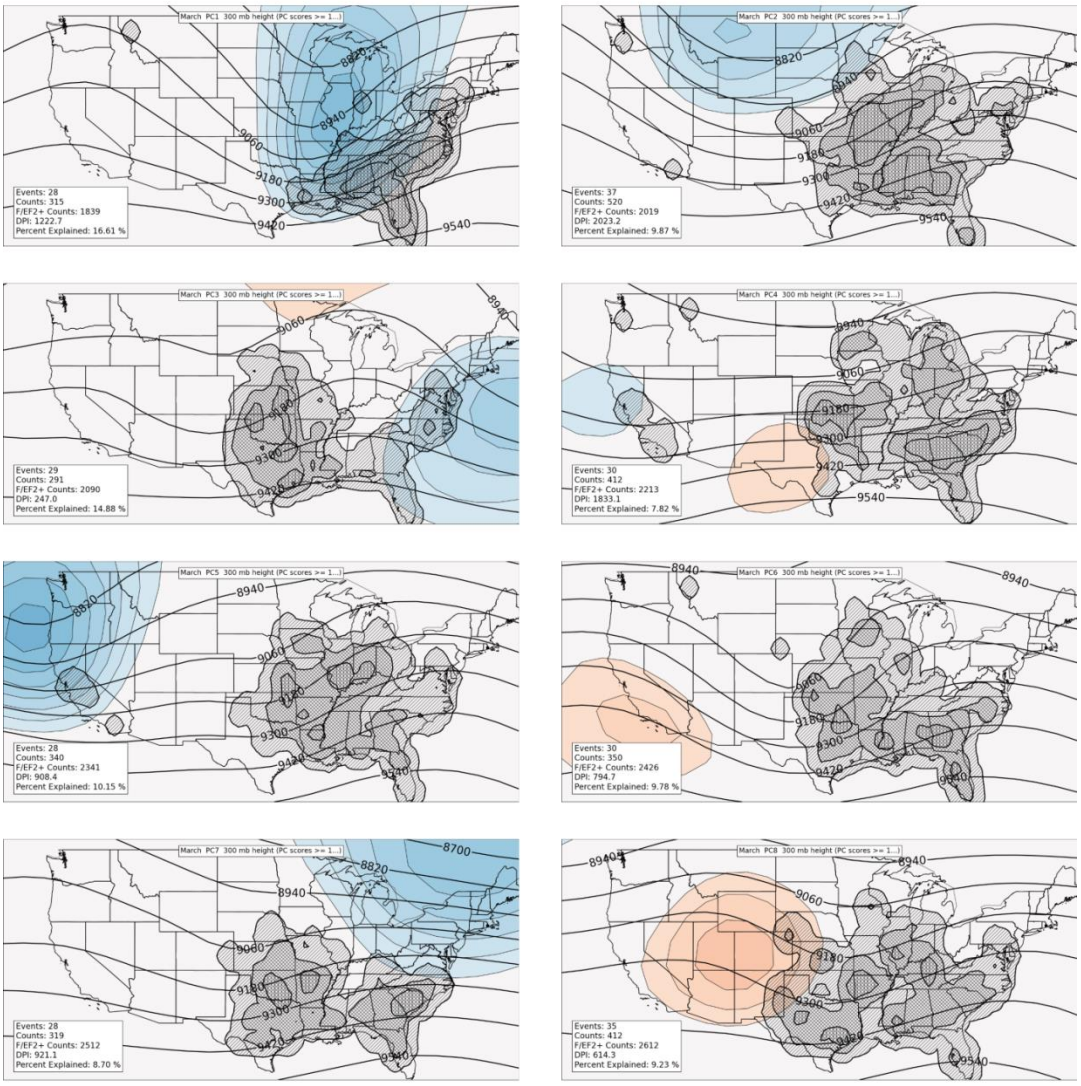

Figure 3.21: Composites of March 300 hPa geopotential heights in tornado outbreaks containing VRPC scores greater than or equal to 1 (black contours). Shaded regions in blue (red) indicate where composited mean height fields are below (above) average of the mean March 300 hPA geopotential height field for all March tornado outbreaks in the entire dataset. Tiers of hatched areas indicate relative concentrations of tornado activity that are counted on a 1° latitude/longitude grid in a manner similar to that outlined in Section 2.1.b.iii. A Gaussian filter with bandwidth = 1° was applied to the data before hatching.

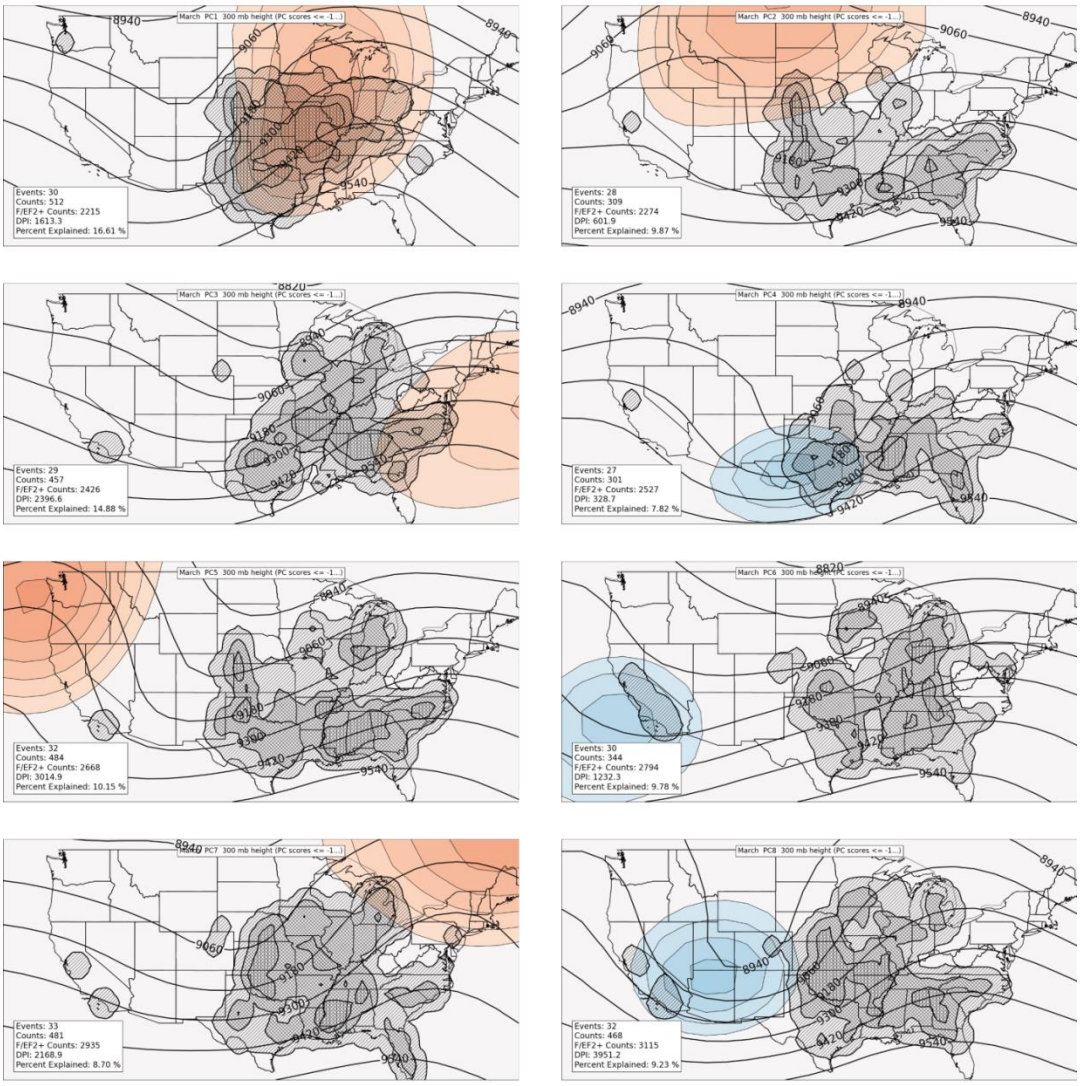

Figure 3.22: As in Figure 3.21, except for events with VRPC scores less than or equal to -1.

during the four-month study period supports the notion that although outbreaks in January are less frequent than their March and April counterparts, tornadoes occurring in those outbreaks can be just as numerous.

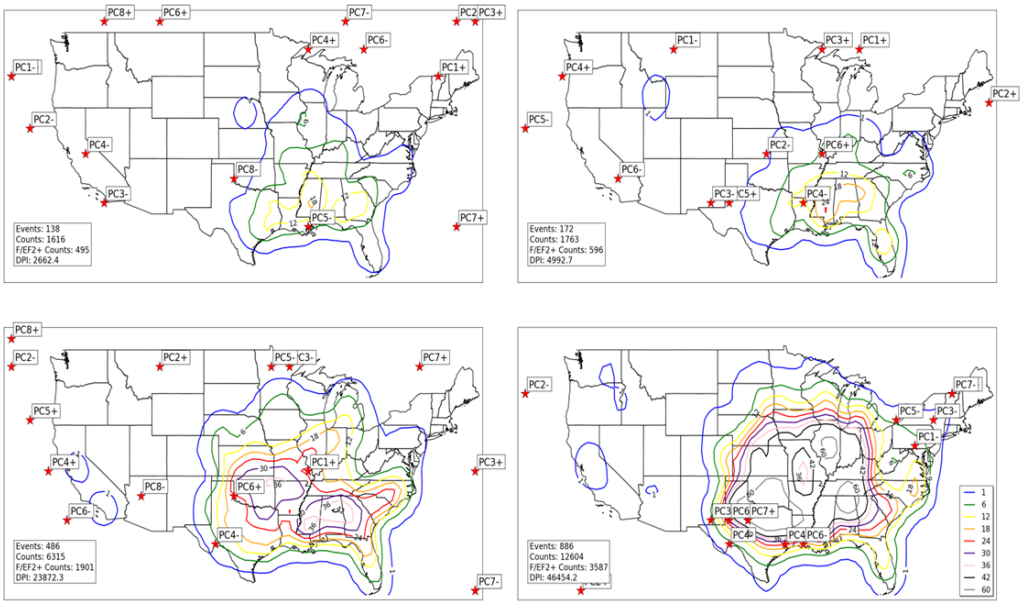

Figure 3.23: As in Figure 3.17, except red stars represent locations of largest negative 300 hPa geopotential height anomalies in composites of 300 hPa geopotential height.

d. Instability

Spatial anomalies of instability (as gauged by Lifted Index) appear to heavily modulate character of tornado activity in outbreaks. Negative (positive) anomalies of lifted index indicate regions of increased (decreased) tornado activity (Figures 3.24-3.27). When these negative anomalies occur

in northern and northeastern parts of the study domain, tornadoes tend to occur at higher latitudes (January PC1+, PC6+; April PC5+, PC1-). Relative decreases in tornado activity occur in regions of strongly positive anomalies of lifted index (indicative of increased static stability), most readily observed in the following composites: January PC2+, PC1-, PC4-; and April PC3+. These findings are consistent with discussion in Section 2.2 indicating increased static instability in regions of tornado outbreaks.

A general increase in instability is noted from January through April across a large part of the U.S. (Figures 3.24-3.27). In January, regions of strongest instability are noted across the southern and southeastern U.S. and adjacent areas of the Gulf of Mexico, with occasional axes of stronger instability (indicated by lifted indices less than zero) located farther inland across the Lower Mississippi Valley (January PC2-). In constrast, outbreak composites of lifted index in April indicate much more expansive areas of static instability, especially in April PC1- and PC3-. These observations are consistent with the notion that maxima in tornado activity expand westward and northward into the Great Plains with progression from January through April and also provide rationale for more frequent and numerous tornado activity in April.

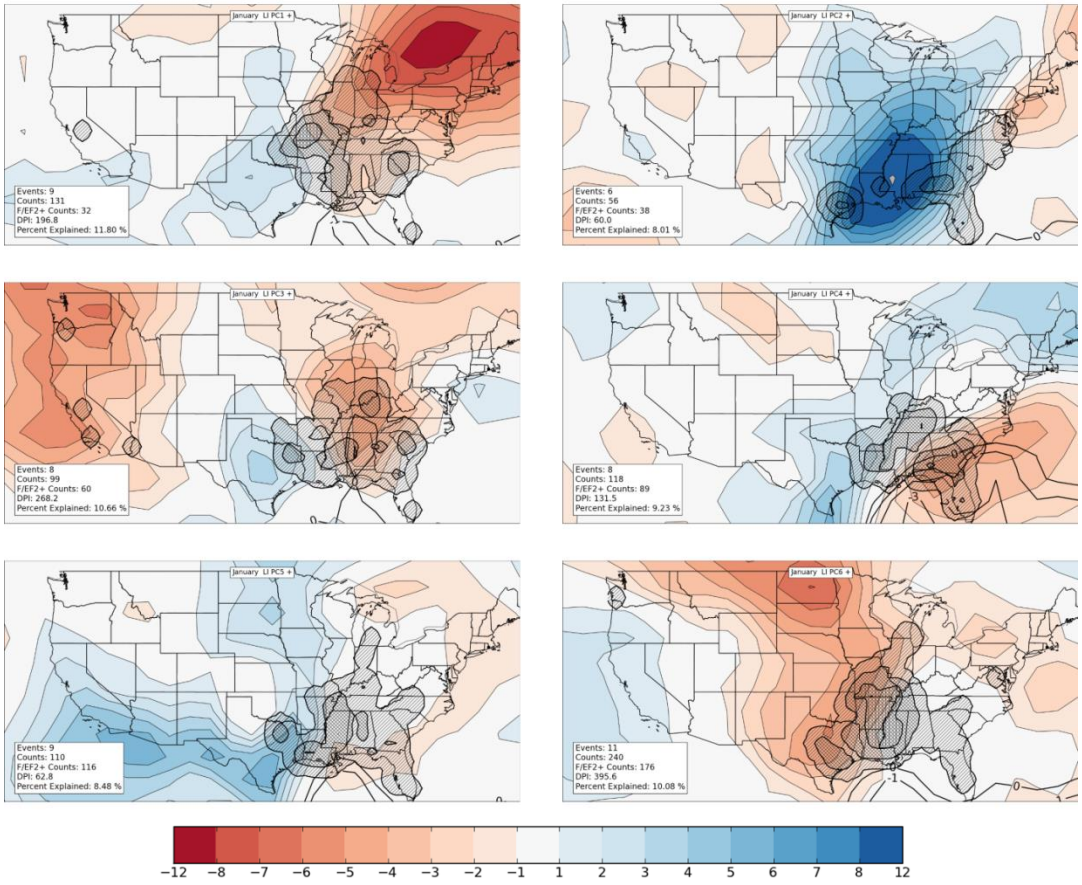

Figure 3.24: Composites of January lifted index in tornado outbreaks containing VRPC scores greater than or equal to 1 (black contours, units in degrees Celsius). Shaded regions in blue (red) indicate where composited mean lifted indices are above (below) average of the mean January lifted index field for all January tornado outbreaks in the entire dataset. Tiers of hatched areas indicate relative concentrations of tornado activity that are counted on a 1° latitude/longitude grid in a manner similar to that outlined in Section 2.1.b.iii. A Gaussian filter with bandwidth = 1° was applied to the data before hatching.

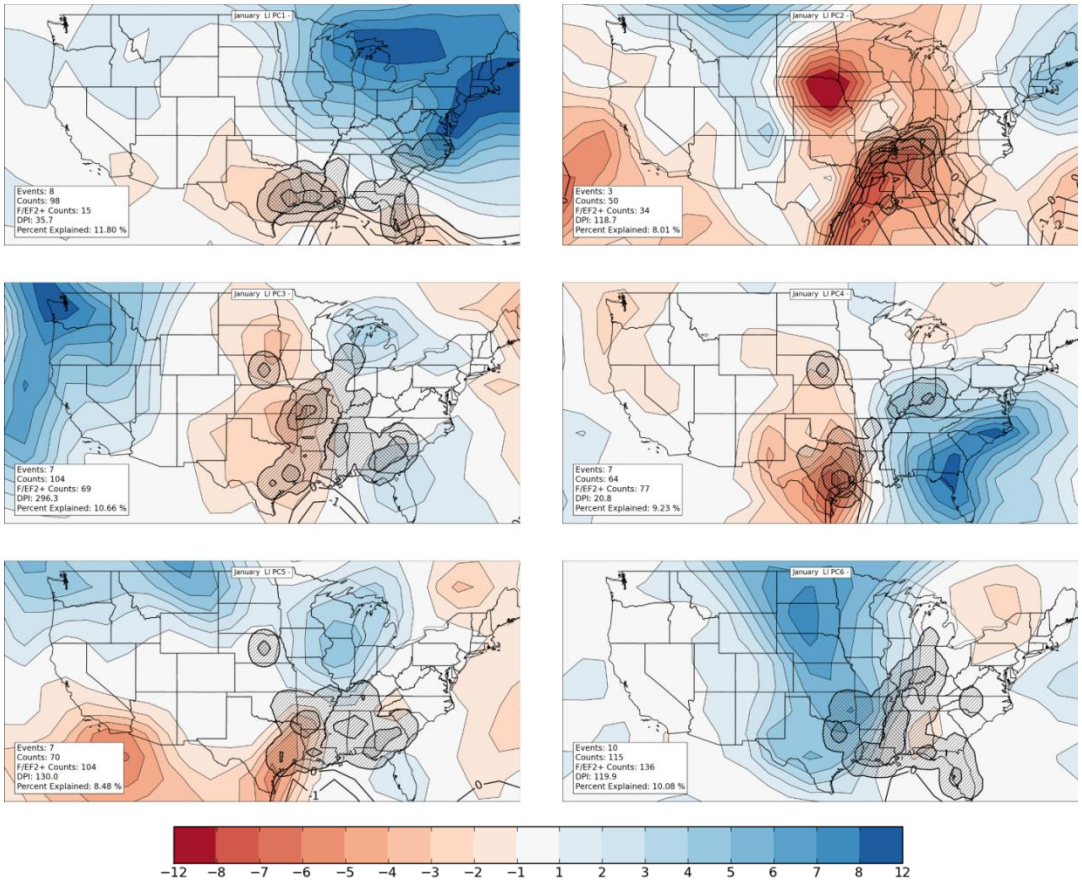

Figure 3.25: As in Figure 3.24, except for events with VRPC scores less than or equal to -1.

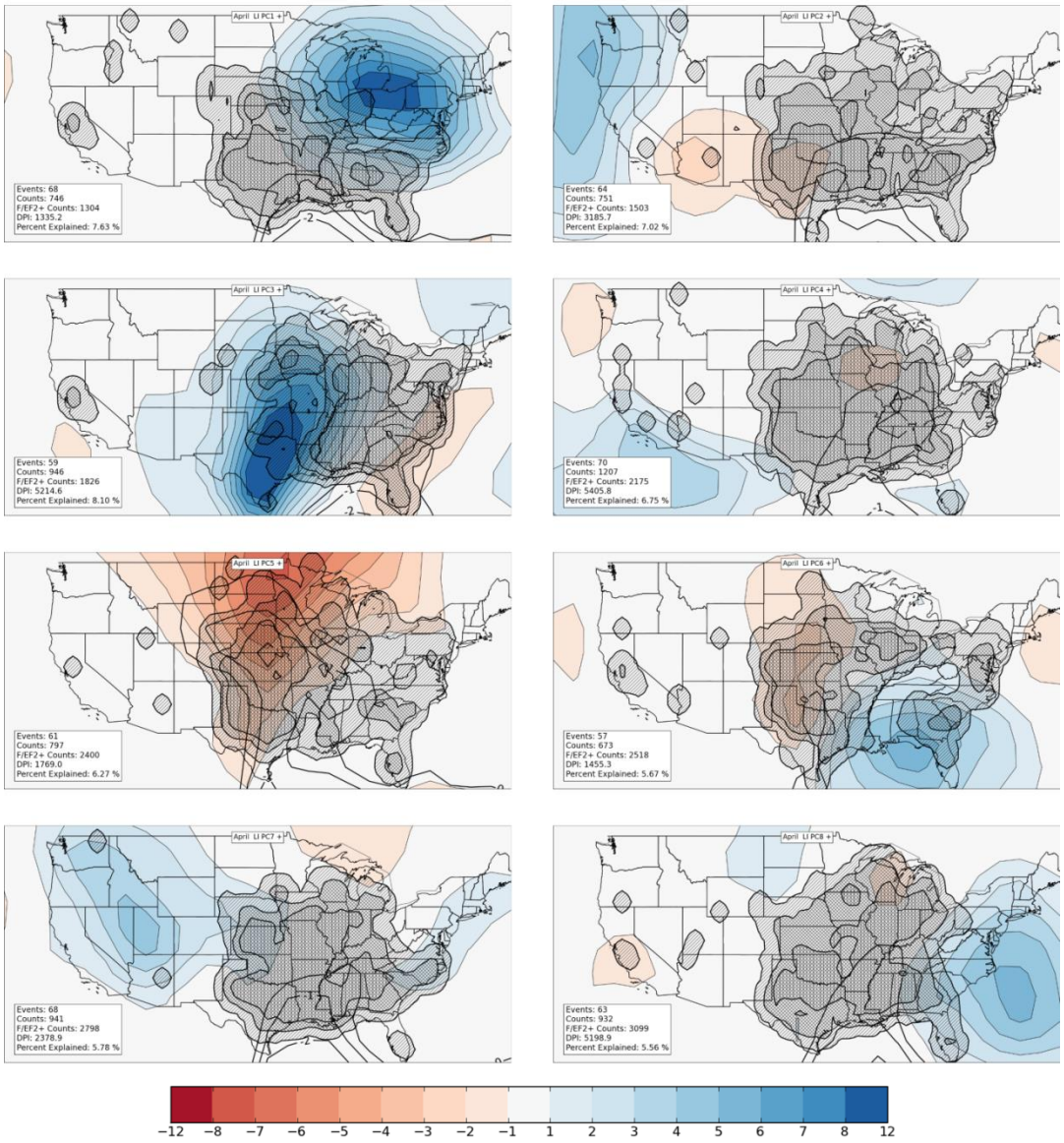

Figure 3.26: Composites of April lifted index in tornado outbreaks containing VRPC scores greater than or equal to 1 (black contours, units in degrees Celsius). Shaded regions in blue (red) indicate where composited mean lifted indices are above (below) average of the mean April lifted index field for all April tornado outbreaks in the entire dataset. Tiers of hatched areas indicate relative concentrations of tornado activity that are counted on a 1° latitude/longitude grid in a manner similar to that outlined in Section 2.1.b.iii. A Gaussian filter with bandwidth = 1° was applied to the data before hatching.

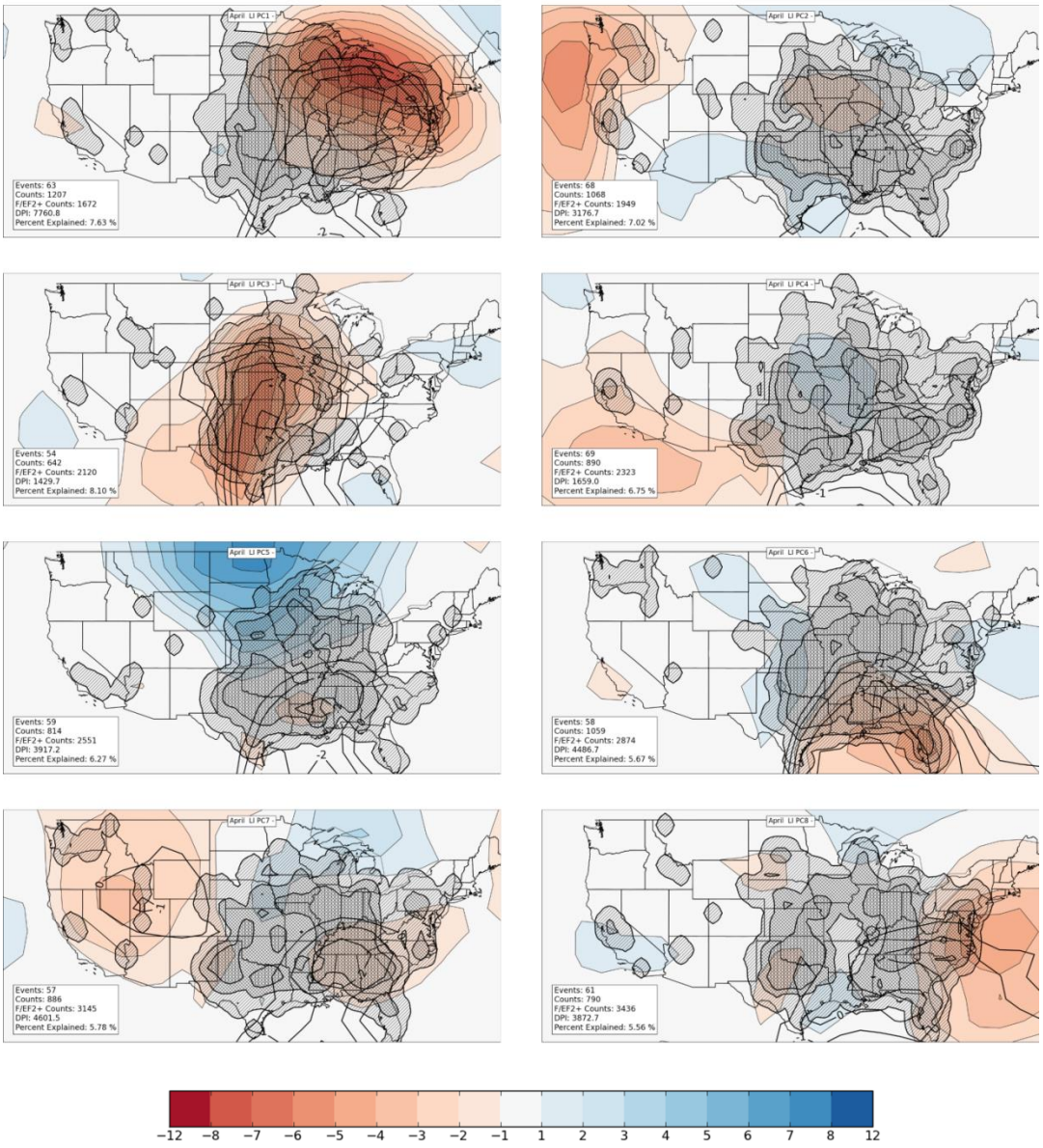

Figure 3.27: As in Figure 3.26, except for events with VRPC scores less than or equal to -1.

e. Moisture

Anomalies in moisture content (gauged through use of precipitable water) exhibit a similar relationship to tornado outbreaks in this study as instability axes do. Areas of increased moisture content tend to favor increased tornado activity, while anomalously dry regions tend to negate tornado activity. The clearest examples of this phenomenon can be found in Figures 3.28-3.31, particularly within the following composites: January PC1+, PC2+, PC1-, PC2-; April PC1+, PC2+, PC1-, PC2-, and PC3-. Some composites even exhibit anomaly dipoles (anomalously moist conditions adjacent to anomalously dry conditions: January PC2+, PC2-; April PC1+, PC3+, PC1-, and PC3-) which occasionally focuses tornado activity into localized regions.

3.5 Conclusions

The preceding sections of this chapter established a basic climatology of tornado outbreaks from January through April 1950-2010. Generally, tornadoes are most concentrated in the southern U.S. in January, but tornado activity increases dramatically with progression toward April. A westward progression of tornado maxima is also noted, with tornado maxima occurring in the southern Great Plains in April. Secular (non-meteorological) trends in tornado activity (i.e., underreporting problems before the 1980s) were also discussed at length. Each of these findings

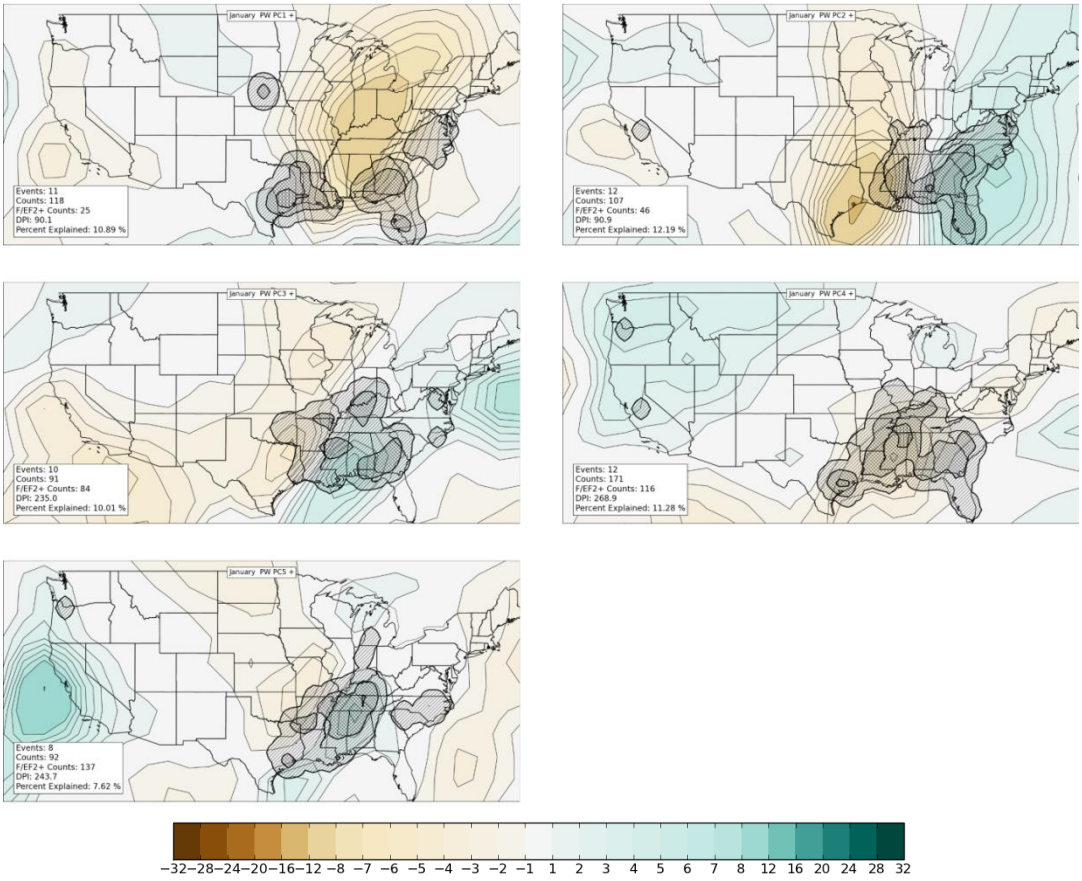

Figure 3.28: Composites of January precipitable water content in tornado outbreaks containing VRPC scores greater than or equal to 1 (black contours, units in kilograms per squared meter). Shaded regions in green (brown) indicate where composited mean precipitable water content are above (below) average of the mean January precipitable water field for all January tornado outbreaks in the entire dataset. Tiers of hatched areas indicate relative concentrations of tornado activity that are counted on a 1° latitude/longitude grid in a manner similar to that outlined in Section 2.1.b.iii. A Gaussian filter with bandwidth = 1° was applied to the data before hatching.

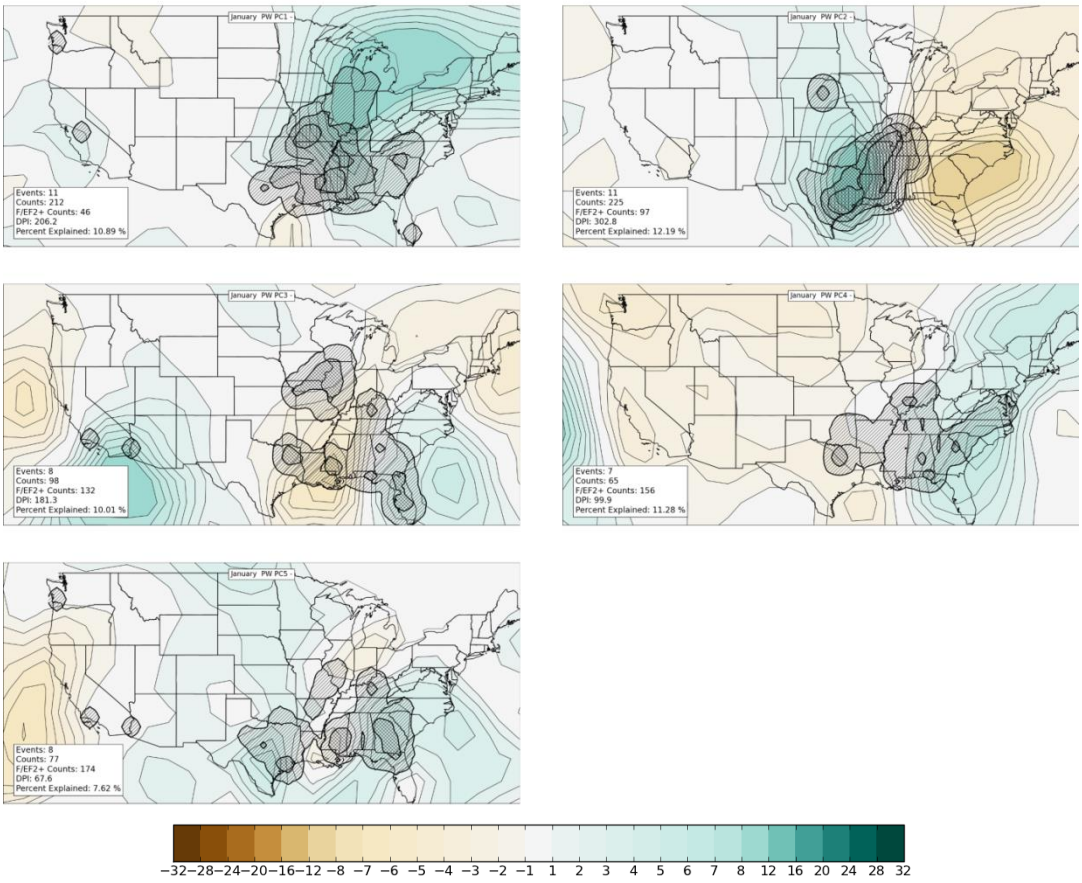

Figure 3.29: As in Figure 3.28, except for events with VRPC scores less than or equal to -1.

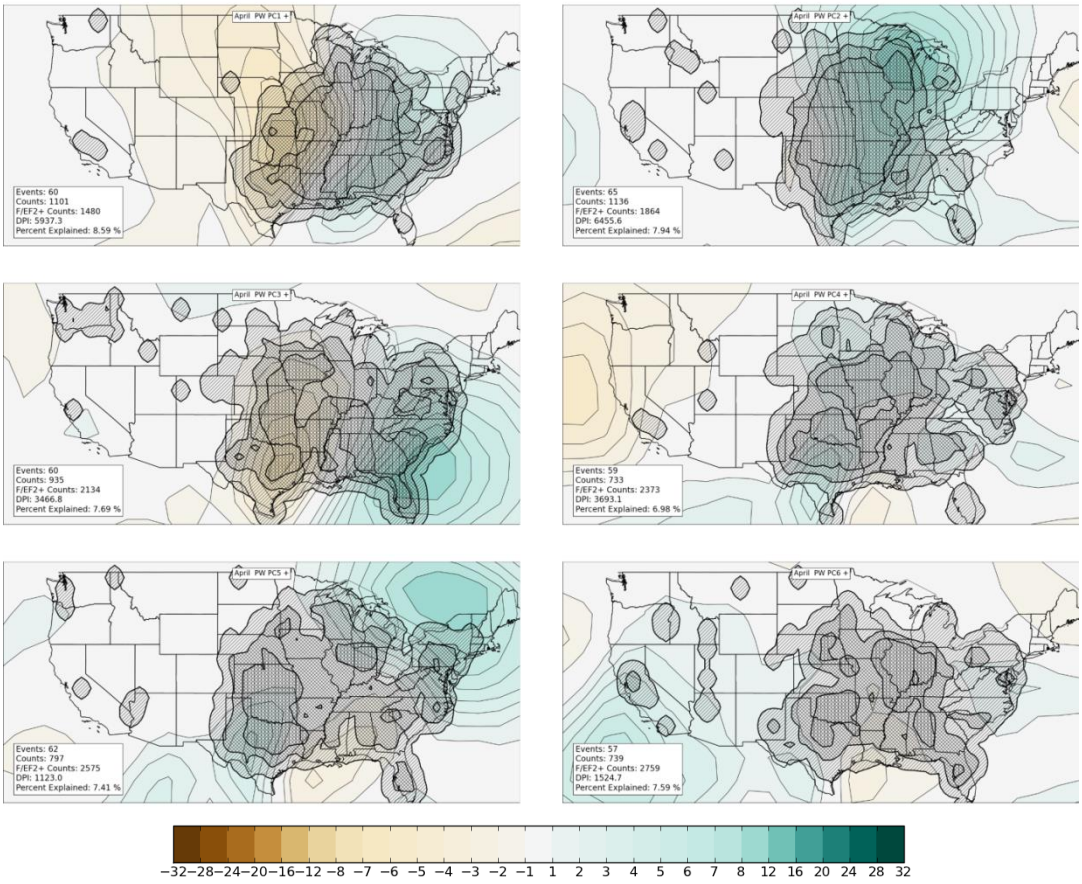

Figure 3.30: Composites of April precipitable water content in tornado outbreaks containing VRPC scores greater than or equal to 1 (units in kilograms per squared meter). Shaded regions in green (brown) indicate where composited mean precipitable water content are above (below) average of the mean April precipitable water field for all April tornado outbreaks in the entire dataset. Tiers of hatched areas indicate relative concentrations of tornado activity that are counted on a 1° latitude/longitude grid in a manner similar to that outlined in Section 2.1.b.iii. A Gaussian filter with bandwidth = 1° was applied to the data before hatching.

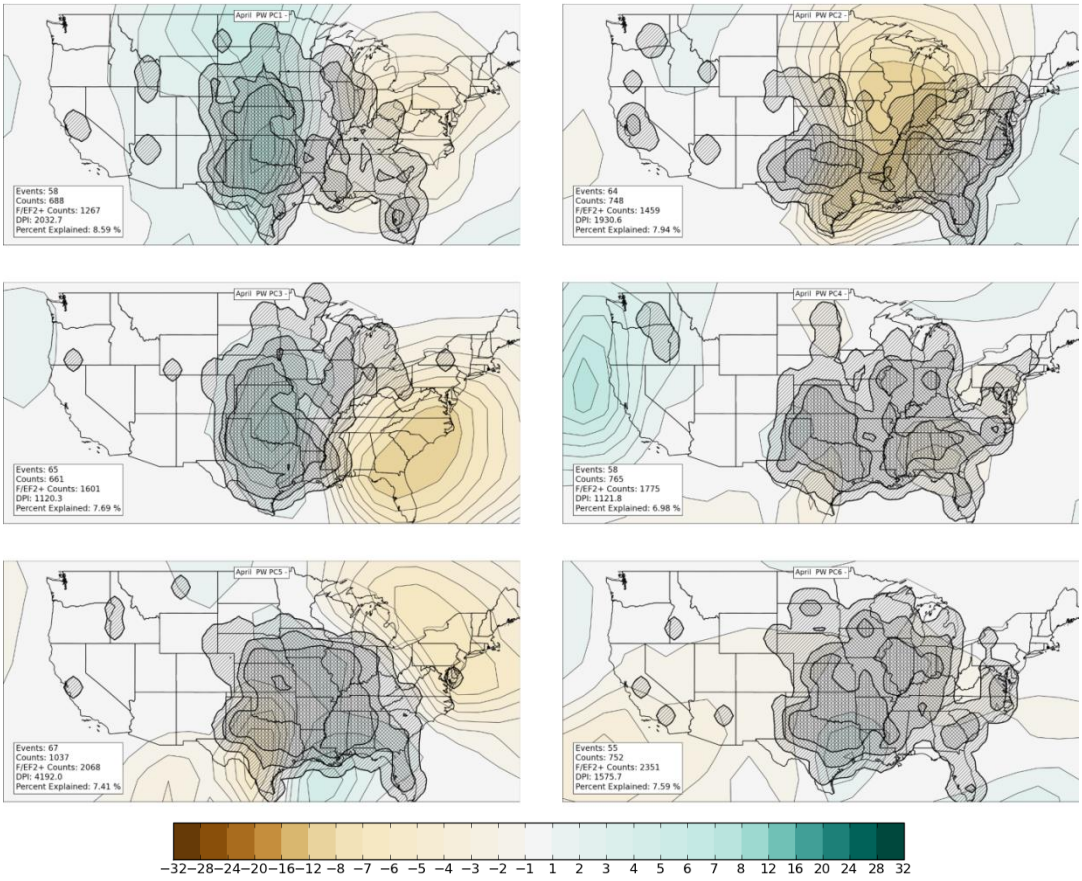

Figure 3.31: As in Figure 3.30, except for events with VRPC scores less than or equal to -1.

were generally consistent with previous tornado climatologies, although this study introduced spatial destruction potential to gauge tornado activity in a way that had never been done before in previous studies.

Section 3.4 provides unique contributions to the state-of-the-science by establishing important information about the locations of atmospheric anomalies (suggesting the presence of important synoptic-scale atmospheric features) and their influence on tornado outbreaks. In general, surface cyclones and low-level jet streams exhibit a westward and northward migration from January through April that appears to be coincident with tornado activity. Instability and moisture heavily modulate tornado activity from January through April and both exhibit northward and/or westward spatial shifts with progression toward the month of April, coincident with the climatological movement of tornado maxima through the period. Spatial shifts in the locations of mid- and upper-level geopotential height anomalies, however, did not exhibit the same movement that aforementioned shifts did.

The next chapter will use some of the same techniques employed in the current chapter to establish shifts in tornado outbreak climatology as a function of ENSO and then attempt to identify related shifts in synoptic-scale atmospheric features in place at the time of those outbreaks. Chapter 4 will focus on the relationship between January-April tornado outbreaks and the El Niño-Southern Oscillation.

4. ENSO AND JANURY-APRIL TORNADO OUTBREAKS

As mentioned in Chapter 1, the El Niño-Southern Oscillation (ENSO) phenomenon is an coupled atmospheric-oceanic oscillation of tropical Pacific winds and resulting anomalous warming (or cooling) of the tropical Pacific sea surface temperatures (SSTs) in a broad region that extends from the western coast of South America westward across the Pacific Ocean (to about 160°E), and spans the 10°N-10°S latitude belt (Bjerknes 1969; Wyrtki 1975; Rasmusson and Carpenter 1982; Ropelewski and Halpert 1987; Peixoto and Oort 1992, pp. 415-426; Federov and Philander 2000),. Many authors have identified ENSO's effects on North American weather (Rasmusson and Carpenter 1982; Ropelewski and Halpert 1987; Peixoto and Oort 1992, pp. 415-426; Smith et al. 1998; Eichler and Higgins 2006; Cook and Schaefer 2008; and others) and a few have discussed relationships between ENSO and tornadoes in the U.S. (Marzban and Schaefer 2001, Knowles and Pielke 2005, Cook and Schaefer 2008, Munoz and Enfield 2011, Lee et al. 2013, Kellner and Niyogi 2014). As alluded to in Chapter 1, this chapter will represent a substantial extension of knowledge of the ENSO/U.S. tornado relationship beyond previous studies because of the use of Reanalysis data and PCA techniques to investigate ENSO-related shifts in synoptic-scale atmospheric features associated with individual tornado outbreaks. Previous studies only briefly considered overall shifts in monthly or seasonally averaged atmospheric patterns (Smith et al. 1998, Munoz and Enfield 2011, Lee et al. 2013) and a few unrefereed studies did not consider concurrent ENSO-related atmospheric

shifts in tornado outbreaks at all. Sections 4.1-4.3 establish a physical climatology assessing the character of tornado outbreaks (location, frequency, and strength) as a function of ENSO phase. Section 4.4 establishes an atmospheric climatology of synoptic-scale features associated with tornado outbreaks that are known to be influenced by ENSO (Section 2.2.b.ii). Section 4.5 concludes the chapter and discusses future work.

4.1 Tornado Location

The annual cycle of all El Niño (EN), La Niña (LN), and Neutral (N) tornado outbreak activity exhibits a similar general increase and westward/northward expansion of tornado activity from January through April as that identified in Section 3.1 (Figures 4.1-4.4). The degree of increase and expansion varies, however, when comparing EN tornado outbreaks to LN and N tornado outbreaks. Tornado activity during EN months appear to occur at farther south latitudes than in other ENSO phases, with most frequent occurrence in east Texas and Mississippi from January to March (Figures 4.1-4.3). By comparison, tornado activity occurs more frequently during LN conditions north of those areas, including maxima in central Arkansas and January-February tornado occurrence as far north as Missouri, southern Illinois, and far southern Indiana (Figures 4.1 and 4.2). During LN conditions, tornado activity is noted as far north as Nebraska and Michigan in March, while in EN conditions, tornado activity

remains limited to southern areas except for an outlier tornado outbreak that occurred in southern Minnesota on March 29, 1998 (Figure 4.3). Figure 4.4 indicates even larger differences between EN and LN appear in the central and northern Great Plains and eastward into Ohio in April, with increased activity during LN years in those areas. In general, N months contain higher tornado counts than EN and LN months, but this difference is at least partially attributed to the frequency of monthly ENSO events (Table 4.1). N months occur nearly twice as frequently as EN months, particularly in February, March, and April.

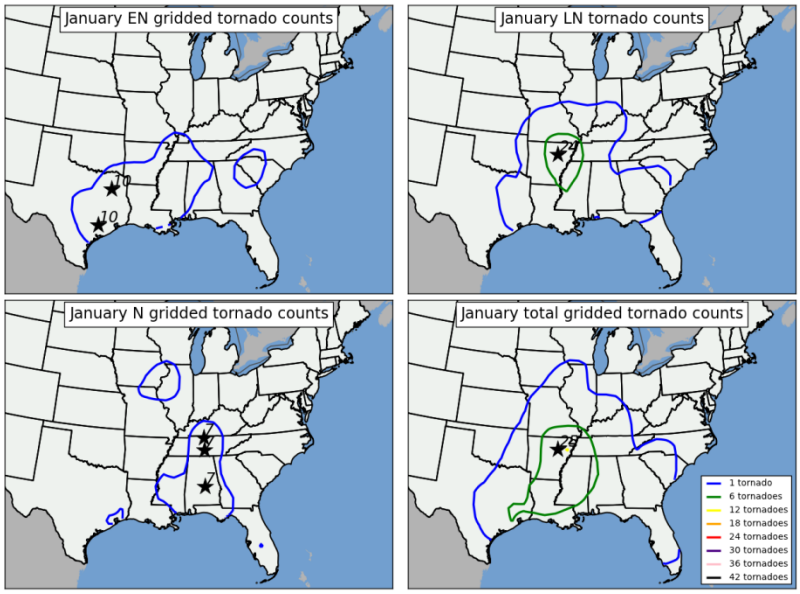

Figure 4.1: Contour plots representing the number of times tornadoes in tornado outbreaks occurred in grid boxes in each ENSO phase during January 1950-2010. Star and associated number indicates location and number of maximum tornado occurrences on the grid. As mentioned in Section 2.1.b, a Gaussian filter with bandwidth = 1° was applied to the data before isoplething.

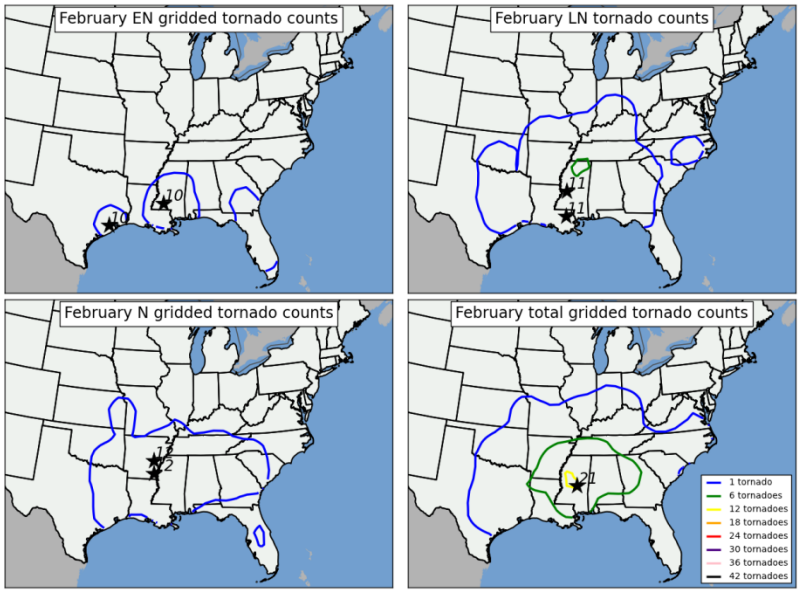

Figure 4.2: Contour plots representing the number of times tornadoes in tornado outbreaks occurred in grid boxes in each ENSO phase during February 1950-2010. Star and associated number indicates location and number of maximum tornado occurrences on the grid. As mentioned in Section 2.1.b, a Gaussian filter with bandwidth = 1° was applied to the data before isoplething.

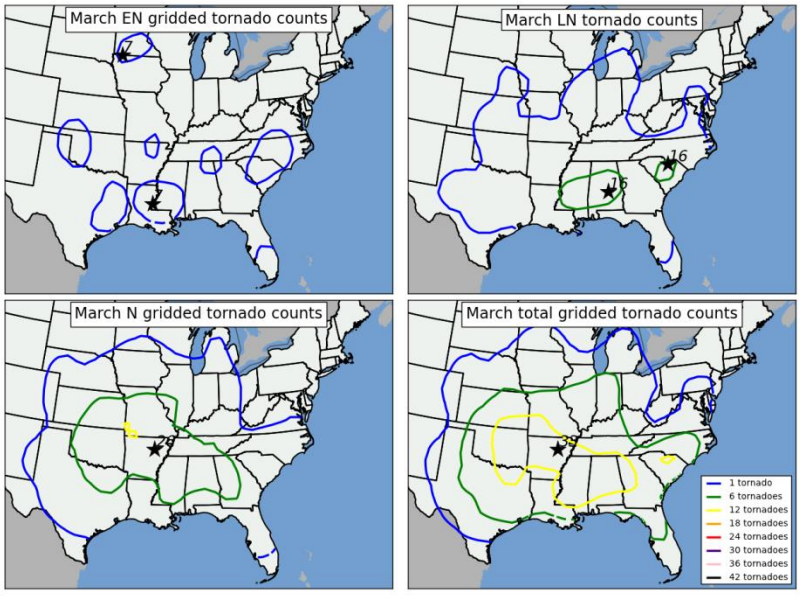

Figure 4.3: Contour plots representing the number of times tornadoes in tornado outbreaks occurred in grid boxes in each ENSO phase during March 1950-2010. Star and associated number indicates location and number of maximum tornado occurrences on the grid. As mentioned in Section 2.1.b, a Gaussian filter with bandwidth = 1° was applied to the data before isoplething.

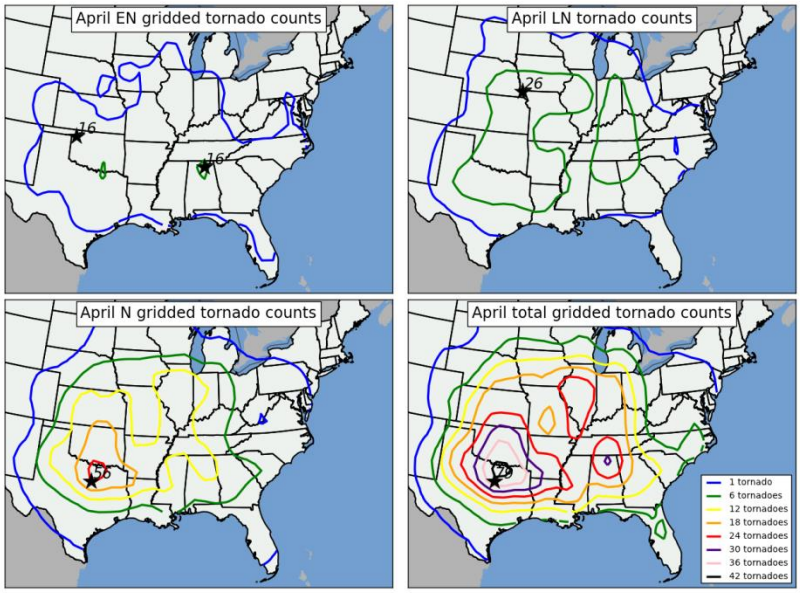

Figure 4.4: Contour plots representing the number of times tornadoes in tornado outbreaks occurred in grid boxes in each ENSO phase during April 1950-2010. Star and associated number indicates location and number of maximum tornado occurrences on the grid. As mentioned in Section 2.1.b, a Gaussian filter with bandwidth = 1° was applied to the data before isoplething.

	January	February	March	April
EN	21	13	10	12
LN	21	18	17	16
N	19	30	34	33

Table 4.1: Number of times each month was classified as an El Nino (EN), La Nina (LN), or Neutral (N) phase of ENSO for the period January-April 1950-2010. Months were classified based on the Nino 3.4 SST anomaly. Months containing a Nino 3.4 SST anomaly greater than or equal to 0.5 were classified as EN. Months with a Nino 3.4 SST anomaly of less than or equal to -0.5 were classified as LN. All other months were classified as N.

Normalization of the data contained in Figures 4.1-4.4 allows for a simpler, more direct comparison of tornado activity between months and phases of ENSO. In Figures 4.5-4.8, gridded tornado counts were normalized against the number of times each month was classified as a particular ENSO phase (expressed in Table 4.1). Tornadoes per month are generally more frequent during LN in all locations east of the Rocky Mountains in the entire study period (January-April), except in Peninsular Florida during February EN months. The increase in tornado activity across the Lower Mississippi Valley in January and February LN months is readily apparent (Figures 4.5 and 4.6). In March, an increase in tornado activity is noted across Illinois and Indiana and also across the southern parts of the U.S. from Mississippi to South Carolina during LN (Figure 4.7). In April, a drastic increase in tornado activity is noted across from Nebraska and northern Kansas eastward to Indiana and Kentucky during LN (Figure 4.8). BCa CIs of tornado counts by ENSO phase (Figures 4.9-4.13) indicate statistically significant differences between EN and LN tornado counts in the Lower Mississippi Valley in January, in northern Alabama in February, Illinois/Indiana and northern Alabama in March, and in northern Kansas and far southern Nebraska in April. Section 4.4 discusses ENSO-related underlying shifts in the atmosphere that result in these drastic, statistically significant shifts in tornado activity.

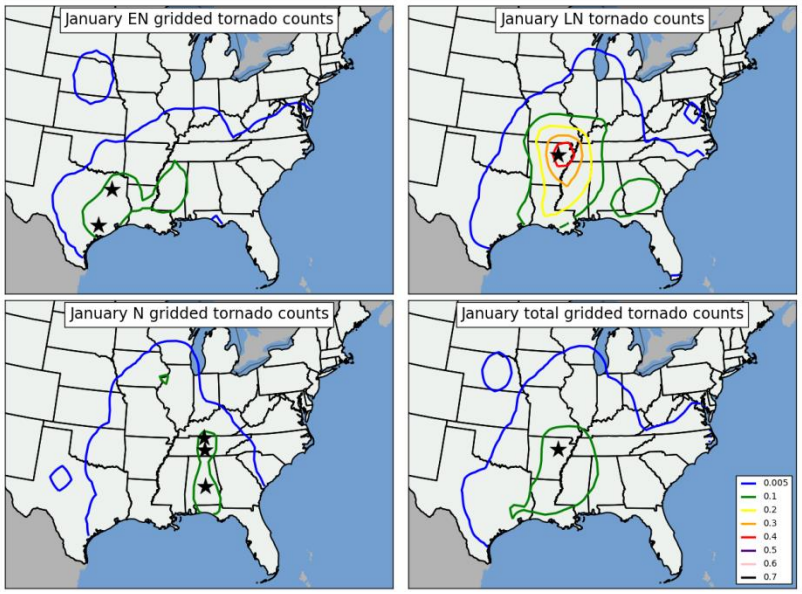

Figure 4.5: Contour plots representing normalized gridded tornado counts in each ENSO phase during January 1950-2010. Tornado data was normalized against the number of months classified as January EN (21), January LN (21), and January N (19). Star indicates location of maximum normalized tornado occurrences on the grid. As mentioned in Section 2.1.b, a Gaussian filter with bandwidth = 1° was applied to the data before isoplething.

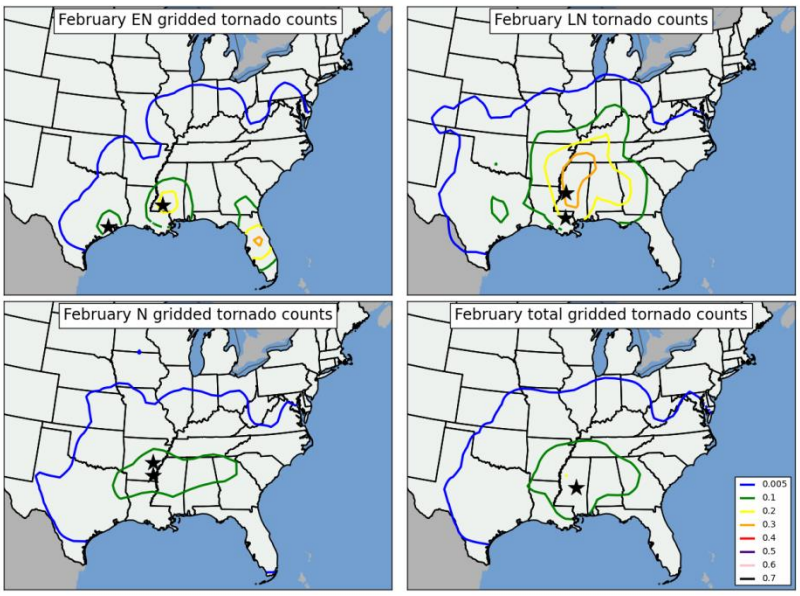

Figure 4.6: Contour plots representing normalized gridded tornado counts in each ENSO phase during February 1950-2010. Tornado data was normalized against the number of months classified as February EN (13), February LN (18), and February N (30). Star indicates location of maximum normalized tornado occurrences on the grid. As mentioned in Section 2.1.b, a Gaussian filter with bandwidth = 1° was applied to the data before isoplething.

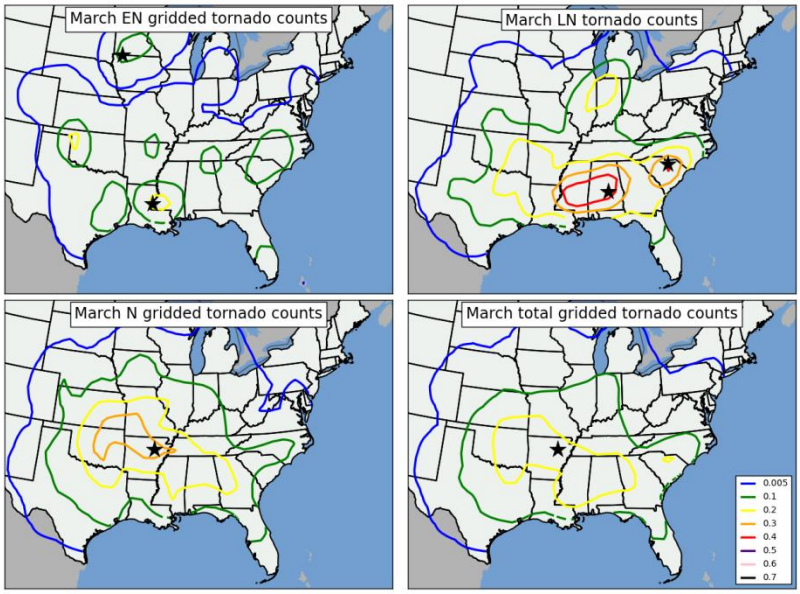

Figure 4.7: Contour plots representing normalized gridded tornado counts in each ENSO phase during March 1950-2010. Tornado data was normalized against the number of months classified as March EN (10), March LN (17), and March N (34). Star indicates location of maximum normalized tornado occurrences on the grid. As mentioned in Section 2.1.b, a Gaussian filter with bandwidth = 1° was applied to the data before isoplething.

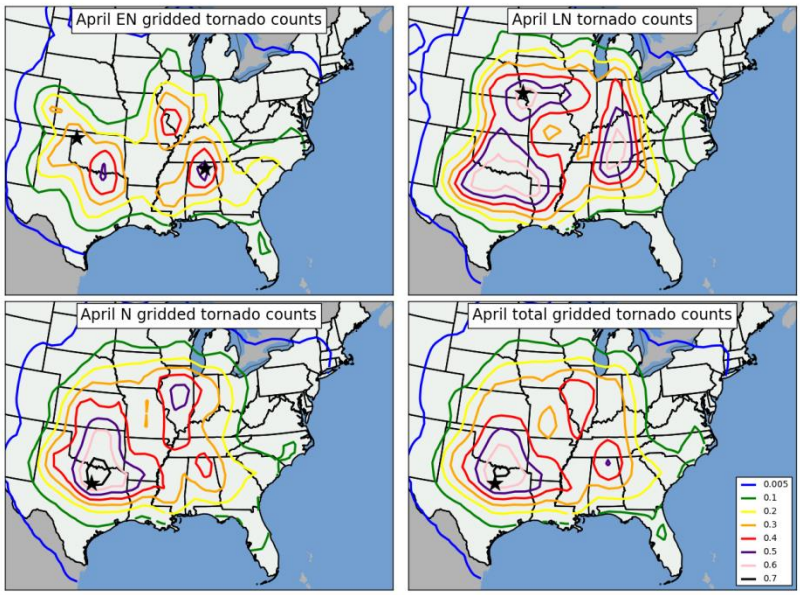

Figure 4.8: Contour plots representing normalized gridded tornado counts in each ENSO phase during March 1950-2010. Tornado data was normalized against the number of months classified as March EN (10), March LN (17), and March N (34). Star indicates location of maximum normalized tornado occurrences on the grid. As mentioned in Section 2.1.b, a Gaussian filter with bandwidth = 1° was applied to the data before isoplething.

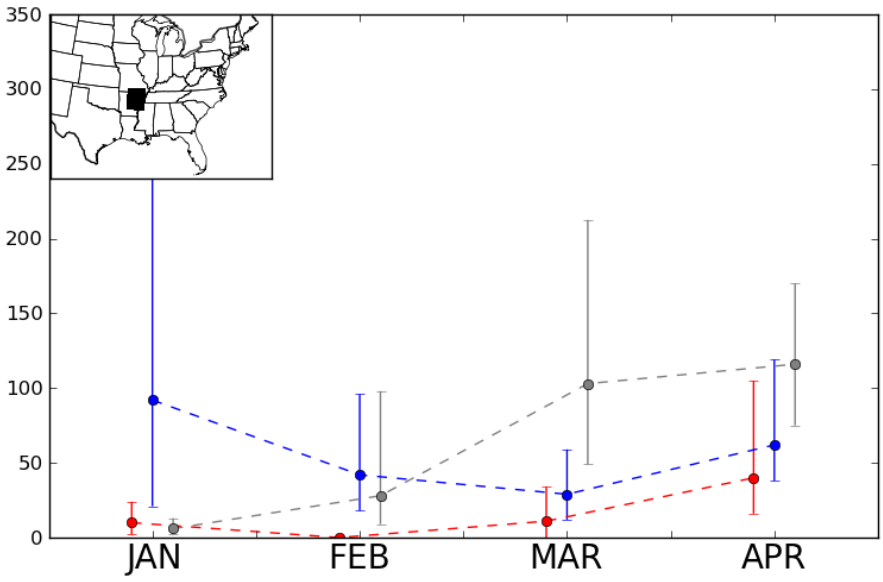

Figure 4.9: Monthly tornado counts (dashed lines) and 95% BCa CIs around the sum of monthly tornado counts (brackets) in the 3° by 3° region shown in inset. Lines and brackets are color-coded based on ENSO phase at the time of tornado occurrence (Red represented EN tornado counts, blue represents LN tornado counts, and gray represents N tornado counts).

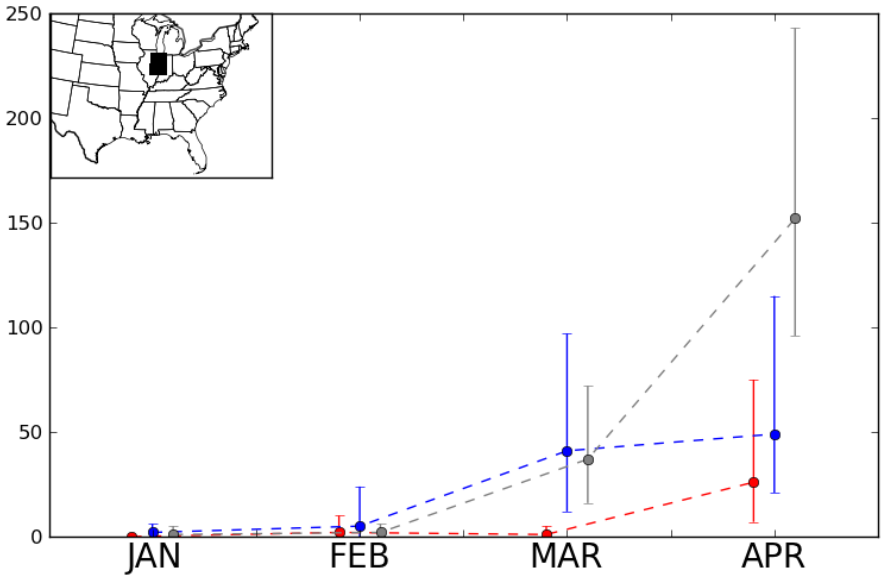

Figure 4.10: Monthly tornado counts (dashed lines) and 95% BCa CIs around the sum of monthly tornado counts (brackets) in the 3° by 3° region shown in inset. Lines and brackets are color-coded based on ENSO phase at the time of tornado occurrence (Red represented EN tornado counts, blue represents LN tornado counts, and gray represents N tornado counts).

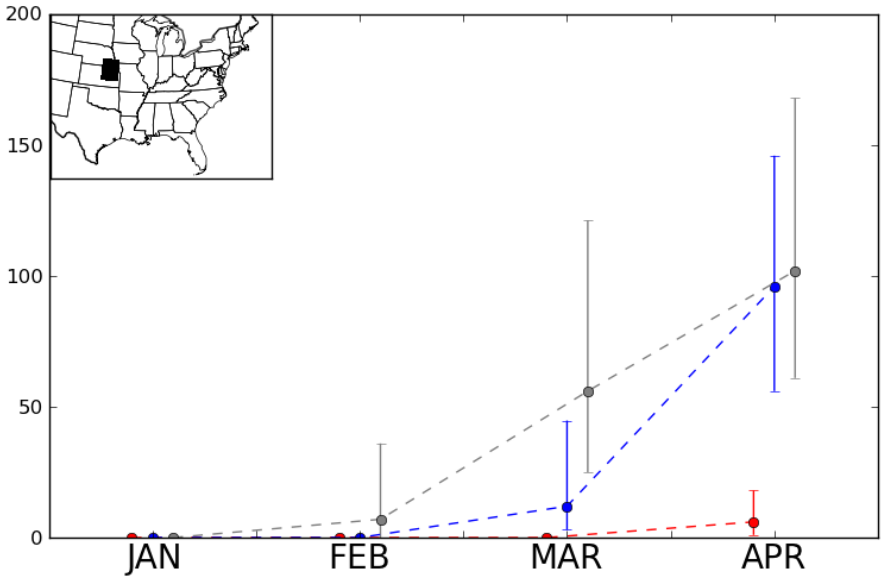

Figure 4.11: Monthly tornado counts (dashed lines) and 95% BCa CIs around the sum of monthly tornado counts (brackets) in the 3° by 3° region shown in inset. Lines and brackets are color-coded based on ENSO phase at the time of tornado occurrence (Red represented EN tornado counts, blue represents LN tornado counts, and gray represents N tornado counts).

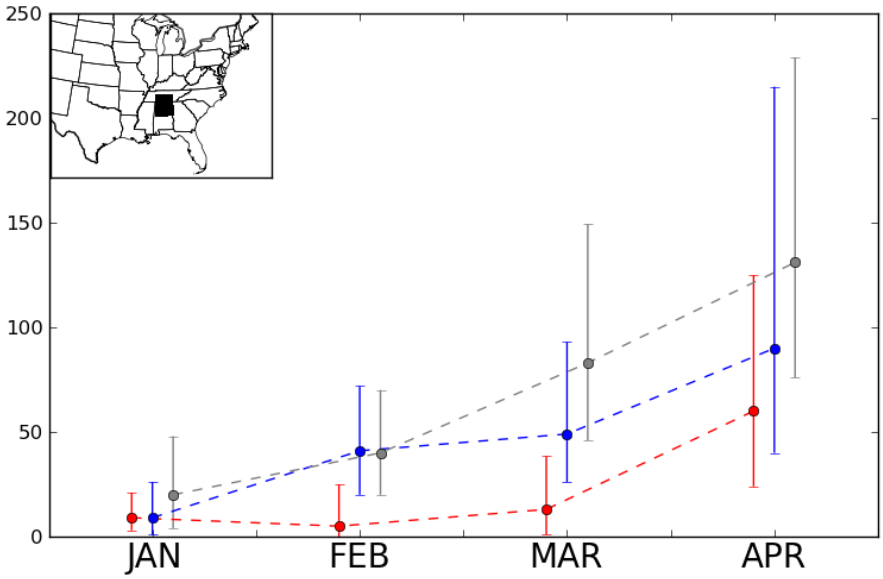

Figure 4.12: Monthly tornado counts (dashed lines) and 95% BCa CIs around the sum of monthly tornado counts (brackets) in the 3° by 3° region shown in inset. Lines and brackets are color-coded based on ENSO phase at the time of tornado occurrence (Red represented EN tornado counts, blue represents LN tornado counts, and gray represents N tornado counts).

4.2 Tornado Frequency

Tornado activity is far more frequent during LN and N conditions in the continental U.S. east of the Rocky Mountains than during EN conditions. Table 4.2 shows monthly tornado counts as a function of ENSO phase for all areas east of the Rocky Mountains (both raw counts and counts normalized against the frequency of respective ENSO phase). Tornadoes on outbreak days during LN conditions in January and February substantially outnumber tornadoes occurring in other phases despite the fact that the number of months that are classified as LN in February (18) is much smaller than the number of events classified as N (30). N tornado days in March and April contain larger numbers of tornadoes, in part because of the N phase being the most frequently observed ENSO phase for those two months. Counts for strong (F/EF2 or greater) tornadoes tended to exhibit similar behavior. These values are consistent with Cook and Schaefer (2008) who found that tornado activity in LN and N was increased in the entire CONUS from January-March 1950-2003. These values are also consistent with Muñoz and Enfield (2011) and Kellner and Niyogi (2014) despite the more limited regional scope in each of those studies.

	January			February			March			April		
	EN	LN	N	EN	LN	N	EN	LN	N	EN	LN	N
Tornadoes on outbreak days	221	412	160	151	418	323	205	788	1492	842	1614	3120
Tornadoes per Number of Months in each ENSO phase	10.52	19.62	8.42	11.62	23.22	10.77	20.50	46.35	43.88	69.67	100.88	94.18
Tornado outbreak days	23	21	12	17	36	30	20	68	100	63	113	214
Outbreak days per Number of Months in each ENSO phase	1.10	1.00	0.63	1.31	2.00	1.00	2.00	4.00	2.94	5.25	7.06	6.48
Tornadoes rated F/EF2 or greater	48	107	74	43	148	114	38	213	556	223	611	818
F/EF2+ tornadoes per number of months in each ENSO phase	2.29	5.10	3.89	3.31	8.22	3.80	3.80	12.53	16.35	18.58	38.19	24.79
Tornadoes rated F/EF4 or greater	2	3	5	1	12	4	1	12	47	19	70	63
F/EF4+ tornadoes per number of months in each ENSO phase	0.10	0.14	0.26	0.08	0.67	0.13	0.10	0.71	1.38	1.58	4.38	1.91
Number of months in each ENSO phase	21	21	19	13	18	30	10	17	34	12	16	33

Table 4.2: January-April 1950-2010 tornado frequency in outbreaks (as defined in Chapter 1) east of the Rocky Mountains. Outbreaks are binned and then tallied according to concurrent ENSO phase.

Tornado outbreak days were similar in EN and LN during January, but more frequent in LN during February, and more frequent during N in March and April. This finding differs from Cook and Schaefer (2008) because of two factors: 1) tornado activity was gauged for an entire seasonal period (January-March) as opposed to the greater detail afforded by month-to-month analyses in the current study, and 2) ENSO events were gauged using an average Nino 3.4 SST anomaly spanning multiple months in that study, whereas the current study classifies an ENSO event based on the Nino 3.4 SST anomaly concurrent with the month being analyzed. In a few of the years in the current study, Nino 3.4 SST anomalies indicated weak EN conditions in January that weakened further into N conditions in February. EN conditions occur in January more often than in any other month in the study because of this.

As mentioned previously, some of the quantities in Table 4.2 were normalized to ensure the ability to compare between ENSO phase by dividing the number of times a particular ENSO phase occurred in a month during the 1950-2010 period of study. Results from this approach generally indicate that the LN phase is consistently the most active for tornado outbreaks, while tornado outbreak activity during EN phase is considerably less frequent. In January and February, tornadoes occur more than twice as frequently during LN phase compared to N phase. This discrepancy isn't nearly as obvious in March and April although tornadoes remain more frequent in LN and N phases compared to EN phase. Tornado outbreaks days per month increase substantially from January through April and this increase is magnified during LN conditions. Strong (rated F/EF2 or greater) and violent (rated F/EF4 or greater) are more frequent during LN conditions as well, especially when compared to EN conditions.

4.3 Tornado Strength

An analysis of the intensity and longevity of tornadoes in outbreaks reveals similar trends in intraseasonal evolution as those discussed in Section 4.1. Table 4.3 indicates the presence of stronger, longer-lived tornadoes in tornado outbreaks occurring during the LN phase, particularly in January and February. Average DPI per tornado outbreak in those months (42.64 and 64.37, respectively) is drastically different from their EN tornado outbreak counterparts (only 9.32 and 8.04, respectively). Additional metrics for comparing intensity of these outbreaks (average DPI per

tornado, cumulative path length per outbreak, and outbreaks with cumulative DPI above 25) are also listed in Table 4.3 and also illustrate the disparity in character of EN tornado outbreaks and LN tornado outbreaks in January and February. Again, the use of DPI in this study affords the opportunity to gauge tornado strength within outbreaks in a more detailed manner than any previous ENSO/tornado study.

The aforementioned trend of stronger LN tornado outbreaks isn't nearly as prominent in March and April, however. N events tend to contain higher DPI in March based on almost all intensity metrics listed in Table 4.3. Interestingly, although the differences in DPI per tornado outbreak in March EN and March LN aren't as large as in the two prior months, the number of tornado outbreaks contributing to the higher DPI average in March EN is far less than the number of March outbreaks contributing to the DPI average in March LN. This suggests that only a limited number of outbreaks with extremely high DPI are contributing to the high average DPI in March EN tornado outbreaks. A similar conclusion can be made regarding April EN tornado outbreaks when compared to April LN tornado outbreaks; a fewer number of outbreaks that occur in April during EN phase contribute to the high average cumulative DPI per tornado outbreak compared to April LN tornado outbreaks.

	January			February			March			April		
	EN	LN	N	EN	LN	N	EN	LN	N	EN	LN	N
Total DPI	214	896	279	137	2317	788	586	2350	7567	3882	7738	9543
Average cumulative DPI per tornado outbreak	9.32	42.64	23.25	8.04	64.37	26.28	29.30	34.56	75.67	61.62	68.48	44.18
Average DPI per tornado in tornado outbreak	0.97	2.17	1.74	0.91	5.54	2.44	2.86	2.98	5.07	4.61	4.79	3.06
Average cumulative Path Length per tornado outbreak	40.05	105.68	55.87	43.92	84.18	57.23	29.84	59.70	99.60	68.17	100.05	69.25
Number of outbreaks with DPI above 25	2	8	4	3	16	8	2	16	43	18	38	63
Number of outbreaks with DPI above 50	1	5	3	0	10	6	1	9	28	12	21	43

Table 4.3: Seasonal evolution of DPI in tornado outbreaks east of the Rocky Mountains binned into separate phases of ENSO.

Intraseasonal spatial evolution of gridded DPI exhibit similar behavior to that already discussed in this section and also in Figures 4.1-4.8 in Section 4.1. The strongest of tornado activity during the EN phase is consistently focused across the southern U.S. in all months of the study (Figures 4.13-4.16). DPI values in EN conditions are consistently small across the entire U.S. east of the Rocky Mountains until March, when a supercell spawned a few strong to violent tornadoes in southern Minnesota on March 29, 1998. (Cook and Schaefer [2008] note that this tornado outbreak was a relative outlier compared to other tornado outbreaks that occurred across the southern parts of the United States during EN.) In April, larger values of DPI appear in the southern U.S. (particularly Mississippi) and much of that is driven by a single violent and long-tracked tornado with a path length of 149 miles and a maximum path width of 1.75 miles. That tornado was part of a larger outbreak of tornadoes that occurred in the Deep South on April 24, 2010. In contrast, tornadoes (and attendant DPI maxima) tended to occur farther north during LN and N

conditions. This difference is most pronounced in April, where powerful tornado outbreaks impacted areas from Nebraska and Kansas eastward to Indiana and western Ohio.

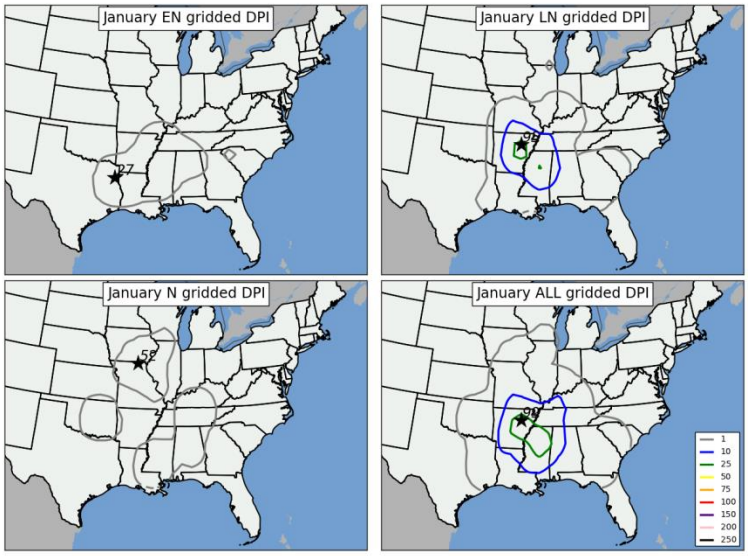

Figure 4.13: Contour plots representing gridded DPI in EN (upper left), LN (upper right), N (lower left), and all (lower right) January tornado outbreaks from 1950-2010. Star and associated number indicates location and number of maximum DPI on the grid. As mentioned in Section 2.1.b, a Gaussian filter with bandwidth = 1° was applied to the data before isoplething.

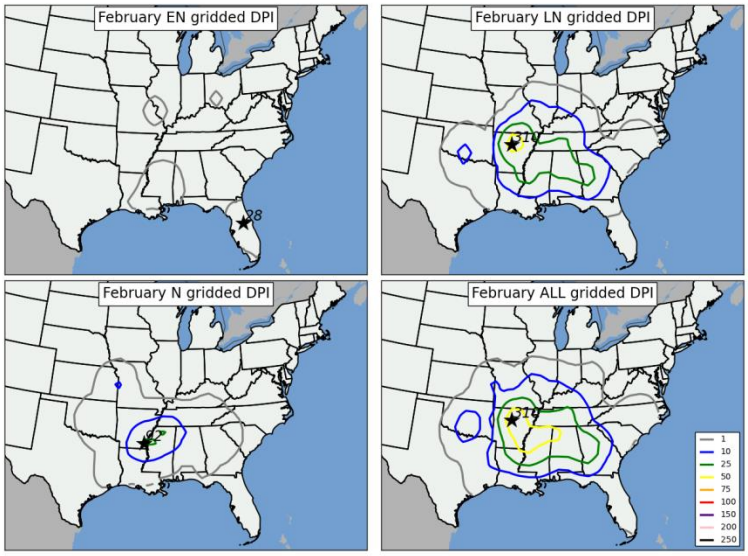

Figure 4.14: As in Figure 4.13, except for February tornado outbreaks.

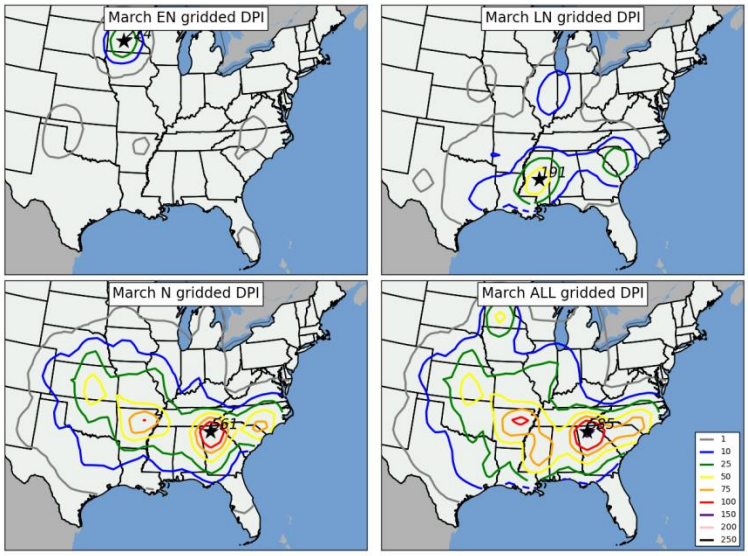

Figure 4.15: As in Figure 4.13, except for March tornado outbreaks.

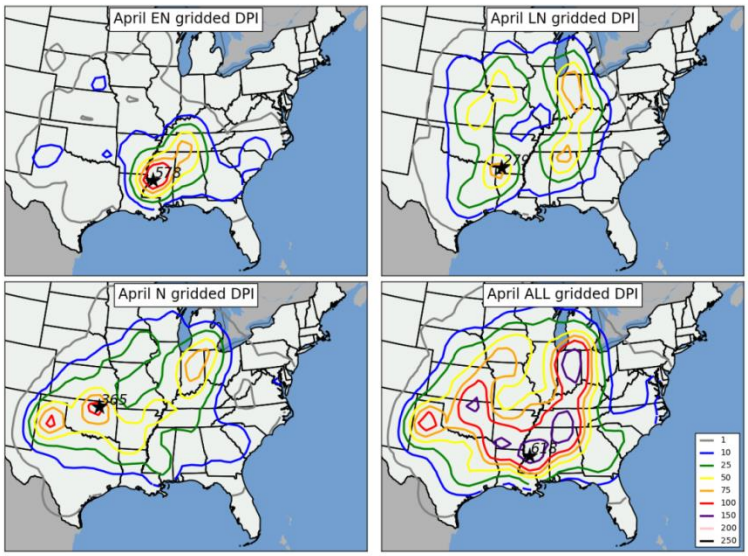

Figure 4.16: As in Figure 4.13, except for April tornado outbreaks.

Despite the marked shifts in DPI across the U.S. east of the Rocky Mountains, BCa CIs indicated statistically significant shifts in DPI in EN and LN conditions in only two areas, both during the month of April: in northern Kansas/far southern Nebraska (Figure 4.17) and in northern Texas (Figure 4.18). In each of these regions, tornado activity was more intense and affected a larger area during LN conditions. Interestingly, BCa CIs indicate stronger tornado activity during EN conditions across the Lower Mississippi Valley in April (Figure 4.19). Although this observation is counter to many others that indicate stronger activity during LN conditions, this shift was not deemed statistically significant given the substantial overlap of the BCa CIs in April LN and April EN conditions.

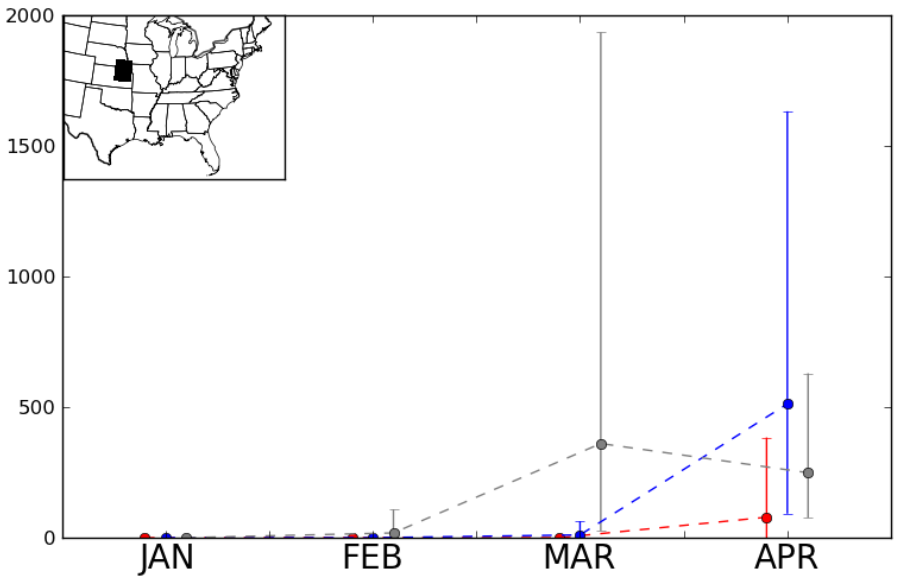

Figure 4.17: Monthly DPI (dashed lines) and 95% BCa CIs around the sum of monthly DPI (brackets) in the 3° by 3° region shown in inset. Lines and brackets are color-coded based on ENSO phase at the time of tornado occurrence (Red represented EN tornado counts, blue represents LN tornado counts, and gray represents N tornado counts).

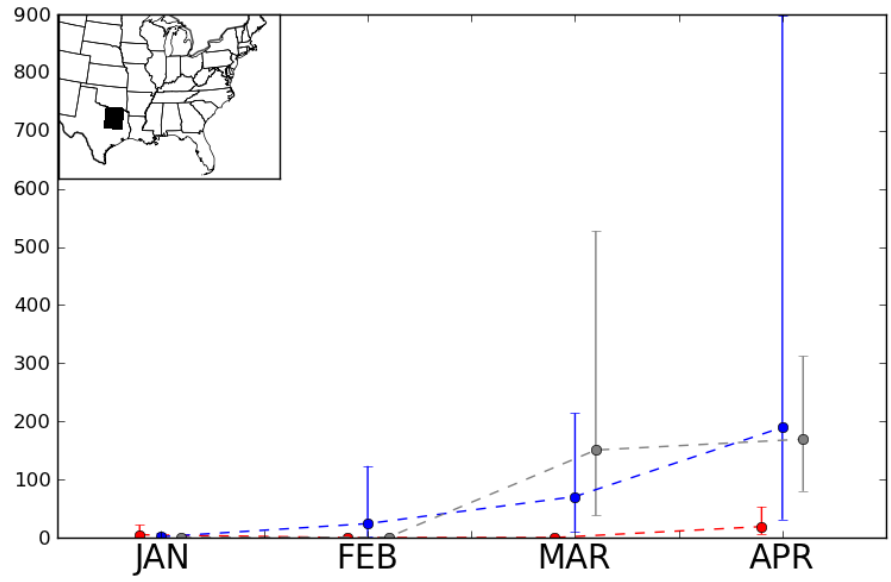

Figure 4.18: Monthly DPI (dashed lines) and 95% BCa CIs around the sum of monthly DPI (brackets) in the 3° by 3° region shown in inset. Lines and brackets are color-coded based on ENSO phase at the time of tornado occurrence (Red represented EN tornado counts, blue represents LN tornado counts, and gray represents N tornado counts).

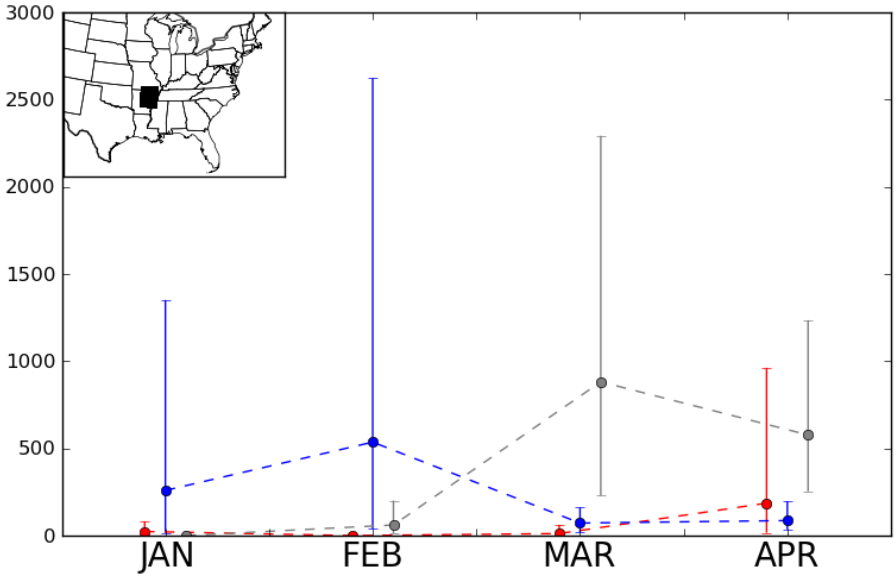

Figure 4.19: Monthly DPI (dashed lines) and 95% BCa CIs around the sum of monthly DPI (brackets) in the 3° by 3° region shown in inset. Lines and brackets are color-coded based on ENSO phase at the time of tornado occurrence (Red represented EN tornado counts, blue represents LN tornado counts, and gray represents N tornado counts).

4.4 ENSO/Atmospheric Tornado Outbreak Climatology

As stated in Sections 2.2 and 3.4, the creation of an atmospheric climatology is expected to apply meteorological reasoning to shifts observed in physical climatology of tornado outbreaks. Two unique key results are apparent from creation of an ENSO/tornado outbreak physical climatology previously discussed in Sections 4.1-4.3:

- While westward and northward shifts in tornado activity and DPI were apparent even when ENSO phase was considered, tornado activity occurring in EN phase were consistently southwardly displaced in every month of the study period, and
- LN tornado activity was consistently more widespread and more intense than EN tornado activity in all four months of the study period. This disparity was most evident in January and February through analysis of tornado counts for all areas east of the Rocky Mountains, although spatial analyses indicated substantial localized shifts in tornado activity, particularly across the parts of the Great Plains and Midwest in April.

The remainder of this chapter discusses the creation of an ENSO/atmospheric tornado outbreak climatology for the purpose of assessing shifts in synoptic-scale atmospheric features (Table 2.2) that appear to be influenced by ENSO. The process for completing this task involved several steps, including: 1) categorizing outbreaks according to ENSO phase and month of occurrence, conducting separate PC analyses

on relevant atmospheric fields from those subsets of outbreaks (i.e., January EN 300 hPa geopotential height, March LN 300 hPa geopotential height, etc.), and then comparing the results of those PC analyses (i.e., composites) to PCA of monthly sets of outbreaks that were conducted independent of any consideration of ENSO (such as those outlined in Section 3.4). This enabled the assessment of potential shifts of relevant synoptic-scale atmospheric features and also the resultant character of tornado outbreak activity. This aspect of the current study, namely the diagnosis of detailed atmospheric information that: 1) is directly tied to the character of tornado outbreak activity, and 2) is also directly tied to ENSO, is perhaps the most important contribution to the understanding of the ENSO/tornado relationship and has never been determined by previous research.

a. January

A key result from Section 4.1 indicated a statistically significant increase in tornado activity in the Lower Mississippi Valley during LN conditions. Although composites of surface cyclone location (i.e., location of absolute minimum in each composite of SLP in EN, LN, and N January Outbreaks, Figure 4.9) did not indicate any substantial shifts that would support the increase in tornadoes in that area, monthly anomalies of SLP indicate anomalously low SLP across the intermountain west during LN conditions (Figure 4.20), which would tend to indicate a more favorable

pattern on average for tornado outbreaks further east across the Lower Mississippi Valley compared to EN conditions.

Composites of 850 hPa maximum V-component wind in EN, LN, and N January tornado outbreaks indicate a distinct northward and westward shift in low-level jet streams during January LN outbreaks compared to January EN outbreaks. In January LN outbreaks, low-level jet streams in outbreaks are focused across the Tennessee and Ohio River Valleys (Figures 4.21.a and 4.21.b) with southerly low-level jet streams indicated as far west as Missouri and Arkansas. In January EN outbreaks, low-level jet streams are focused farther south and east in an area from Louisiana to the Carolinas. Low-level vertical shear (Figure 4.22) also exhibit these trends. Monthly anomalies of 850 hPa V-component (Figure 4.23) wind also indicate distinct shifts across the eastern two-thirds of the CONUS, with the largest positive anomalies centered across the “Ark-La-Tex” region of the southern U.S., suggesting that these westward shifts in the low-level jet persist even in the absence of tornado outbreaks. Each of these shifts in the low-level jet appear to be directly tied to shifts in tornado activity.

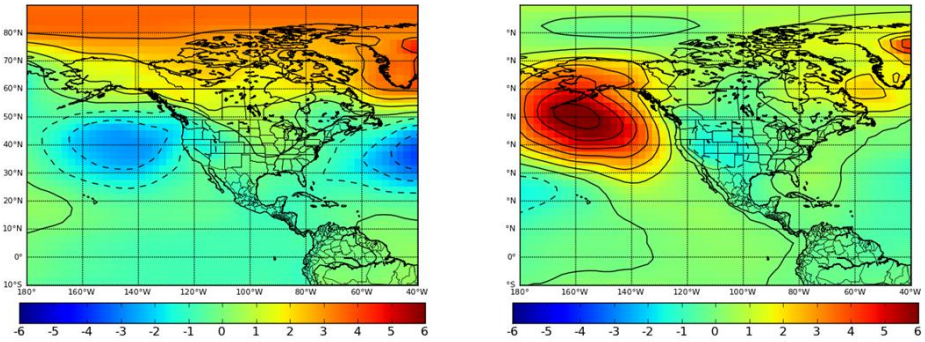

Figure 4.20: Monthly anomalies of SLP during January EN (left) and LN (right) conditions. Units are in millibars.

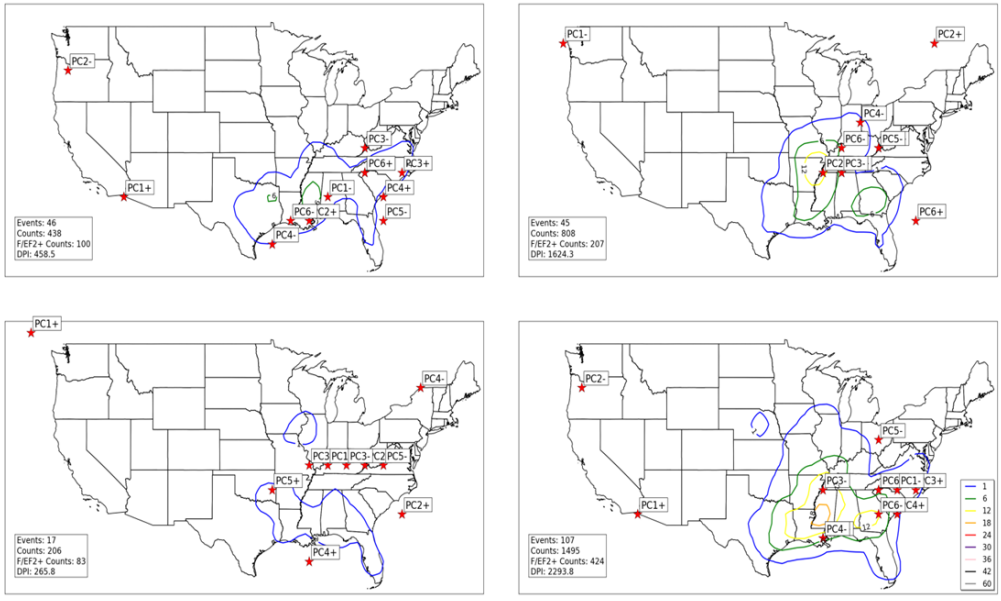

Figure 4.21.a: Locations of maximum 850 V-component wind (noted by red stars) for all EN January tornado outbreak 850 hPa geopotential height composites (upper left), all LN January tornado outbreak 850 hPa geopotential height composites (upper right), all N January tornado outbreak 850 hPa geopotential height composites (lower left), and all January tornado outbreak 850 hPa geopotential height composites (lower right). Contours represent concentrations of tornado activity concurrent with events used to create composites. Tornado counts are on a 1° by 1° grid as described in Section 2. 1.b.ii.

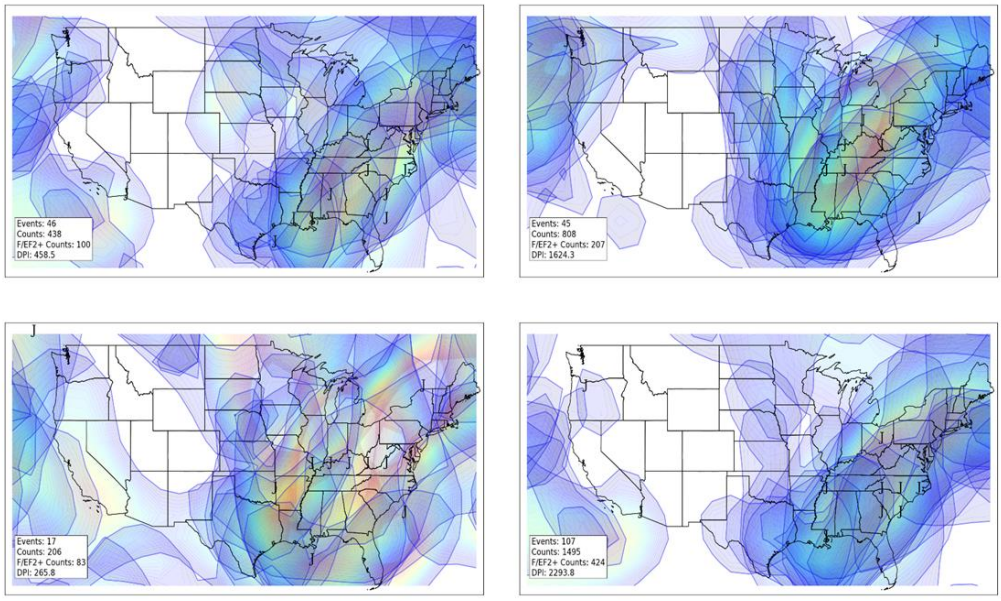

Figure 4.21.b: Similar to 4.21.a, except for jet streams in individual composites. "J" indicates jet stream wind maxima, while shaded areas indicate location of winds associated with individual jet streams of at least 20 knots. Lighter shading (yellow, red) indicates stronger winds.

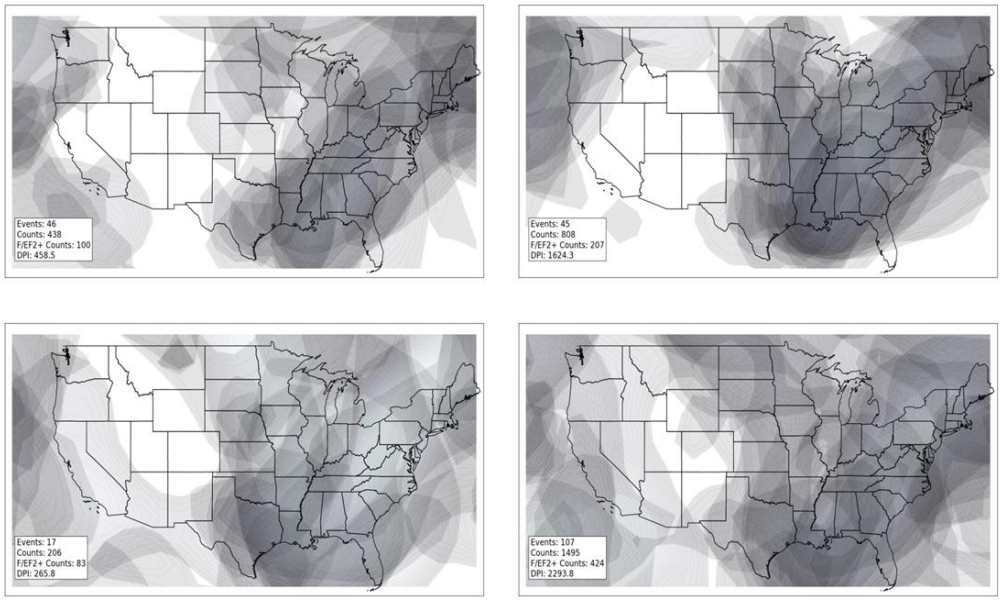

Figure 4.22: Low-level shear greater than 20 knots for all EN January tornado outbreak composites (upper left), all LN January tornado outbreak composites (upper right), all N January tornado outbreak composites (lower left), and all January tornado outbreak composites (lower right). Composites were based on result from PCA of 850 hPa geopotential height fields and low-level shear was calculated via the difference between the 850 hPa wind and surface wind.

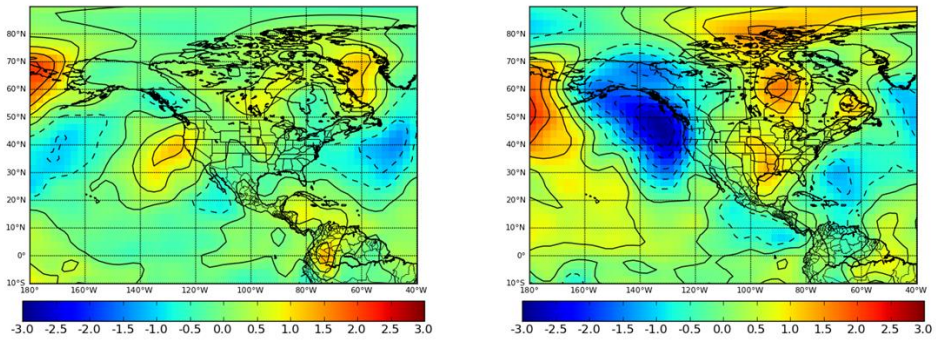

Figure 4.23: Monthly anomalies of 850 hPa V-component wind during January EN (left) and LN (right) conditions. Units are in meters per second.

ENSO-related shifts in instability (lifted index) and moisture fields (precipitable water) also exhibit similar westward/northward shifts during LN conditions as those shifts exhibited in aforementioned ENSO-related low-level jet streams (Figures 4.24 and 4.25). In January EN conditions, instability axes in outbreaks are located across areas adjacent to the Gulf of Mexico from Texas into Florida. During January LN conditions, instability is drastically decreased across much of Florida and southern Georgia and also increased along the Middle Mississippi and Ohio River Valleys, helping to explain the increase in tornado activity during January LN in those locations. Similar shifts are noted in moisture fields, with higher moisture values (i.e. precipitable water values above 1 inch or 25.4 mm) noted as far west as Missouri and northwestern Arkansas in LN outbreaks. However, high precipitable water values are noted across a large part of the continental U.S. east of the Mississippi River regardless of ENSO phase, suggesting that ENSO does not influence moisture values in those regions

in the same manner that it influences other atmospheric features. Additionally, high moisture values can be present in regions that are statically stable.

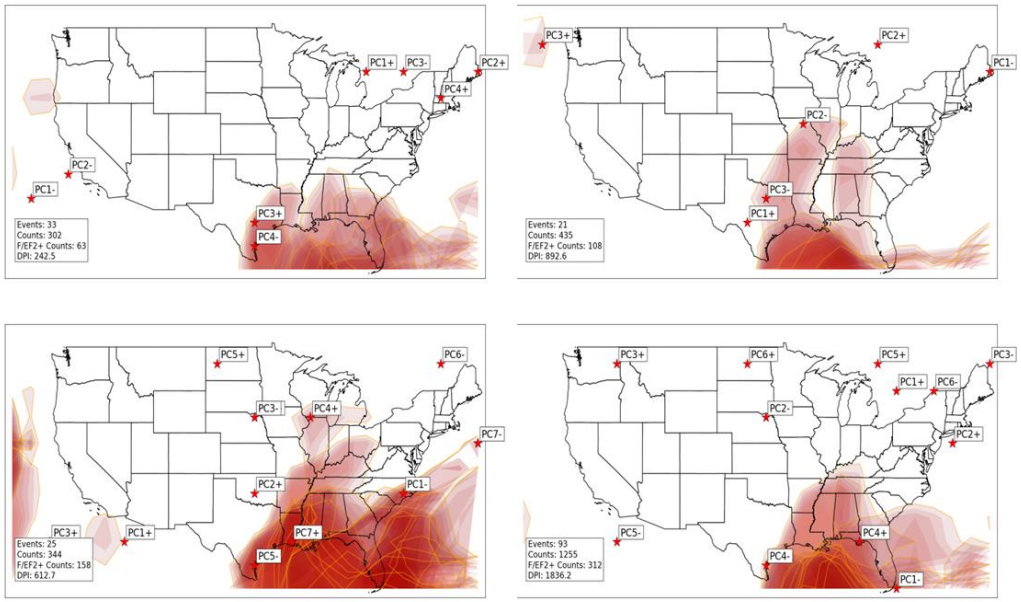

Figure 4.24: Instability axes (noted by shaded regions where lifted index is less than 0) in each composite during January EN (upper left), January LN (upper right), January N (lower left) and all January (lower right) tornado outbreaks. Stars indicate location of largest negative anomaly (departure from mean of all January tornado outbreaks) of lifted index. Darker red shading indicates stronger instability (i.e., lower lifted index).

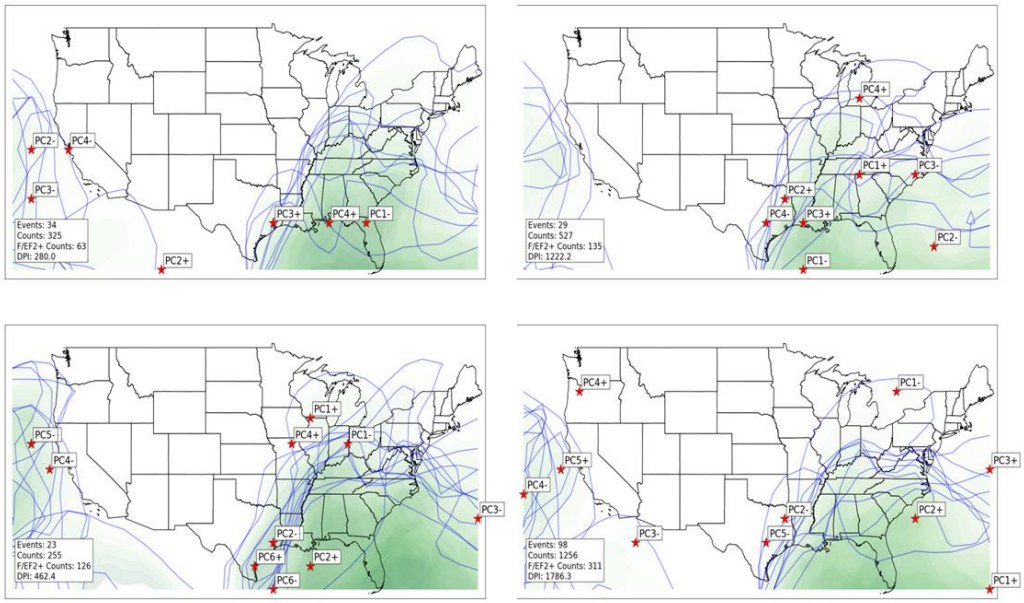

Figure 4.25: Moisture axes (noted by shaded regions where precipitable water is greater than 1 inch) in each composite during January EN (upper left), January LN (upper right), January N (lower left) and all January (lower right) tornado outbreaks. Stars indicate location of largest anomaly (departure from mean of all January tornado outbreaks) of precipitable water. Darker green shading indicates greater moisture values (i.e., lower precipitable water).

Evidence of shifts in upper-level jet streams and wind maxima as a function of ENSO are clearly indicated in monthly anomalies of 300 hPa scalar wind fields (Figure 4.26), but not clearly indicated in composites of 300 hPa wind field maxima in EN, LN, and N January tornado outbreaks (Figures 4.27.a and 4.27.b), nor are they clearly indicated in composites of deep-layer vertical wind shear (Figure 4.28). Monthly anomalies during EN conditions indicate an anomalously strong 300 hPa scalar wind field from the Pacific, through Mexico, and into Florida, which is likely an extension of the southwardly displaced jet stream influenced by ENSO that has been identified in past studies (Rasmussen and Mo 1993; Cook and Schaefer

2008; Climate Prediction Center 2012, website: http://www.cpc.ncep.noaa.gov/products/analysis_monitoring/ensocycle/nawinter.shtml). Given the relationship between upper-level jet streams and synoptically-driven low-level jet streams as described by Uccelini and Johnson (1979), it is plausible that the southward displacement of the low-level jet is directly tied to the southward displacement of the upper-level jet. This is observed both within outbreaks (as assessed by individual composites in Figures 4.21.a and 4.21.b) and within the atmosphere independent of outbreaks (as assessed by monthly anomalies in Figure 4.23). The combined influence of southward shifts in low- and upper-level jet position due to EN conditions appear to contribute to the statistically significant decrease in tornado activity across the Lower Mississippi Valley.

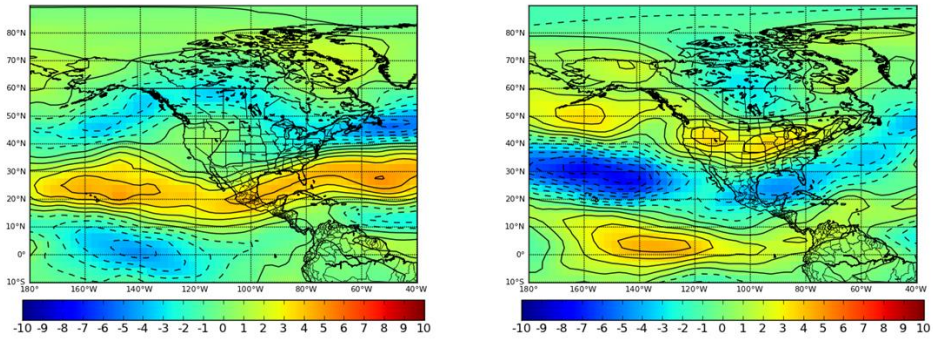

Figure 4.26: Monthly anomalies of 300 hPa scalar wind during January EN (left) and LN (right) conditions. Units are in meters per second.

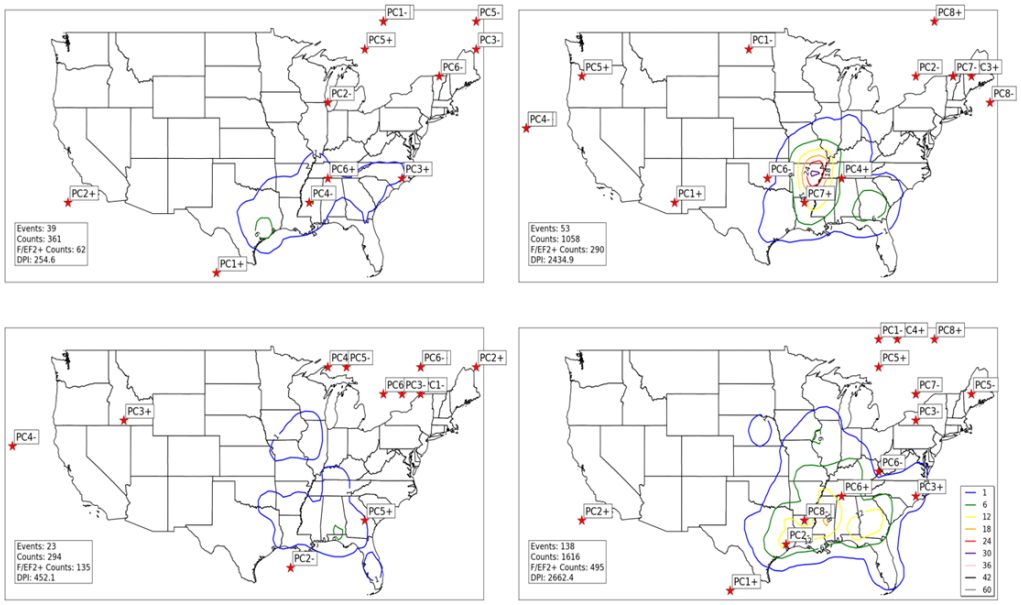

Figure 4.27.a: Locations of maximum 300 hPa scalar wind (noted by red stars) for all EN January tornado outbreak 300 hPa geopotential height composites (upper left), all LN January tornado outbreak 300 hPa geopotential height composites (upper right), all N January tornado outbreak 300 hPa geopotential height composites (lower left), and all January tornado outbreak 300 hPa geopotential height composites (lower right). Contours represent concentrations of tornado activity concurrent with events used to create composites. Tornado counts are on a 1° by 1° grid as described in Section 2. 1.b.ii.

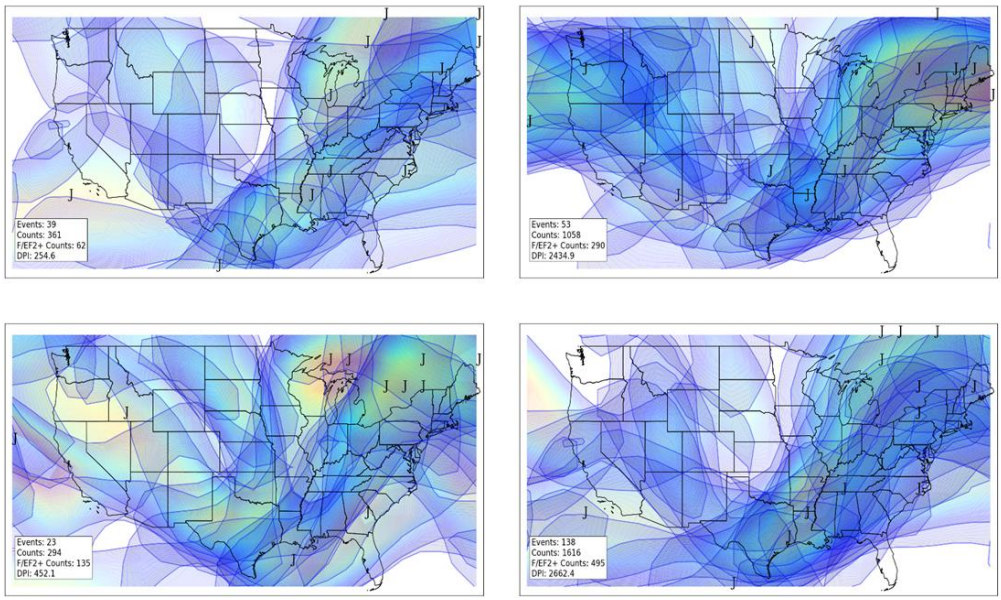

Figure 4.27.b: Similar to 4.27.a, except for jet streams in individual composites. "J" indicates jet stream wind maxima, while shaded areas indicate location of winds associated with individual jet streams of at least 70 knots. Lighter shading (yellow, red) indicates stronger winds.

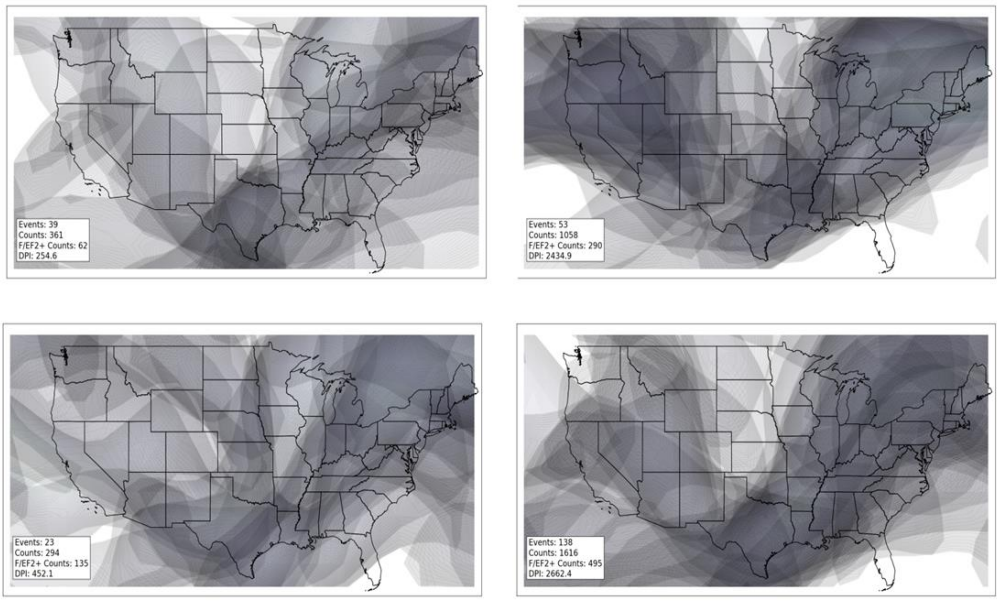

Figure 4.28: Deep-layer (surface to 300 hPa) shear greater than 60 knots for all EN January tornado outbreak composites (upper left), all LN January tornado outbreak composites (upper right), all N January tornado outbreak composites (lower left), and all January tornado outbreak composites (lower right). Composites were based on result from PCA of 300 hPa geopotential height fields and low-level shear was calculated via the difference between the 300 hPa wind and surface wind.

No clear explanation exists for the lack of similarity between monthly anomalies of geopotential height and wind fields at 300 hPa as a function of ENSO and individual composites of 300 hPa geopotential height and wind fields concurrent to January outbreaks in various ENSO phases. While it is possible that the individual dominant patterns identified through the compositing methodology are substantially deviant from the means and anomalies shown on a monthly basis, it is also important to note that results in subsequent months do not exhibit this behavior and individual composites appear to be much more closely related to monthly anomaly fields of geopotential heights and wind fields at the 300 hPa level.

b. February

Another key result from Section 4.1 indicated that while maxima of tornado activity reside in the general vicinity of Mississippi during both EN and LN conditions, tornado activity was more frequent in LN conditions in that area than in EN conditions. Additionally, the state of Florida experiences more frequent tornado activity during EN (a finding consistent with CS08). Several atmospheric features appear to support these shifts in tornado activity. Southward shifts in surface cyclone location during EN are far more dramatic in February than they are in January (Figure 4.29). During LN conditions, a greater concentration of surface cyclones exists in the Great Lakes region. This is consistent with the LN corridor present in CS08 and also identified in Eichler and Higgins (2006). Both CS08 and the current study indicate that this northward shift in surface cyclone track during LN contributed to increased tornado activity in the Lower Mississippi Valley.

A very distinct shift in 300 hPa wind fields as a function of ENSO are noted in composites shown in Figures 4.30.a and 4.31.b. This difference is far more striking than indicated in January 300 hPa wind field composites (Figures 4.27.a and 4.27.b), but also more in line with monthly anomalies of 300 hPa wind fields during EN February (Figure 4.32) and even in EN January (Figure 4.26). The southward shift in the upper-level jet stream indicated in these figures is consistent with several previous studies (Rasmussen and Mo 1993; Cook and Schaefer 2008; Climate Prediction

Center 2012), consistent with the southward displacement in surface cyclone track identified in Figure 4.29 and in Eichler and Higgins (2006), and is also consistent with a the southward shift in location of low-level jet streams shown in Figures 4.33, 4.34.a, and 4.34.b. The southward shift in tornado activity (including the decrease in the Lower Mississippi Valley and increase in Florida) is also supported by these atmospheric trends. Deep-layer and low-layer vertical wind shear composites (Figures 4.31 and 4.35) are closely related to the jet displacement identified in composites in Figures 4.30.a, 4.30.b, 4.34.a, and 4.34.b and also support a southward displacement in tornado activity.

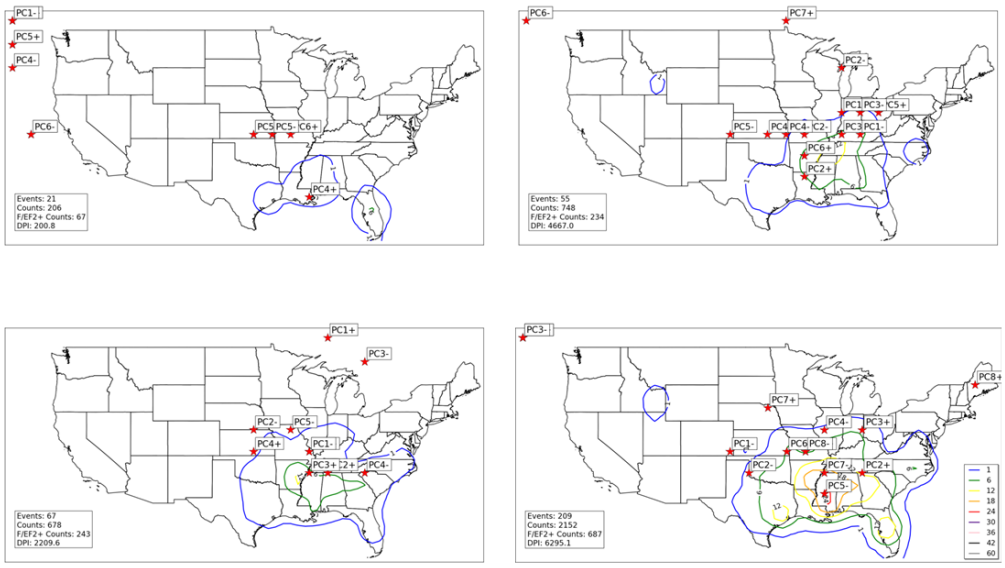

Figure 4.29: Locations of minimum SLP (noted by red stars) for all EN February tornado outbreak SLP composites (upper left), all LN February tornado outbreak SLP composites (upper right), all N February tornado outbreak SLP composites (lower left), and all January tornado outbreak SLP composites (lower right). Contours represent concentrations of tornado activity concurrent with events used to create composites. Tornado counts are on a 1° by 1° grid as described in Section 2. 1.b.ii.

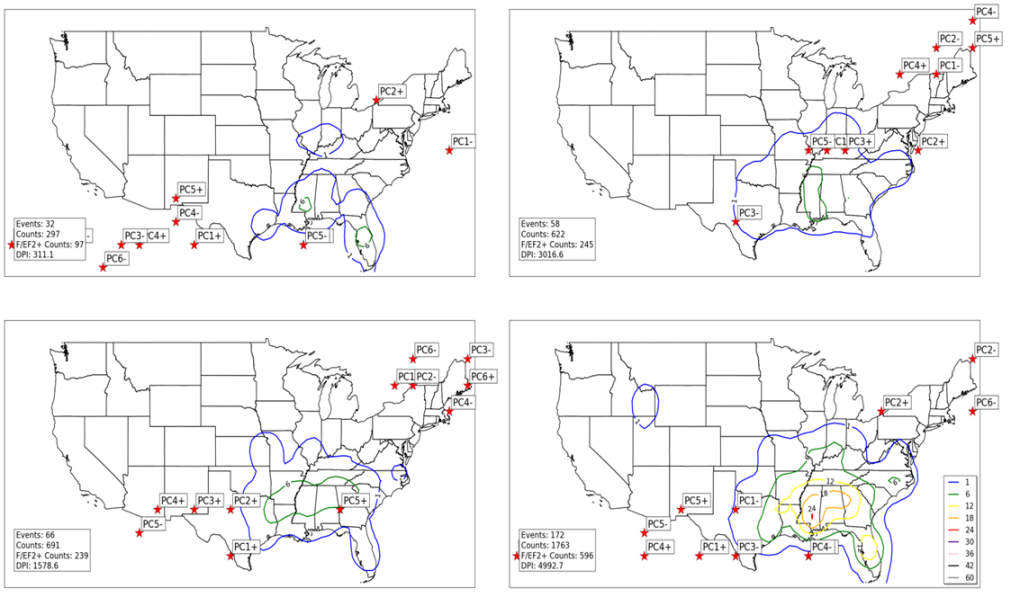

Figure 4.30.a: Locations of maximum 300 hPa scalar wind (noted by red stars) for all EN February tornado outbreak 300 hPa geopotential height composites (upper left), all LN February tornado outbreak 300 hPa geopotential height composites (upper right), all N February tornado outbreak 300 hPa geopotential height composites (lower left), and all February tornado outbreak 300 hPa geopotential height composites (lower right). Contours represent concentrations of tornado activity concurrent with events used to create composites. Tornado counts are on a 1° by 1° grid as described in Section 2. 1.b.ii.

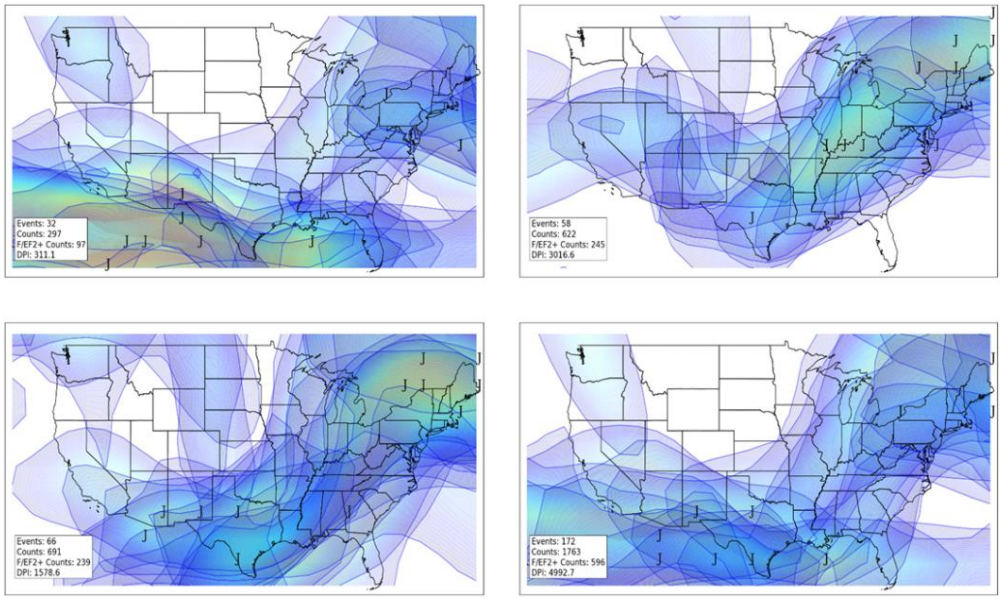

Figure 4.30.b: Similar to 4.30.a, except for jet streams in individual composites. "J" indicates jet stream wind maxima, while shaded areas indicate location of winds associated with individual jet streams of at least 70 knots. Lighter shading (yellow, red) indicates stronger winds.

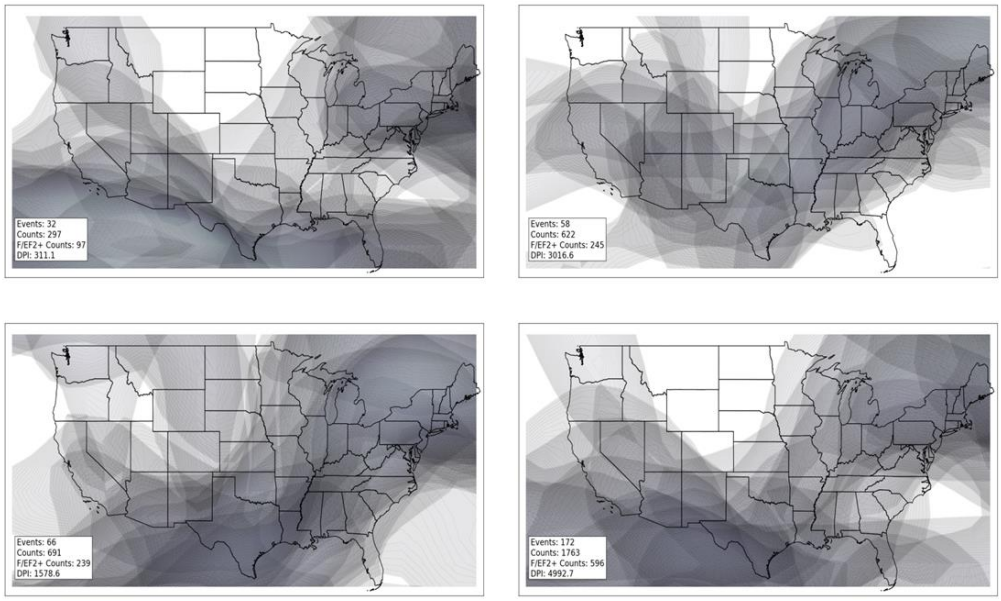

Figure 4.31: Deep layer (surface to 300 hPa) shear calculated as described in Figure 4.28 for all EN February composites (upper left), all LN February composites (upper right), all N February composites (lower left), and all February composites (lower right).

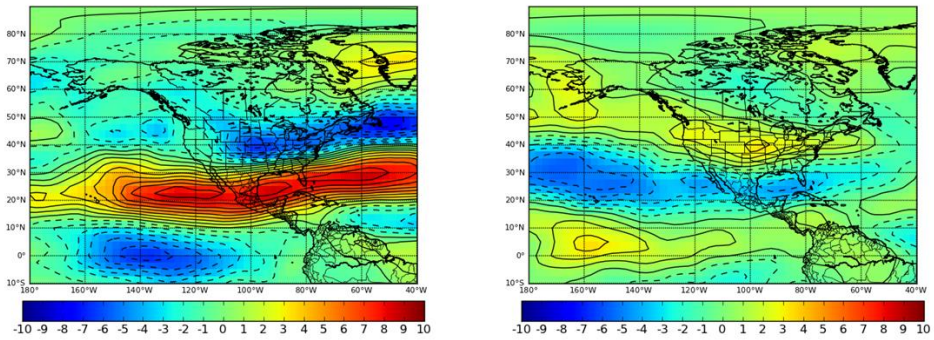

Figure 4.32: Monthly anomalies of 300 hPa scalar wind during February EN (left) and LN (right) conditions. Units are in meters per second.

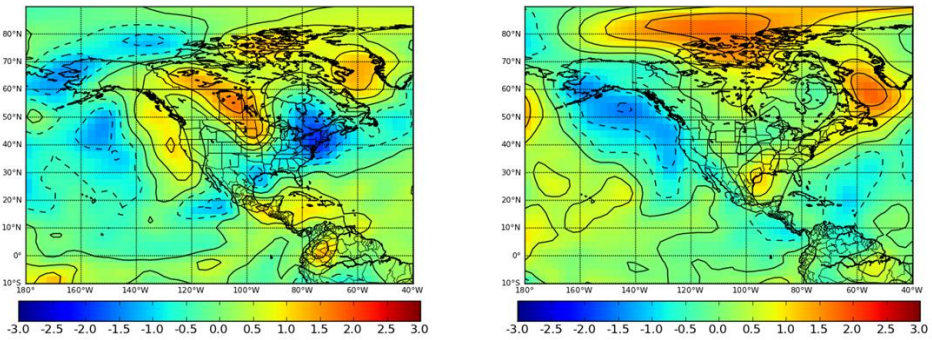

Figure 4.33: Monthly anomalies of 850 hPa V-component wind during February EN (left) and LN (right) conditions. Units are in meters per second.

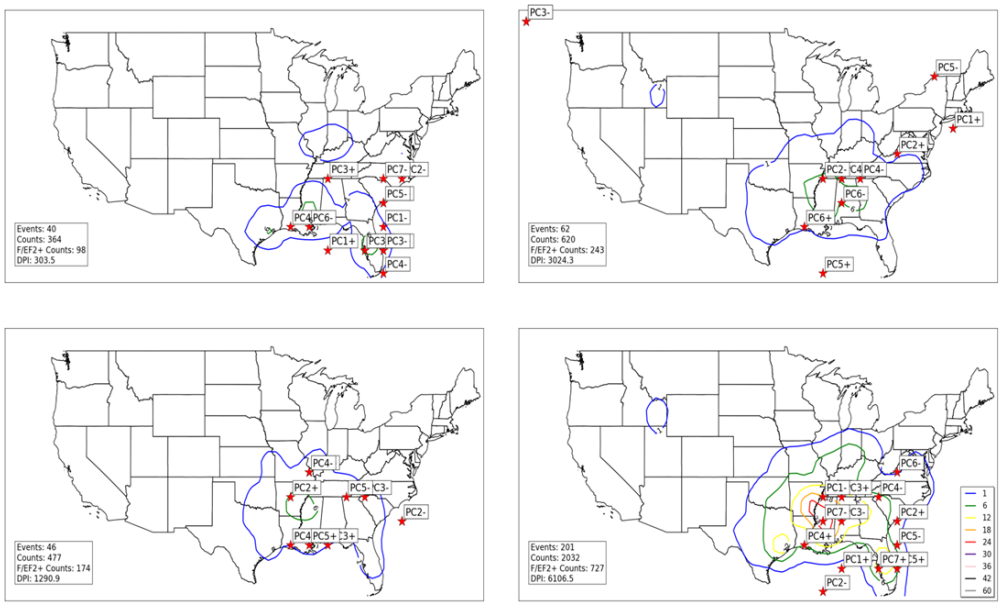

Figure 4.34.a: Locations of maximum 850 V-component wind (noted by red stars) for all EN February tornado outbreak 850 hPa geopotential height composites (upper left), all LN February tornado outbreak 850 hPa geopotential height composites (upper right), all N February tornado outbreak 850 hPa geopotential height composites (lower left), and all February tornado outbreak 850 hPa geopotential height composites (lower right). Contours represent concentrations of tornado activity concurrent with events used to create composites. Tornado counts are on a 1° by 1° grid as described in Section 2. 1.b.ii.

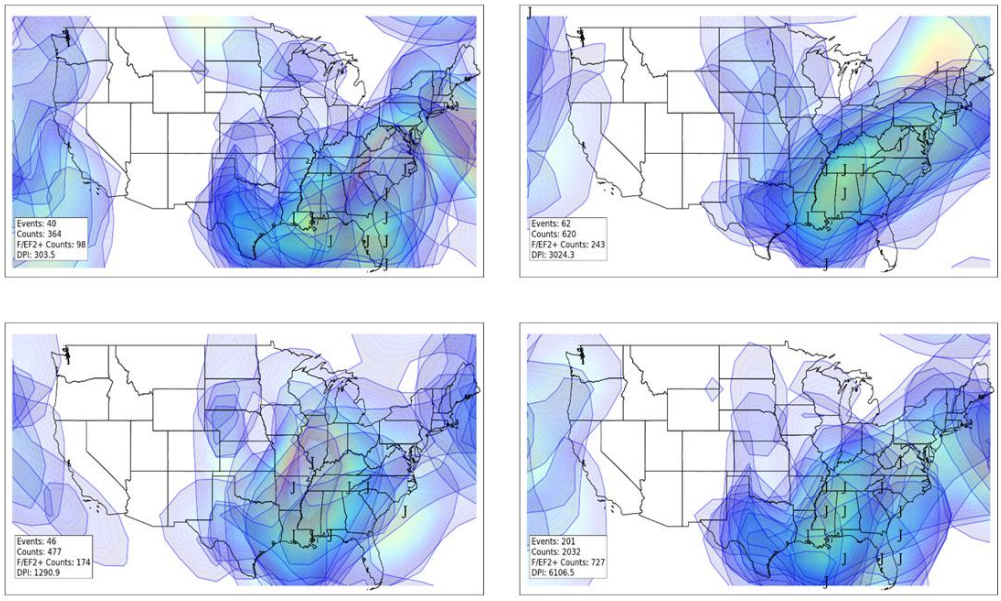

Figure 4.34.b: Similar to 4.34.a, except for jet streams in individual composites. "J" indicates jet stream wind maxima, while shaded areas indicate location of winds associated with individual jet streams of at least 20 knots. Lighter shading (yellow, red) indicates stronger winds.

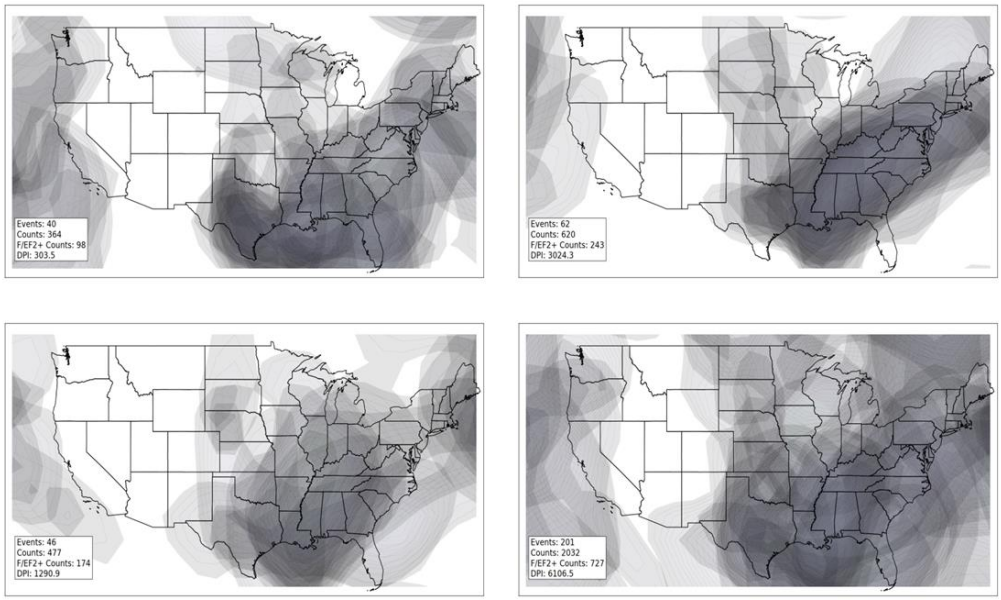

Figure 4.35: Low-level shear calculated as described in Figure 4.22 for all EN February composites (upper left), all LN February composites (upper right), all N February composites (lower left), and all February composites (lower right).

Interestingly, the distinct ENSO-related shifts that appear in upper- and lower-level jets do not appear as strongly in instability and moisture fields (Figures 4.36 and 4.37). In February outbreaks in all three phases of ENSO, instability tends to be most focused across the Gulf of Mexico and northward into the Lower Mississippi Valley. Only in February N tornado outbreaks does instability extend farther northwest into Kansas and Missouri. In other February EN and LN outbreaks, instability extends northeastward into Kentucky and Tennessee. Similar statements can be made regarding moisture fields in February tornado outbreaks, with slightly northward displacement of moisture fields in February N tornado outbreaks compared to February EN and February LN outbreaks. These results indicate that while instability and moisture are necessary conditions for tornado outbreaks, they alone are not sufficient for tornado outbreak development. Tornado outbreak activity appears to be more readily modulated by the orientation of low-level and upper-level jet streams.

c. March

Tornado activity tends to increase across the entire study domain east of the Rocky Mountains in March coincident with a general increase of tornado activity during the study period as discussed in Chapter 3. These increases are most dramatic during LN conditions across Illinois/Indiana and the southern tier of the U.S. (from Texas to South Carolina).

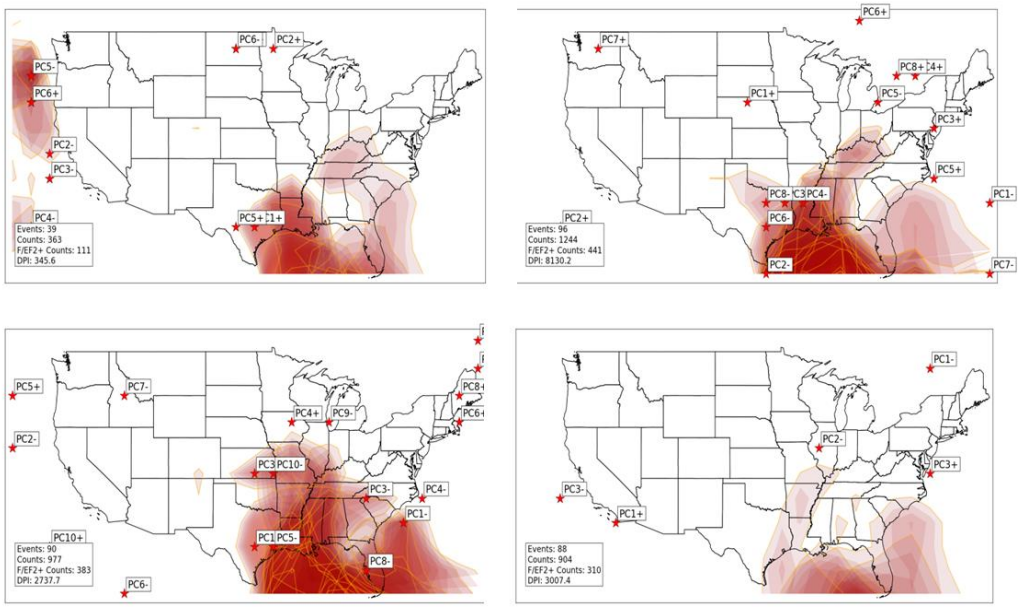

Figure 4.36: Instability axes (noted by shaded regions where lifted index is less than 0) in each composite during February EN (upper left), February LN (upper right), February N (lower left) and all February (lower right) tornado outbreaks. Stars indicate location of largest negative anomaly of lifted index. Darker red shading indicates stronger instability (i.e., lower lifted index).

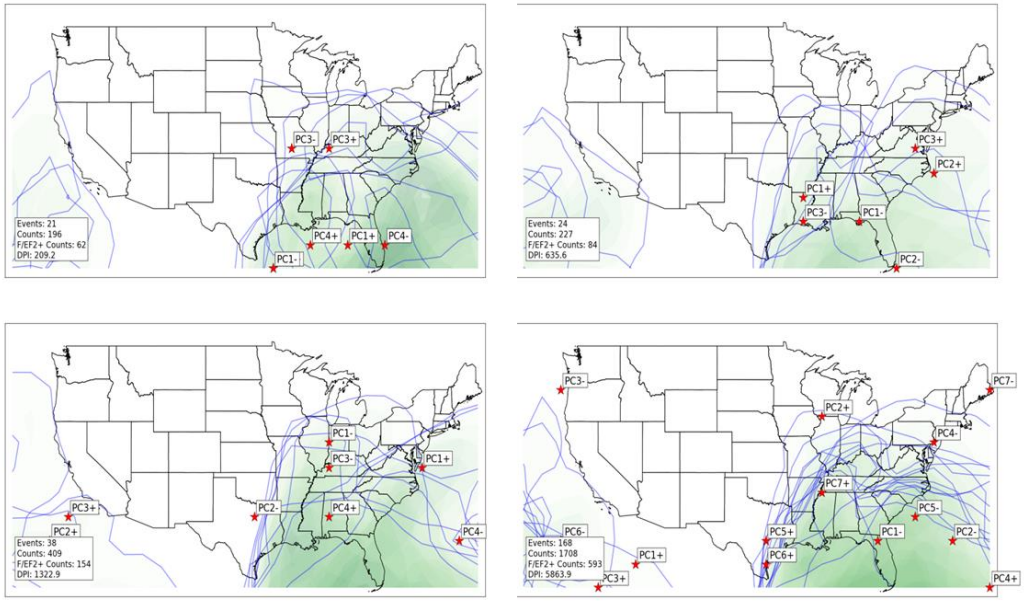

Figure 4.37: Moisture axes (noted by shaded regions where precipitable water is greater than 1 inch) in each composite during February EN (upper left), February LN (upper right), February N (lower left) and all February (lower right) tornado outbreaks. Stars indicate location of largest anomaly of precipitable water. Darker green shading indicates greater moisture values (i.e., lower precipitable water).

Composites of SLP (used for identification of surface cyclones; Figure 4.38) are not particularly conclusive in supporting the ENSO-related shifts in activity. These composites indicate a surface low across southern Wisconsin associated with tornado activity across Illinois and Indiana. Other SLP minima indicated in composites across the Ohio/Tennessee River Valleys and southern Appalachians support increased tornado activity in the Southern U.S. from Alabama to the Carolinas. In EN March composites of SLP, minima are located from southern Colorado to Ohio, but tornado activity associated with these minima is not nearly as extensive in vicinity of those minima in LN March composites, suggesting the likelihood of additional atmospheric factors not shown in SLP composites that may be influencing tornado activity.

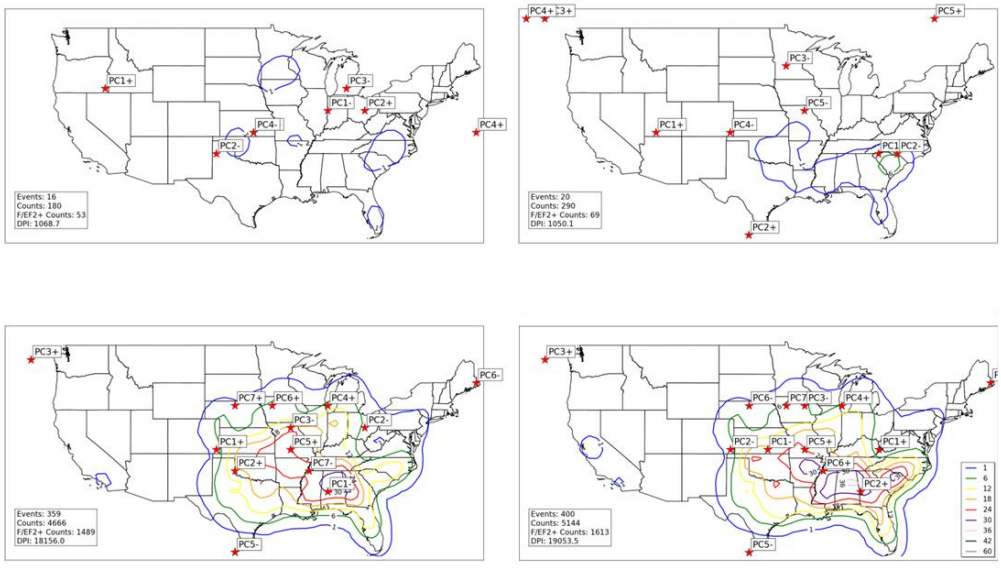

Figure 4.38: Locations of minimum SLP (noted by red stars) for all EN March tornado outbreak SLP composites (upper left), all LN March tornado outbreak SLP composites (upper right), all N March tornado outbreak SLP composites (lower left), and all March tornado outbreak SLP composites (lower right). Contours represent concentrations of tornado activity concurrent with events used to create composites. Tornado counts are on a 1° by 1° grid as described in Section 2. 1.b.ii.

Monthly anomalies of SLP indicate weak negative anomalies across the intermountain west during LN conditions, which would support more frequent surface cyclones in that region (Figure 4.39). This would also support more frequent/anomalous warm advection immediately downstream of this anomaly, as indicated in monthly anomalies of 850 hPa meridional wind (Figure 4.40). Each of these factors support tornado activity in those warm advection regions and areas immediately downstream.

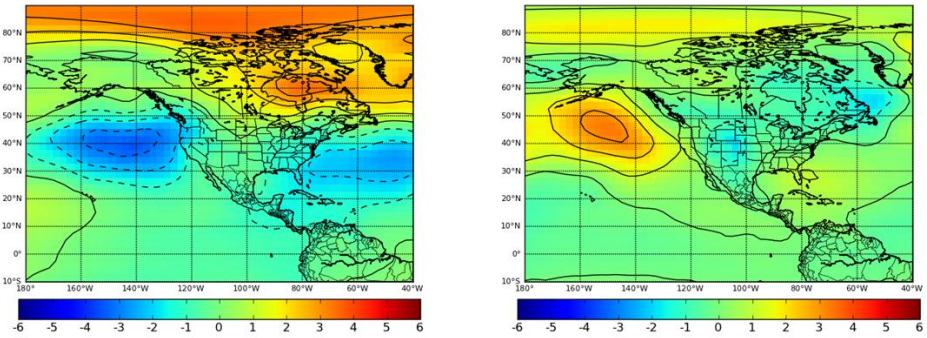

Figure 4.39: Monthly anomalies of SLP during March EN (left) and LN (right) conditions. Units are in millibars.

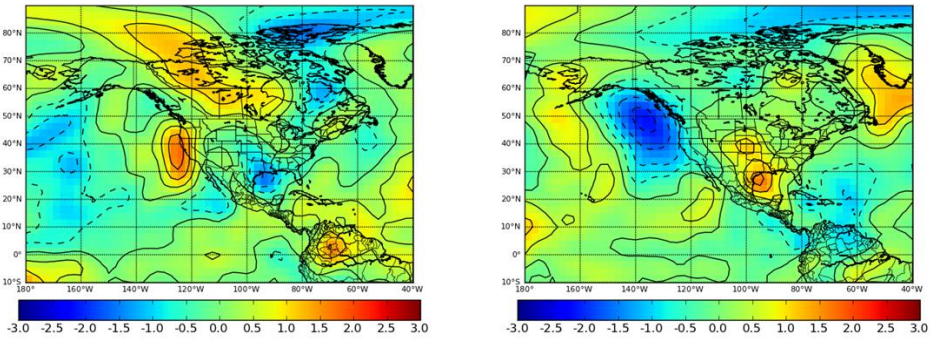

Figure 4.40: Monthly anomalies of 850 hPa V-component wind during March EN (left) and LN (right) conditions. Units are in meters per second.

In the upper levels, a more distinct, ENSO-related bi-modal shift in upper level jet streams is indicated in composites (Figures 4.41.a and 4.41.b), with a southwardly displaced jet stream noted in EN March tornado outbreaks across southern Texas, southern New Mexico, and Mexico. The southward shift is consistent with southward displacement of monthly anomalies of 300 hPa scalar wind fields (Figure 4.43) particularly within areas of stronger positive wind anomalies across the eastern Pacific, Mexico, the Gulf of Mexico, and Florida. During LN conditions, 300 hPa wind maxima in composites are noted mainly across the southern Great Plains and also the northeastern U.S. Similar southward shifts in maxima of deep-layer vertical wind shear are noted in composites during EN March outbreaks (Figure 4.42). These shifts impact tornado activity also indirectly through their influence on surface cyclone activity and low-level jets.

Results from PCA of instability fields in March outbreaks indicate substantial shifts (Figure 4.44). During EN March outbreaks, areas of static instability are located across a large part of the U.S., including the Pacific Northwest, southwestern U.S. and Great Plains from the Gulf Coast to as far north as southeastern South Dakota. In contrast, instability is focused from the Lower Mississippi Valley northward to northern Indiana during LN March outbreaks. The widespread nature of static instability in some of the EN March outbreaks is not consistent with the decreased tornado activity observed during EN March across those areas (particularly north of the

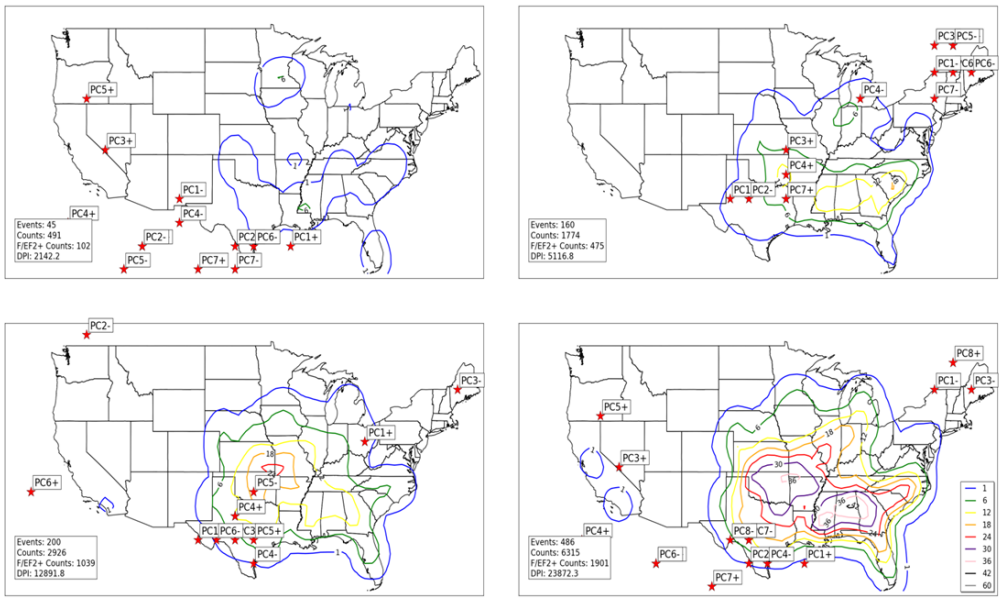

Figure 4.41.a: Locations of maximum 300 hPa scalar wind (noted by red stars) for all EN March tornado outbreak 300 hPa geopotential height composites (upper left), all LN March tornado outbreak 300 hPa geopotential height composites (upper right), all N March tornado outbreak 300 hPa geopotential height composites (lower left), and all March tornado outbreak 300 hPa geopotential height composites (lower right). Contours represent concentrations of tornado activity concurrent with events used to create composites. Tornado counts are on a 1° by 1° grid as described in Section 2. 1.b.ii.

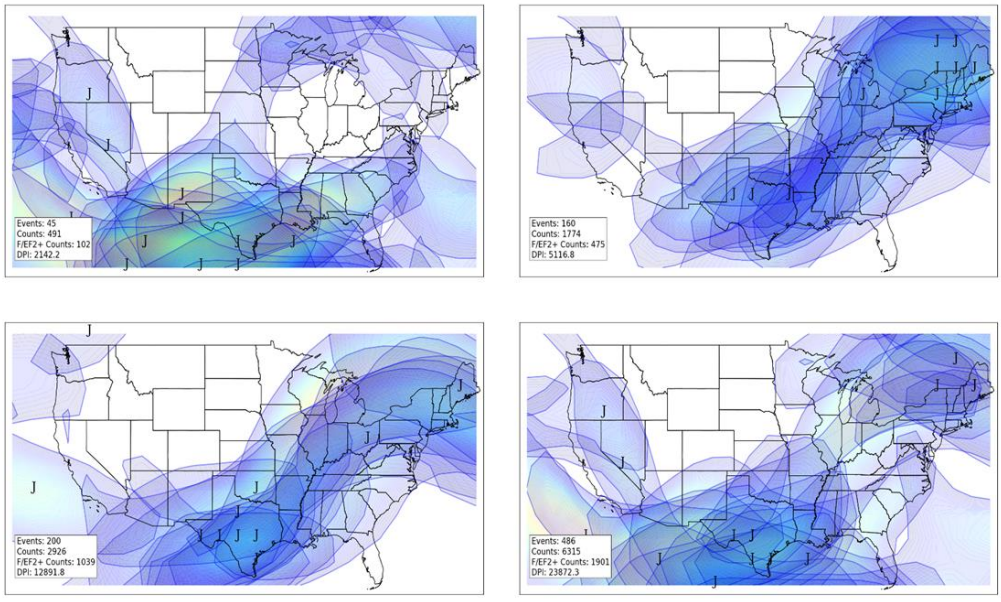

Figure 4.41.b: Similar to 4.41.a, except for jet streams in individual composites. "J" indicates jet stream wind maxima, while shaded areas indicate location of winds associated with individual jet streams of at least 70 knots. Lighter shading (yellow, red) indicates stronger winds.

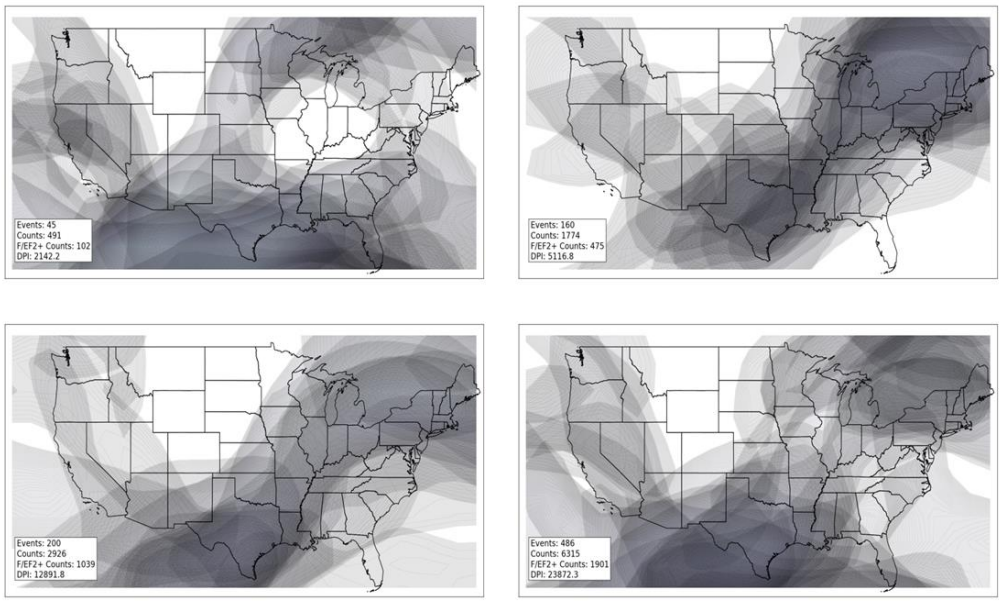

Figure 4.42: Deep layer (surface to 300 hPa) shear calculated as described in Figure 4.28 for all EN March composites (upper left), all LN March composites (upper right), all N March composites (lower left), and all March composites (lower right).

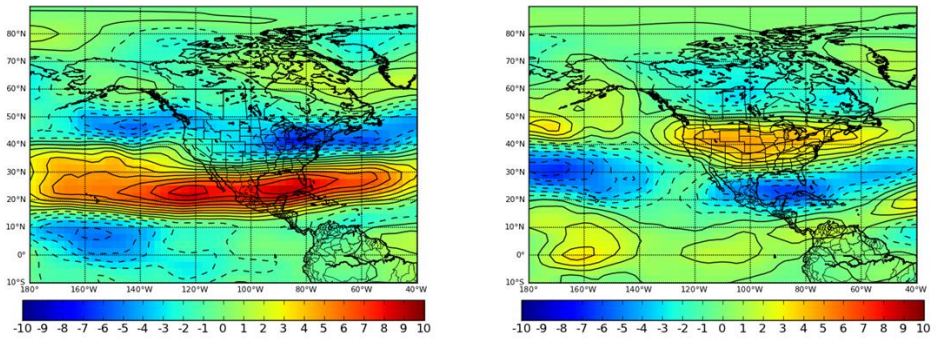

Figure 4.43: Monthly anomalies of 300 hPa scalar wind during March EN (left) and LN (right) conditions. Units are in meters per second.

central Great Plains eastward to the upper Midwest), suggesting that either 1) additional synoptic-scale atmospheric features for producing tornado outbreaks in those areas (i.e., lift, shear) are absent or 2) smaller-scale atmospheric phenomenon not resolved by the present analysis are not supportive of tornado outbreak development in those areas. Shifts in moisture axes (Figure 4.45) are consistent with aforementioned shifts in instability axes, particularly with increased moisture across the central Great Plains during EN March outbreaks and moisture axes located farther to the east of those regions during LN March outbreaks.

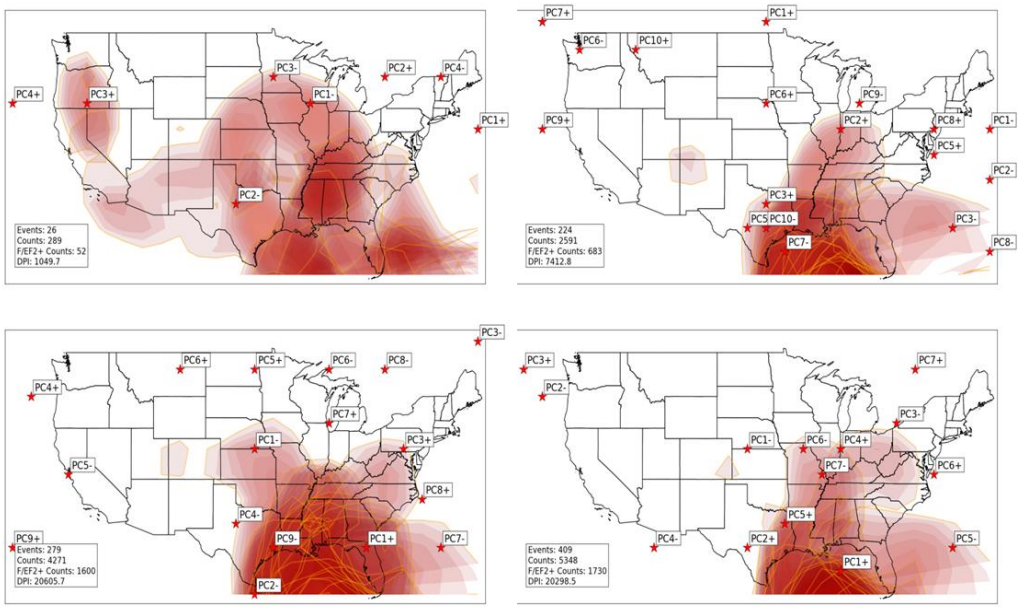

Figure 4.44: As in Figure 4.24, except for March EN outbreaks (upper left), March LN outbreaks (upper right), March N outbreaks (lower left), and all March outbreaks (lower right).

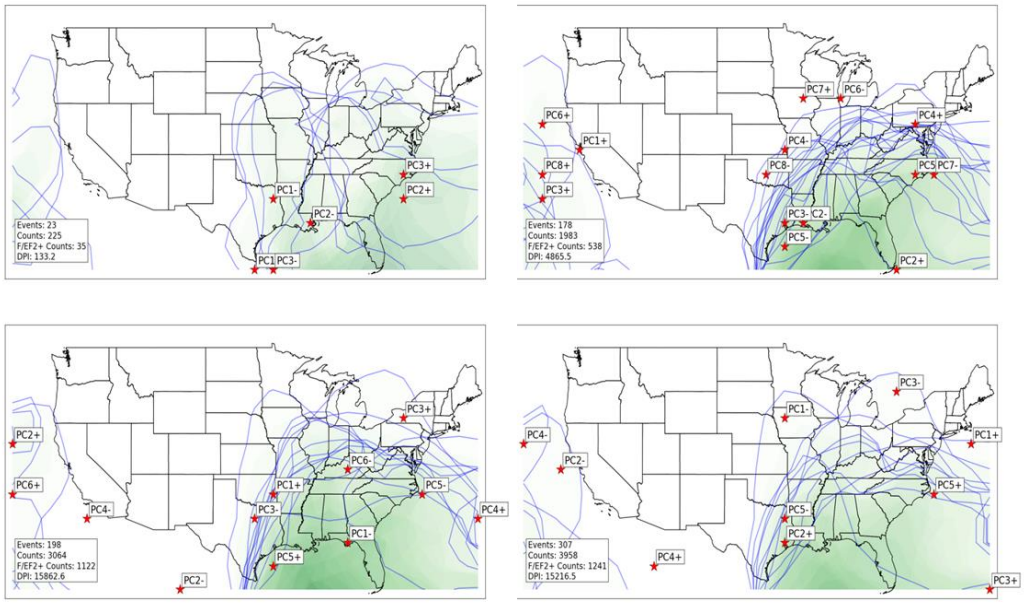

Figure 4.45: As in Figure 4.25, except for March EN outbreaks (upper left), March LN outbreaks (upper right), March N outbreaks (lower left), and all March outbreaks (lower right).

d. April

As discussed in Chapter 3, April is by far the most active month in the study period for tornado activity. Some areas from the southern Great Plains eastward to northern Alabama experience frequent tornadoes regardless of ENSO phase. However, slightly more frequent tornado activity in these areas and dramatically increased tornado activity across the northern Great Plains (Nebraska and Kansas) eastward to Indiana and western Ohio during LN. Several ENSO-related shifts in the atmosphere support these shifts.

In the lowest levels of the atmosphere, distinct shifts in surface cyclone locations are noted in composites of SLP (Figure 4.46). Surface

cyclone activity is focused in an area from Kansas northeastward to Wisconsin in LN conditions. Low-level jet streams also exhibit a distinct northward shift during LN conditions (Figure 4.47.a and 4.47.b), monthly anomalies of 850 hPa meridional wind are also maximized across the Great Plains during LN conditions (Figure 4.48), and distinct northward shifts in instability (i.e., lifted index; Figure 4.49) and low-level shear (Figure 4.50) are also noted especially from Nebraska eastward to northern Ohio. During EN conditions, some composites indicate surface cyclones farther southeast across Kentucky, southeastern Missouri, and Pennsylvania. Each of these atmospheric shifts are among the most dramatic ENSO-influenced shifts documented by this research and support increased tornado activity across the entire U.S., particularly across the central/northern Great Plains and areas to the east across Indiana and western Ohio.

Although ENSO-related shifts in upper-level wind maxima (indicated by maximum 300 hPa wind in composites; Figures 4.51.a and 4.51.b) aren't as distinct as in previous months, there are particularly important shifts involving the enhancement of the upper-level jet (and associated deep-layer vertical wind shear; Figure 4.52) that has an impact on tornado outbreaks across the southern tier of the U.S. from Texas to Alabama. On a monthly time scale, some shift in wind anomalies at 300 hPa as a function of ENSO are apparent (Figure 4.53), particularly in the eastern Pacific east of Hawaii and also across Mexico. Geopotential height anomalies at 300 hPa and 500 hPa (Figures 4.54 and 4.55) suggest favorable patterns for tornado

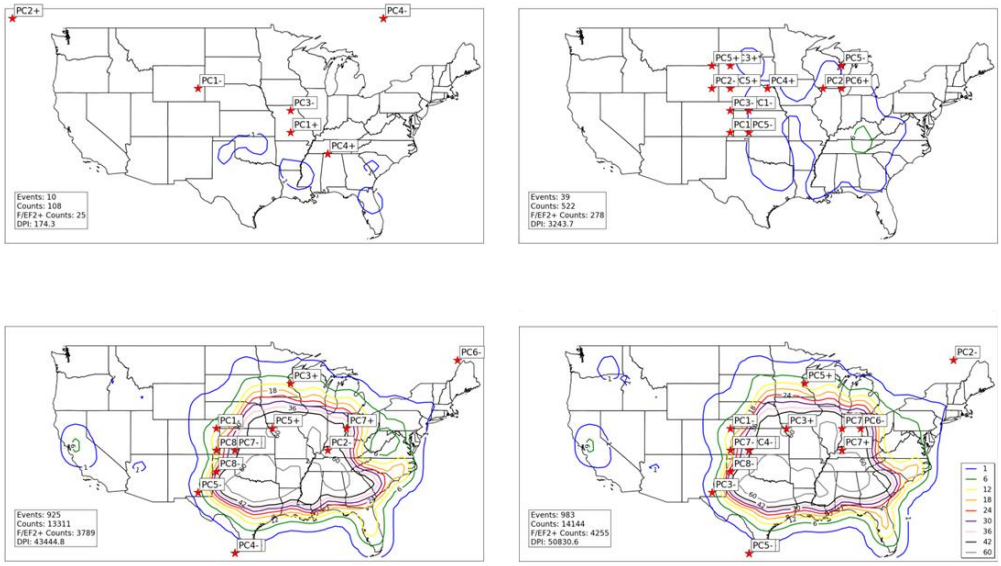

Figure 4.46: Locations of minimum SLP (noted by red stars) for all EN April tornado outbreak SLP composites (upper left), all LN April tornado outbreak SLP composites (upper right), all N April tornado outbreak SLP composites (lower left), and all April tornado outbreak SLP composites (lower right). Contours represent concentrations of tornado activity concurrent with events used to create composites. Tornado counts are on a 1° by 1° grid as described in Section 2. 1.b.ii.

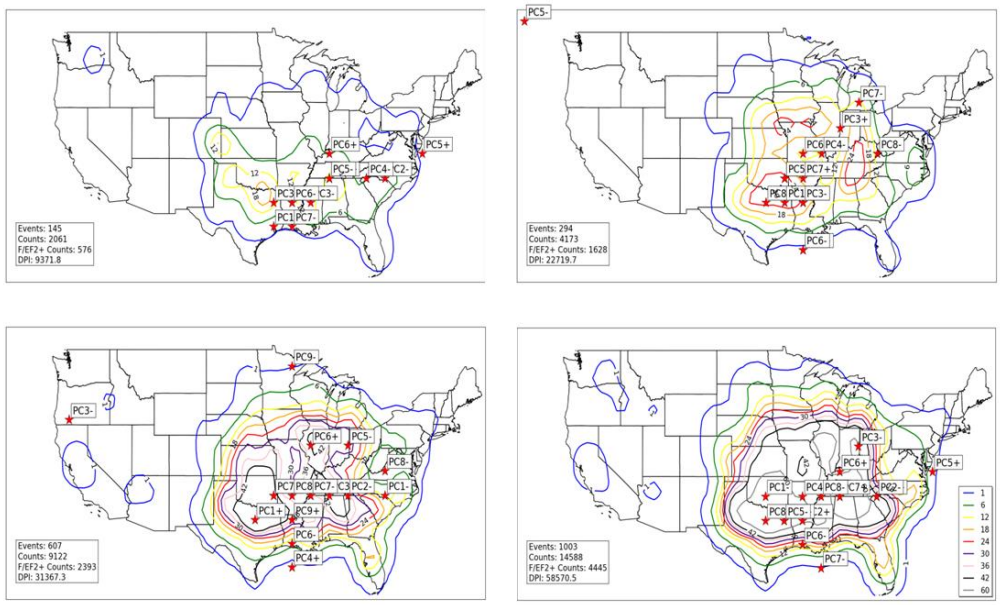

Figure 4.47.a: Locations of maximum 850 V-component wind (noted by red stars) for all EN April tornado outbreak 850 hPa geopotential height composites (upper left), all LN April tornado outbreak 850 hPa geopotential height composites (upper right), all N April tornado outbreak 850 hPa geopotential height composites (lower left), and all April tornado outbreak 850 hPa geopotential height composites (lower right). Contours represent concentrations of tornado activity concurrent with events used to create composites. Tornado counts are on a 1° by 1° grid as described in Section 2. 1.b.ii.

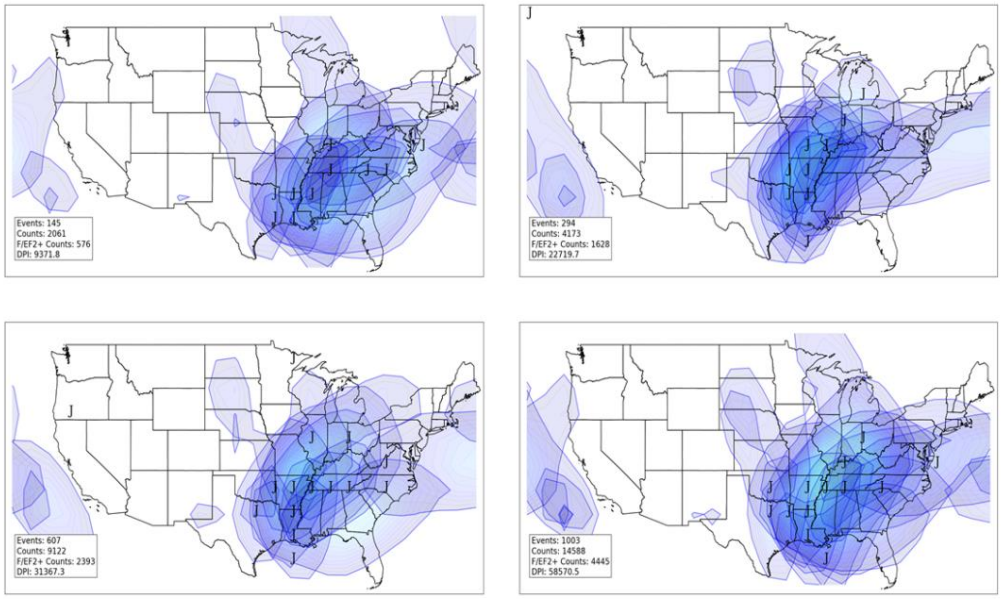

Figure 4.47.b: Similar to 4.47.a, except for jet streams in individual composites. "J" indicates jet stream wind maxima, while shaded areas indicate location of winds associated with individual jet streams of at least 20 knots. Lighter shading (yellow, red) indicates stronger winds.

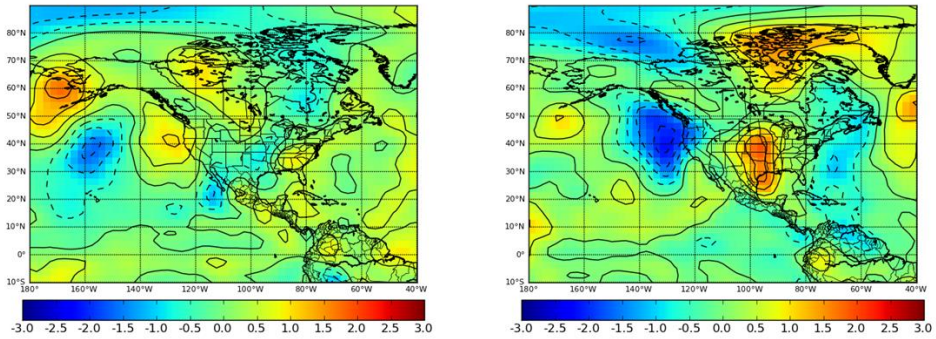

Figure 4.48: Monthly anomalies of 850 hPa V-component wind during April EN (left) and LN (right) conditions. Units are in meters per second.

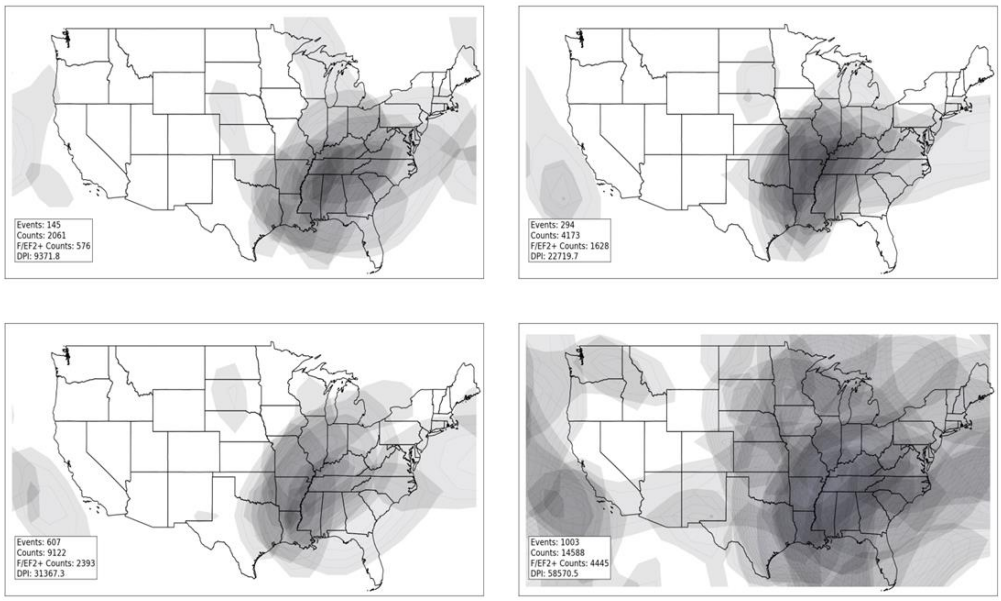

Figure 4.49: Low-level shear calculated as described in Figure 4.22 for all EN April composites (upper left), all LN April composites (upper right), all N April composites (lower left), and all April composites (lower right).

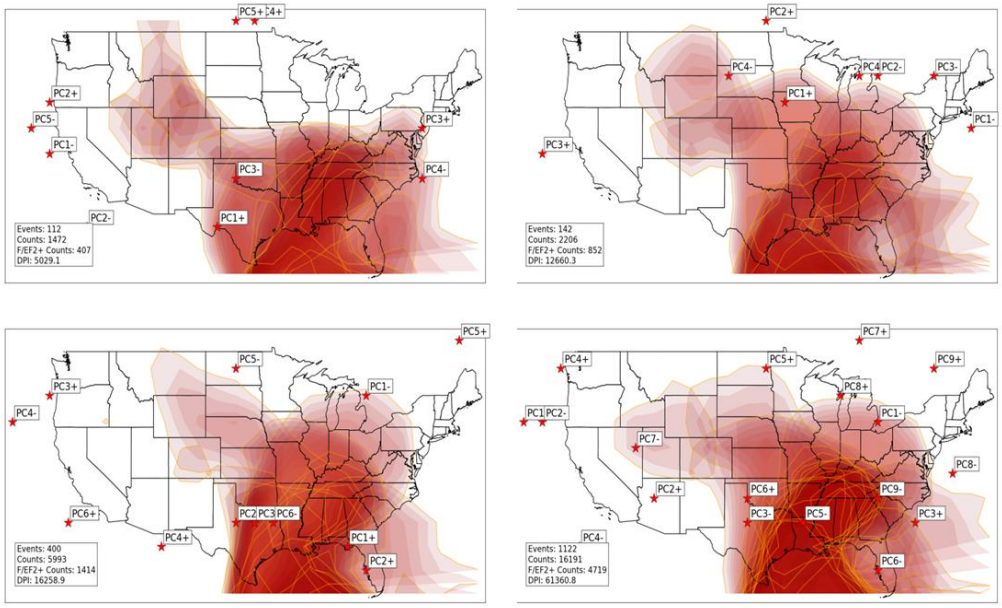

Figure 4.50: As in Figure 4.24, except for April EN outbreaks (upper left), April LN outbreaks (upper right), April N outbreaks (lower left), and all April outbreaks (lower right).

outbreaks in the Plains due to 1) increased southwesterly flow aloft just east of anomaly centers located over the intermountain west, 2) synoptic-scale low-level jet response due to increased southwesterly flow aloft and negative geopotential height anomalies west of the low-level jet axis, and 3) resulting warm, moist advection due to the enhanced meridional synoptically-driven low-level jet. It is important to note that a few of the larger outbreaks in the dataset that occurred east of the Rocky Mountains occurred in particular geopotential height/jet stream configurations for classic tornado outbreaks that are favored during April LN patterns, which is consistent with Lee et al. (2013).

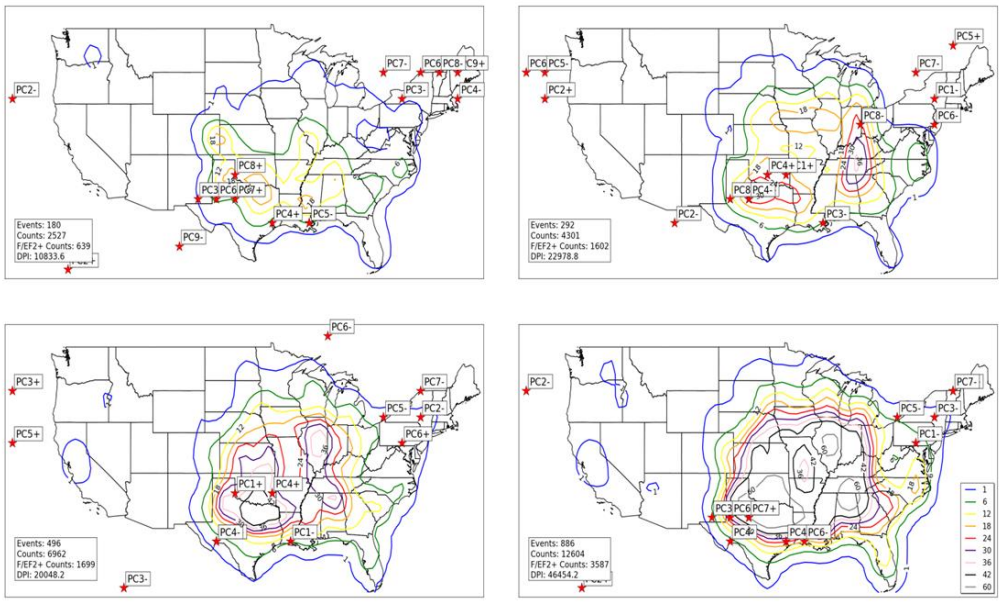

Figure 4.51.a: Locations of maximum 300 hPa scalar wind (noted by red stars) for all EN April tornado outbreak 300 hPa geopotential height composites (upper left), all LN April tornado outbreak 300 hPa geopotential height composites (upper right), all N April tornado outbreak 300 hPa geopotential height composites (lower left), and all April tornado outbreak 300 hPa geopotential height composites (lower right). Contours represent concentrations of tornado activity concurrent with events used to create composites. Tornado counts are on a 1° by 1° grid as described in Section 2. 1.b.ii.

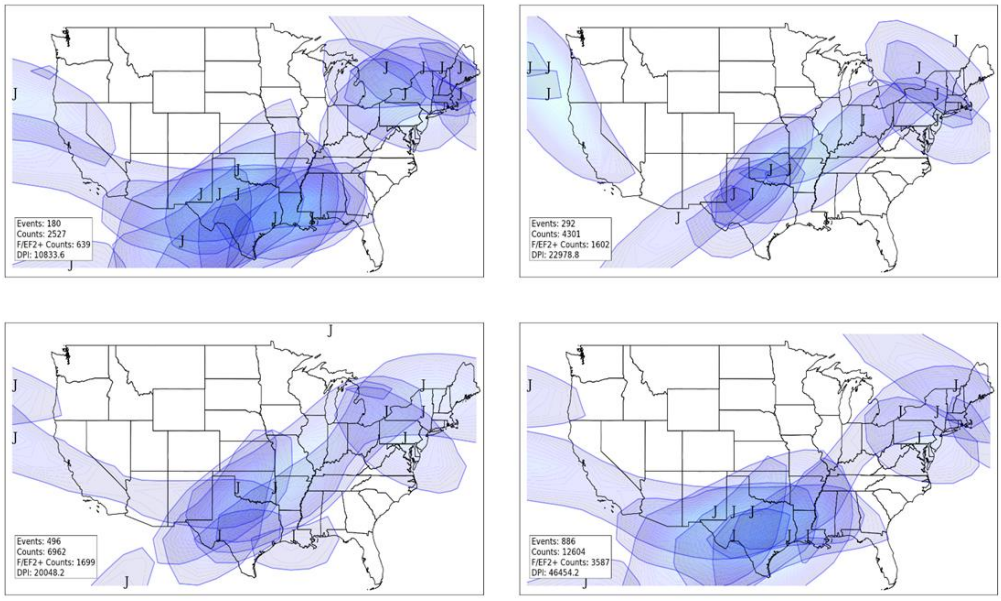

Figure 4.51.b: Similar to 4.51.a, except for jet streams in individual composites. "J" indicates jet stream wind maxima, while shaded areas indicate location of winds associated with individual jet streams of at least 70 knots. Lighter shading (yellow, red) indicates stronger winds.

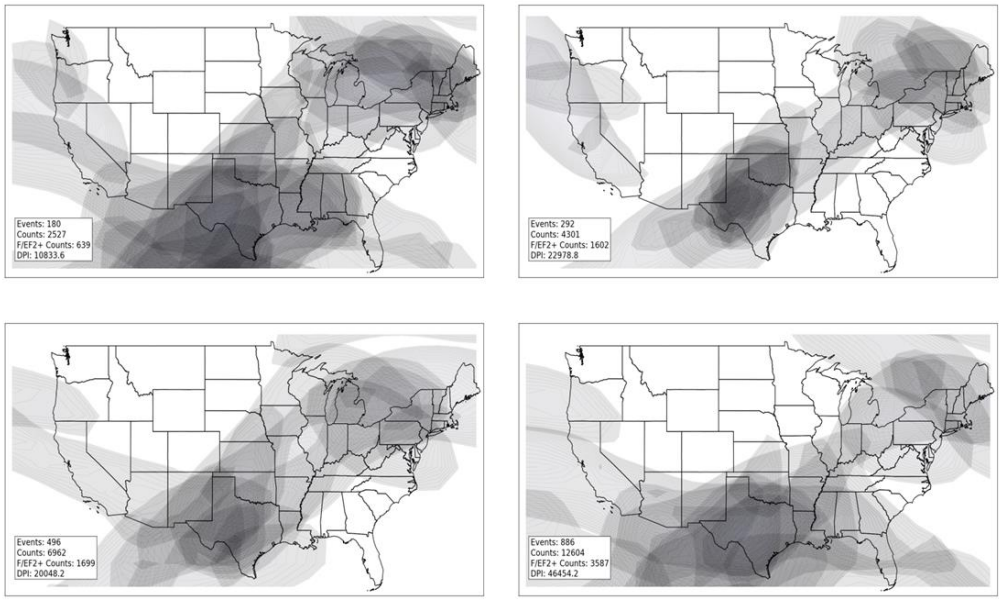

Figure 4.52: Deep layer (surface to 300 hPa) shear calculated as described in Figure 4.28 for all EN April composites (upper left), all LN April composites (upper right), all N April composites (lower left), and all April composites (lower right).

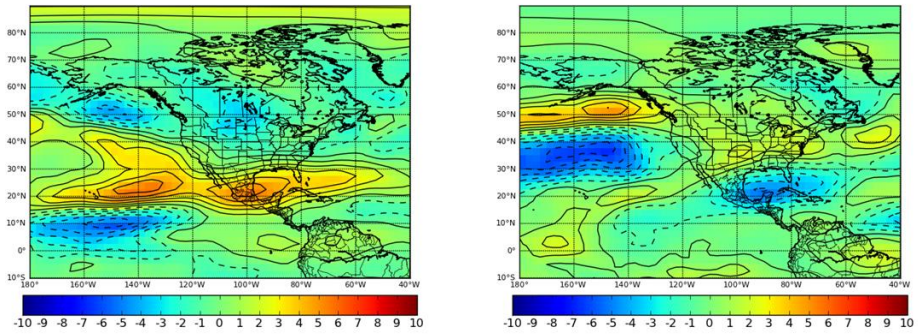

Figure 4.53: Monthly anomalies of 300 hPa scalar wind during April EN (left) and LN (right) conditions. Units are in meters per second.

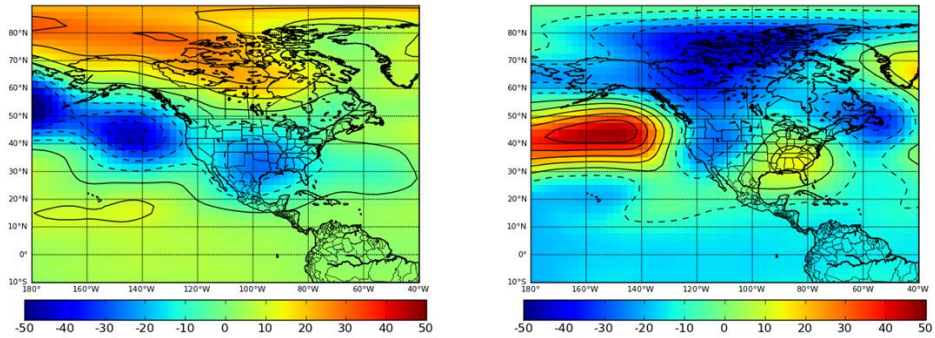

Figure 4.54: Monthly anomalies of 300 hPa geopotential height during April EN (left) and LN (right) conditions. Units are in meters per second.

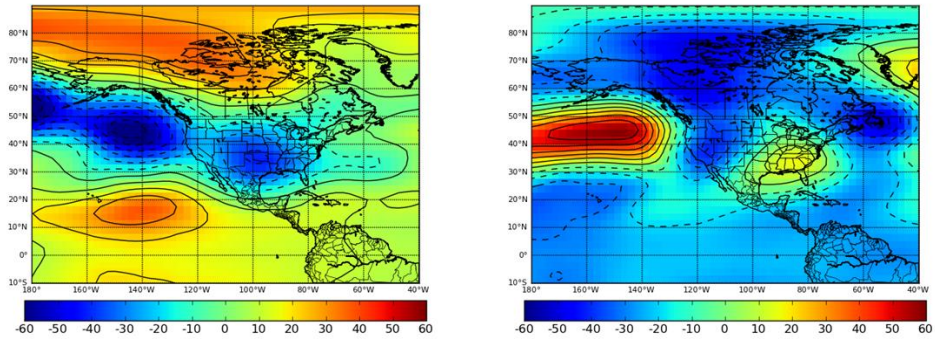

Figure 4.55: Monthly anomalies of 500 hPa geopotential height during April EN (left) and LN (right) conditions. Units are in meters per second.

4.5 Conclusions

The preceding sections of this chapter illustrated the changes in the basic climatology of tornado outbreaks as a function of ENSO. In each monthly period from January-April, tornadoes occur less frequently and at farther south latitudes during EN conditions in the equatorial Pacific and a distinct increase and northward extension of tornadoes in outbreaks occurs during LN conditions. Using normalized and gridded metrics for tornado outbreaks along with bootstrap resampling, ENSO-related shifts in the physical tornado climatology proved to be statistically significant.

The atmospheric climatology discussed in this chapter represents a substantial extension beyond previous work regarding the investigation of an ENSO-related climatology of individual tornado outbreaks. Section 4.5 illustrated that synoptic-scale atmospheric conditions across the continental U.S. are indeed influenced by ENSO and, in turn, affect the location of tornado activity. Some of these atmospheric features are more directly tied to ENSO (i.e., upper-level jet streams) while others are more indirectly associated (i.e., surface cyclones, instability and moisture axes, and low-level jet streams). During EN conditions, upper-level jets are abnormally strong and southwardly displaced, affecting the location of low-level jet formation, surface cyclone formation, and subsequent development of instability axes to foster a southward shift in tornado activity from January through April. During LN conditions, upper-level jets occur farther north, encouraging development of low-level jet streams, and instability axes

farther north and west across the continental U.S., thereby resulting in increased tornado activity farther north and west of the locations experiencing more frequent tornado outbreaks in EN conditions (i.e., the Great Plains and western Great Lakes areas). As mentioned in Chapter 1, previous studies (Cook and Schaefer 2008, Muñoz and Enfield 2011, Lee et al. 2013) only considered monthly or seasonal averages to infer related shifts in tornado activity rather than researching individual outbreaks. Some studies in this regard (Kellner and Niyogi 2014) did not consider any ENSO-related atmospheric shifts that would alter tornado activity.

5. CONCLUSIONS, SEASONAL FORECAST IMPLICATIONS, AND FUTURE WORK

ENSO-related influences on tornado outbreaks were identified in this body of work via the establishment of a physical tornado climatology. This physical tornado climatology was first used to identify shifts in tornado outbreak activity from January through April without any regard to ENSO (Chapter 3) and then developed to determine shifts in tornado activity as a function of ENSO (Chapter 4). Additionally, an PCA-based atmospheric climatology of synoptic-scale features attributed to tornado outbreaks was developed (Chapters 2 and 3) and ENSO-related influences on that climatology was identified (Chapter 4). In general, tornado activity exhibits a westward and northward shift with progression from winter to early spring and although shifts in several synoptic-scale atmospheric features support the shifts in tornado activity, similar geopotential height configurations were noted in winter as in early spring. ENSO tended to alter the tornado climatology by southwardly displacing the upper-level jet stream during its warm phase, which in turn led to southwardly displaced surface cyclones, low-level jets, instability axes, and ultimately tornado outbreaks. During the cold phase of ENSO, tornado activity was stronger, more impactful, occurred more frequently, and occurred at higher latitudes compared to their warm phase counterparts.

ENSO-related evolution of sea surface temperatures tends to slowly evolve over time. Given its slow evolution and its strong influence on

Northern Hemispheric weather that can last many months, the potential for a seasonal tornado forecast is apparent. This body of work has the following implications for such a forecast:

1) The direct and indirect influences of ENSO on synoptic-scale atmospheric features associated with tornado outbreaks and related influences on tornado activity are much clearer because of this study. These relationships have been established not only on a seasonal or monthly averaged basis as has been done in previous studies, but has been established for individual tornado outbreaks as well. As a result, influences of ENSO on upper-level jet streams, low-level jet streams, instability, moisture, and surface cyclogenesis *within* individual outbreaks are much clearer.
2) The ENSO-related physical climatology established in Chapter 4 affords an opportunity to approximate an expected number of tornado outbreaks in a particular month or season. Cook and Schaefer (2008) provided the foundation for this type of forecast, but the current study has presented a deeper, more detailed investigation into this type of forecast potential than previously afforded in any literature. This is primarily due to the systematic identification and inclusion of all invididual January-April tornado outbreaks dating to 1950.
3) Given the geographic shifts outlined in both ENSO-related physical and atmospheric tornado outbreak climatologies (Section 4.5), a

forecast of locations expected to experience more frequent and more impactful tornado activity in a particular season can be inferred based on time of year and ENSO phase. Identification of spatial shifts in tornado activity have been made in previous studies, but only limited to the spring (April and May) time frame (Muñoz and Enfield 2011, Lee et al. 2013), but no identification of such shifts have been made in the refereed literature during January-March, a timeframe in which many impactful and damaging tornado outbreaks have been observed since 1950.

Although the overall result of this body of work demonstrates clear potential for seasonal forecasts of tornado outbreaks, several important caveats need to be considered. Outlier outbreaks that do not match the overall ENSO/tornado climatology have occurred (e.g., March 29, 1998 in southern Minnesota). Additionally, one composite of lifted index indicated widespread instability across much of the CONUS east of the Rocky Mountains during EN March, contradicting other atmospheric signals (i.e., southwardly displaced upper-level jet streams and low-level jet development) that would support a southward shift of tornado occurrence. Extensive experimentation in an operational environment is needed before official seasonal tornado forecasts can be disseminated. As more development in this topic area occurs, research efforts should focus on effective communication of seasonal tornado outbreak risk, with the

understanding that tornadoes will occasionally occur outside of climatologically favored areas.

Two distinct areas of future work have emerged from this research. Although ENSO appears to be a key influence for winter and early spring tornado outbreaks in the U.S., additional areas of localized sea surface temperature anomalies appear to play a role on synoptic-scale atmospheric features associated with outbreaks (e.g., eastern Pacific Ocean) and appear to modulate the availability of low-level moisture and potential instability in tornado outbreak development (e.g., Gulf of Mexico and far western Atlantic Ocean). These factors need to be considered to create a robust seasonal tornado prediction tool. Additionally, the use of PCA to assess synoptic-scale atmospheric features on a climatological basis has opened up interesting possibilities for application of the methodology to 1) develop an environment-based historical tornado record that addresses inaccuracies in historical tornado records and 2) addresses tornado outbreak risk in future climate scenarios.

References

Agee, E., and S. Zurn-Birkhimer, 1998: Variations in USA tornado occurrences during El Niño and La Niña. Preprints, *19th Conf. Severe Local Storms,* Minneapolis, MN*,* Amer. Meteor. Soc., 287-290.

Ambaum, M. H., B. J. Hoskins, and D. B. Stephenson, 2001: Arctic Oscillation or North Atlantic Oscillation?. *J. Climate*, **14**, 3495-3507.

Ashley, W. S., 2007: Spatial and temporal analysis of tornado fatalities in the United States: 1880–2005. *Wea. Forecasting*, **22**, 1214–1228.

Barnes, S. L., and C. W. Newton, 1983: Thunderstorms in the synoptic setting. In *Thunderstom Morphology and Dynamics* (E. Kessler, Ed.), Univ. of Oklahoma, 75-112.

Barnston, A. G., and R. E. Livezey, 1987: Classification, seasonality and persistence of low-frequency atmospheric circulation patterns. *Mon. Wea. Rev.*, **115**, 1083–1126.

Beebe, R. G., and F. C. Bates, 1955: A mechanism for assisting in the release of convective instability. *Mon. Wea. Rev.*, **83,** 1–10.

Betts, A.K., and W. Ridgway, 1989: Climatic equilibrium of the atmospheric convective boundary layer over a tropical ocean. *J. Atmos. Sci.*, **46**, 2621-2641.

Bjerknes, J., 1969: Atmospheric teleconnections from the equatorial Pacific. *Mon. Wea. Rev.*, **97**, 163-172.

Blackadar, A. K., 1957: Boundary layer wind maxima and their significance for the growth of nocturnal inversions. *Bull. Amer. Meteor. Soc.*, **38**, 283-290.

Bonner, W. D., and Paegle, J., 1970: Diurnal Variations in Boundary Layer Winds Over the South-Central United States in Summer. *Mon. Wea. Rev.*, **98**, 735-744.

Bove, M.C., 1998: Impacts of ENSO on United States tornado activity. Preprints, *19th Conf. Severe Local Storms,* Minneapolis, MN, Amer. Meteor. Soc., 313-316.

Brooks, H. E., C. A. Doswell III, and M. P. Kay, 2003: Climatological estimates of local daily tornado probability for the United States. *Wea. Forecasting*, **18**, 626–640.

Brooks, H. E., 2012: Personal Communication.

Browning, P., 1998: ENSO related severe thunderstorm climatology of Northwest Missouri. Preprints*, 19th Conf. Severe Local Storms, Amer. Meteor. Soc., Minneapolis MN*, 291-292.

Bruening, S. L., M. P. Kay, and H. E. Brooks, 2002: A new perspective on the climatology of tornadoes in the United States. Preprints, *16th Conf. on Probability and Statistics,* Orlando, FL, Amer. Meteor. Soc., J96–J103.

Burgess, D. W., L. R. Lemon, and R. A. Brown, 1975: Tornado characteristics revealed by Doppler radar. *Geophys. Res. Lett.*, 2, 183-184.

Cahir, J. J., 1971: Implications of circulations in the vicinity of jet streaks at subsynoptic scales. Ph.D. thesis, Pennsylvania State University, 170 pp.

Carlson, T. N., S. G. Benjamin, G. S. Forbes, Y. F. Li, 1983: Elevated mixed layers in the regional severe storm environment: Conceptual model and case studies. *Mon. Wea. Rev.*, **11**, 1453-1474.

Carr, J. A., 1952: A preliminary report on the tornadoes of March 21–22, 1952. *Mon. Wea. Rev.*, **80**, 50–58.

Cook, A.R., and J. T. Schaefer, 2008: The relation of El Niño Southern Oscillation to winter tornado activity. *Mon. Wea. Rev.*, **136**, 3121-3137.

Corfidi, S. F., 1999: The birth and early years of the Storm Prediction Center. *Wea. Forecasting*, **14**, 507–525.

Crum, T. D., and R. L. Alberty, 1993: The WSR-88D and the WSR-88D Operational Support Facility. *Bull. Amer. Meteor. Soc.,* **74**, 1669-1687.

Danielson, E. P., 1975: A conceptual theory of tornadogenesis based on macro-, meso-, and microscale processes. Preprints, *9th Conf. on Severe Local Storms,* Norman, OK, Amer. Meteor. Soc., 376-383.

Dixon, P. G., A. E. Mercer, J. Choi, and J. S. Allen, 2011: Tornado risk analysis: Is Dixie Alley an extension of Tornado Alley? *Bull. Amer. Meteor. Soc.*, **92**, 433-441

Doswell, C. A. III, 2007: Small sample size and data quality issues illustrated using tornado occurrence data. *Electronic J. Severe Storms Meteor.,* **2**, 1-16.

Doswell, C**. A. III**, and D. W. Burgess, 1988: On some issues of United States tornado climatology. *Mon. Wea. Rev.,* **116,** 495–501.

Doswell, C. A. III, H. E. Brooks, and R. A. Maddox, 1996: Flash flood forecasting: an ingredients-based methodology. *Wea. Forecasting*, **11**, 560–581.

Doswell, C. A. III, R. Edwards, R. L. Thompson, J. A. Hart, and K. C. Crosbie, 2006: A simple and flexible method for ranking severe weather events. *Wea. Forecasting*, **21**, 939–951.

Efron, B. and R. J. Tibshirani, 1993: An Introduction to the Bootstrap. Chapman and Hall, London. 436 pp.

Eichler, T. and R. W. Higgins, 2006: Climatology and ENSO-related Variability of North American Extratropical Cyclone Activity. *J. Climate*, **19**, 2076-2093.

Enloe, J., J. J. O'Brien, and S. R. Smith, 2004: ENSO Impacts on Peak Wind Gusts in the United States. *J. Climate*, **17**, 1728-1737.

Enthought Python Distribution (Version 7.2) [Software]. (2010). Retrieved from http://www.enthought.com

Federov, A. V., and S. G. Philander, 2000: Is El Niño Changing? *Science*, **288**, 1997-2002

Feldstein, S. B., 2000: The timescale, power spectra, and climate noise properties of teleconnection patterns. *J. Climate,* **13,** 4430–4440.

Feldstein, S. B., 2002: Fundamental mechanisms of the growth and decay of the PNA teleconnection pattern. *Quart. J. Royal Meteor. Soc.*, **128**, 775–796.

Finley, J.P., 1884: Tornado predictions. *Amer. Meteor. J.*, **1**, 85-88.

Finley, J.P., 1888: The relation of tornado regions to areas of low pressure. *Amer. Meteor. J.*, **5**, 83-87.

Flora, S. D., 1953: *Tornadoes of the United States*. The University of Oklahoma Press: Norman, 221 pp.

Fujita, T. T., 1971: Proposed characteristics of tornadoes and hurricanes by area and intensity. Chicago: University of Chicago. 42 pp.

Galway, J. G., 1975: Relationship of tornado deaths to severe weather watch areas**.** *Mon. Wea. Rev.*, **103**, 737–741.

Galway, J. G., 1977: Some climatological aspects of tornado outbreaks. *Mon. Wea. Rev.*, **105**, 477–484.

Galway, J. G., 1985: J.P. Finley: The first severe storms forecaster. *Bull. Amer. Meteor. Soc.*, **66**, 1389–1395.

Galway, J. G., 1992: Early severe thunderstorm forecasting and research by the United States Weather Bureau. *Wea. Forecasting*, **7**, 564–587.

Galway, J. G., and A. Pearson, 1981: Winter tornado outbreaks. *Mon. Wea. Rev.*, **109**, 1072-1080.

Glickman, T. S., Ed., 2000: *Glossary of Meteorology*. 2d ed. Amer. Meteor. Soc., 782 pp.

Grazulis, T. P., 1993: *Significant Tornadoes 1680-1991, A Chronology and Analysis of Events*. The Tornado Project of Environmental Films: St. Johnsbury, VT. 526 pp.

Grice, G. K., R. J. Trapp, S. F. Corfidi, R. Davies-Jones, C. C. Buonanno, J. P. Craven, K. K. Droegemeier, C. Duchon, J. V. Houghton, R. A. Prentice, G. Romine, K. Schlachter, and K. K. Wagner, 1999: The golden anniversary celebration of the first tornado forecast. *Bull. Amer. Meteor. Soc.*, **80**, 1341–1348.

Hales, J. E., Jr., 1985: Synoptic features associated with the Los Angeles tornado occurrences. *Bull. Amer. Meteor. Soc.*, **66**, 657-662.

Hagemeyer, B.C., 1998: Significant extratropical tornado occurrences in Florida during strong El Niño and strong La Niña events. **Preprints, *19th Conference on Severe Local Storms,*** Minneapolis, MN, Amer. Meteor. Soc., 412-415.

Horel, J. D., 1981: A rotated principal component analysis of the interannual variability of the Northern Hemisphere 500 mb height field. *Mon. Wea. Rev.*, **109**, 2080–2092.

Horel, J. D., and J. M. Wallace, 1981: Planetary-scale atmospheric phenomenon associated with the Southern Oscillation. *Mon.Wea. Rev.,* **109,** 813–829.

Hurrell, J. W., 1995: Decadal trends in the *North Atlantic Oscillation*: Regional temperatures and precipitation. *Science*, **269**, 676-679.

Johns, R. H., and C. A. Doswell III, 1992: Severe local storms forecasting. *Wea. Forecasting,* **7,** 588–612.

Kalnay, E. and Coauthors, 1996: The NCEP/NCAR 40-Year Reanalysis Project. Bull. Amer. Meteor. Soc., 77, 437-471.

Kellner, O. and D. Niyogi, 2014: Land Surface Heterogeneity Signature in Tornado Climatology? An Illustrative Analysis over Indiana, 1950-2012. *Earth Interact.*, **18**, 1-32.

Kelly, D. L., J. T. Schaefer, R. P. McNulty, C. A. Doswell, and R. F. Abbey, 1978: An augmented tornado climatology. *Mon. Wea. Rev.*, **106**, 1172–1183.

Kessler, E., and J. T. Lee, 1976: Normalized indices of destruction and deaths by tornadoes. NOAA Tech. Memo. ERL NSSL-77, National Severe Storms Laboratory.

Knowles, J. B., and R.A. Pielke, 2005: The Southern Oscillation and its effects on tornadic activity in the United States. Atmospheric Sciences Paper No. 755, Colorado State University, Fort Collins, CO 80523. 15pp.

Lamb, P. J., and R. A. Peppler, 1987: North Atlantic oscillation: Concept and an application. *Bull. Amer. Meteor. Soc.*, **68,** 1218–1225.

Lanicci, J. M., and T. T. Warner, 1991: A synoptic climatology of the elevated mixed-layer inversion over the southern Great Plains in spring. Part 3: Relationship to severe-storms climatology. *Wea. Forecasting*, **6**, 214-226.

Lee, J. T., and J. G. Galway, 1956: Preliminary report on the relationship between the jet at 200-mb level and tornado occurrence. *Bull. Amer. Meteor. Soc.*, **37,** 327–332.

Lee, S-K., R. Atlas, D. Enfield, C. Wang, and H. Liu, 2013: Is there an optimal ENSO pattern that enhances large-scale atmospheric processes conducive to tornado outbreaks in the U.S.? *J. Climate*, **26**, 1626-1642.

Li, Y., and N. –C. Lau, 2012: Impact of ENSO on the Atmospheric Variability over the North Atlantic in Late Winter—Role of Transient Eddies. *J. Climate*, **25**, 320–342.

Ludlum, D. M., 1970: *Early American tornadoes 1586-1870*. American Meteorological Society, Boston. 219 pp.

Madden., R. A., and P. R. Julian, 1971: Description of global-scale circulation cells in the tropics with a 40-50 day period. *J. Atmos. Sci.*, **29**, 1109-1123.

Maddox, R. A., L. R. Hoxit, and C. F. Chappell, 1980: A study of tornadic thunderstorm interactions with thermal boundaries. *Mon. Wea. Rev.*, **108**, 322–336.

Marzban, C., and J. T. Schaefer. 2001: The correlation between U.S. tornadoes and Pacific sea surface temperatures. *Mon. Wea. Rev*, **129**, pp. 884–895.

McDonald, J. R. and K. C. Mehta, 2006: A Recommendation for an Enhanced Fujita Scale. [Available Online at http://www.spc.noaa.gov/efscale/]

McNulty, R. P., 1978: On upper tropospheric kinematics and severe weather occurrence. *Mon. Wea. Rev.*, **106**, 662–672.

Mead, C. M., and R. L. Thompson, 2011: Environmental characteristics associated with nocturnal significant-tornado events in the central and southern Great Plains. *Electronic J. Severe Storms Meteor.*, **6**, 1-35.

Mercer, A. E., 2008: Discrimination of tornadic and non-tornadic severe weather outbreaks. Ph.D. Dissertation, University of Oklahoma, 152 pp.

Mercer, A. E., C.M. Shafer, C. A. Doswell, L. M. Leslie, and M. B. Richman, 2011: Synoptic composites of tornadic and nontornadic outbreaks. *Mon. Wea. Rev.*, in press.

Miller, R. C., 1972: Notes on analysis and severe storm forecasting procedures of the Air Force Global Weather Central. Tech. Rep. 200 (rev. ed.), Air Force Weather Agency, 190 pp.

Muñoz, E., and D. Enfield, 2011: The boreal spring variability of the Intra-Americas low-level jet and its relation with precipitation and tornadoes in the eastern United States. *Climate Dynamics* **36**:1-2, 247-259.

Murphy, A. H., 1996: The Finley Affair: A Signal Event in the History of Forecast Verification. *Wea. and Forecasting*, **11**, 3-20.

National Climatic Data Center, 2011: Storm Events Database. [Available online at: http://www4.ncdc.noaa.gov/cgiwin/wwcgi.dll?wwevent~Storms]

National Oceanic and Atmospheric Administration, 2014: 2011 Tornado Information. Web link: http://www.noaanews.noaa.gov/2011_tornado_information.html

Newton, C. W., 1967: Severe convective storms. Adv. Geophys., 12, 257-308.

Parsons, D. B., M. A. Shapiro, and E. Miller, 2000: A mesoscale structure of a nocturnal dryline and a frontal-dryline merger. *Mon. Wea. Rev.*, **128**, 3824-3838.

Pautz, M. E., 1969: Severe local storm occurrences, 1955-1967. ESSA Tech. Memo. WBTM FCST12, Washington, DC, 3-4.

Peixoto, J. P., and A. H. Oort, 1992: *Physics of Climate*. Springer-Verlag, 520 pp.

Portis, D. H., J. E. Walsh, M. E. Hamly, and P. J. Lamb, 2000: Seasonality of the North Atlantic Oscillation. J. Climate, 13, 2069-2078.

R Development Core Team, 2012. R; A language and environment for statistical computing. R Foundation for Statistical Computing, Vienna, Austria. URL http://www.R-project.org/.

Ramsdell, J. V., and J. P. Rishel. 2007: Tornado climatology of the contiguous United States, NUREG/CR-4461, Rev.2, Pacific Northwest Laboratory.

Rasmusson, E. M., and T. H. Carpenter, 1982: Variations in tropical sea surface temperature and surface wind fields associated with the Southern Oscillation/El Niño. *Mon. Wea. Rev.* **110**, 354-384.

Rasmusson, E. M., and K. Mo, 1993: Linkages between 200-mb tropical and extratropical circulation anomalies during the 1986-1989 ENSO cycle. *J. Climate*, **6**, 595-616.

Rogers, J. C., 1984: The association between the North Atlantic Oscillation and the Southern Oscillation in the Northern Hemisphere. *Mon. Wea. Rev.,* **112**, 1999-2015.

Ropelewski, C. F., and M. S. Halpert, 1987: Global and regional scale precipitation patterns associated with the El Niño/Southern Oscillation. *Mon. Wea. Rev.,* **115**, 1606–1626.

Rhea, J. O., 1966: A study of thunderstorm formation along drylines. *J. Appl. Meteor.,***5,** 58–63.

Richman, M. B., 1986: Rotation of principal components. *J. Climatol.*, **6**, 293-335.

Sasaki, Y., and S. A. Tegtmeier, 1974: An experiment of subjective tornado forecasting using hourly surface observations. Preprints, *8th Conf. on Severe Local Storms,* Denver, CO, Amer. Meteor. Soc., 276-279.

Schaefer, J. T., 1974: The life cycle of the dryline. *J. Appl. Meteor.*, **13**, 444–449.

Schaefer, J. T., 1986: Severe thunderstorm forecasting: A historical perspective. *Wea. Forecasting*, **1**, 164–189.

Schaefer, J. T., and C. A. Doswell, 1984: Empirical orthogonal function expansion applied to progressive tornado outbreaks. *J. Meteor. Soc. Japan*, **62,** 929–936.

Schaefer, J. T., and R. Edwards, 1999: The SPC tornado/severe thunderstorm database. Preprints, *11th Conf. on Applied Climatology,* Dallas, TX, Amer. Meteor. Soc., 215–220.

Schaefer, J. T., D. L. Kelly, and R. F. Abbey, 1980: *Tornado Track Characteristics and Hazard Probabilities.* Pergamon Press, 650 pp.

Schaefer, J. T., D. L. Kelly, and R. F. Abbey, 1986: A Minimum Assumption Tornado-Hazard Probability Model. *J. Climate Appl. Meteor.*, **25**, 1934–1945.

Schaefer, J. T., and F. B. Tatom, 1998: The Relationship between El Niño, La Niña and United States Tornado Activity. Preprints, *19th Conf. Severe Local Storms,* Minneapolis MN, Amer. Meteor. Soc., 416-419.

Schneider, R. S., J. T. Schaefer, and H. E. Brooks, 2004: Tornado outbreak days: An updated and expanded climatology (1875-2003). Preprints, *22nd Conf. Severe Local Storms,* St. Louis, MO. CD-ROM. [Available online at: http://www.spc.noaa.gov/publications/schneider/otbrkday.pdf]

Shafer, C. M., and C. A. Doswell III, 2011: Using kernel density estimation to identify, rank, and classify severe weather outbreak events. *Electronic J. Severe Storms Meteor.*, **6**, 1-28.

Showalter, A. K., 1953: A stability index for thunderstorm forecasting. *Bull. Amer. Meteor. Soc*., **34**, 250-252.

Showalter, A. K., and J. R. Fulks, 1943: Preliminary report on tornadoes. U.S. Weather Bureau, Washington, 162 pp.

Simmons, K. M. and Sutter, D., 2005: WSR-88D radar, tornado warnings, and tornado casualties. *Wea. and Forecasting*, **20**, 301-310.

Smith, S. R., P. M. Green, A. P. Leonardi, and J. J. O'Brien, 1998: Role of Multiple-Level Tropospheric Circulations in Forcing ENSO Winter Precipitation Anomalies. *Mon. Wea. Rev.*, **126**, 3102-3116.

Stensrud, D. J., 1996: Importance of low-level jets to climate: a review. *J. Climate*, **9**, 1698–1711.

Thom, H. C. S., 1963: Tornado Probabilities. *Mon. Wea. Rev.*, **91**, 730–736.

Thompson, D. W., and J. M. Wallace, 1998. The Arctic oscillation signature in the wintertime geopotential height and temperature fields. *Geophys. Res. Lett.*, **25**, 1297–1300.

Thompson, R. L., and M.D. Vescio, 1998. The Destruction Potential Index - a method for comparing tornado days. Preprints, *19th Conf. Severe Local Storms,* Minneapolis, MN, Amer. Meteor. Soc., 280-282.

Thompson, R. L., R. Edwards, J. A. Hart, K. L. Elmore, and P. M. Markowski, 2003: Close proximity soundings within supercell environments obtained from the Rapid Update Cycle. *Wea. Forecasting*, **18**, 1243–1261.

Uccelini, L. W., and D. R. Johnson, 1979: The coupling of upper and lower tropospheric jet streaks and implications for the development of severe convective storms. *Mon. Wea. Rev.*, **107**, 682-703.

van Loon, H., and J.C. Rogers, 1978: The Seesaw in Winter Temperatures Between Greenland and Northern Europe. Part I: General Description. *Mon. Wea. Rev*., **106**, 296-310.

Verbout, S. M., H. E. Brooks, L. M. Leslie, and D. M. Schultz, 2006: Evolution of the US tornado database: 1954-2003. *Wea. Forecasting*, **21**, 86-93.

Verbout, S. M., L. M. Leslie, H. E. Brooks, and S. L. Bruening, 2004: Leveling the field for tornado reports through time: Inflation-adjustment of annual tornado reports and objective identification of extreme tornado reports. Preprints, *22nd Conf. on Severe Local Storms*, Hyannis, MA, Amer. Meteor. Soc., CD-ROM.

Walker, G. T., and E. W. Bliss, 1932: World Weather V. Mem. *Roy. Meteor. Soc*., **4,** 36, 53-84.

Wallace, J. M., and D. S. Gutzler, 1981: Teleconnections in the geopotential height field during the Northern Hemisphere Winter. *Mon. Wea. Rev.,* **109,** 784-812.

Weaver. S. J., S. Baxter, and A. Kumar, 2012: Climatic Role of North American Low-Level Jets on U.S. Regional Tornado Activity. *J. Climate*, **25**, 6666-6683.

Weisman, M. L., and J. B. Klemp, 1984: The structure and classification of numerically simulated convective storms in directionally varying wind shears. *Mon. Wea. Rev.,* **112,** 2479-2498.

Wilks, D. S., 2006: Statistical Methods in the Atmospheric Sciences. Academic Press, Burlington, MA. 627 pp.

Wolford, L. V., 1960: Tornado occurrences in the United States. *Technical Paper No. 20*, U.S. Weather Bureau, Washington, D.C., 71 pp.

Wyrtki, K. 1975: El Niño -- The dynamic response of the equatorial Pacific Ocean to atmospheric forcing. *J. Phys. Oceanogr.* **4**, 91-103.

Zhong, S., J. D. Fast, and X. Bian, 1996: A case study of the Great Plains low-level jet using wind profiler network data and a high-resolution mesoscale model. *Mon. Wea. Rev.*, **124**, 785-806.